MICROCOPY RESOLUTION TEST CHART

NATIONAL BUREAU OF STANDARDS-1963-A

REPORT DOCUMENTATION PAGE		READ INSTRUCTIONS BEFORE COMPLETING FORM
1. REPORT NUMBER	2. GOVT ACCESSION NO.	3. RECIPIENT'S CATALOG NUMBER
4. TITLE (and Subtitle) BASIC ADHESION MECHANISMS IN THICK AND THIN FILMS.		5. TYPE OF REPORT & PERIOD COVERED Final Report. 1 Jan-31 Dec 77, (1-1-77 to 12-31-77)
		6. PERFORMING ORG. REPORT NUMBER PRRL-78-CR-5
7. AUTHOR(s) Kenneth R. Bube Thomas T. Hitch		8. CONTRACT OR GRANT NUMBER(s) N00019-77-C-0176
9. PERFORMING ORGANIZATION NAME AND ADDRESS RCA Laboratories Princeton, New Jersey 08540		10. PROGRAM ELEMENT, PROJECT, TASK AREA & WORK UNIT NUMBERS
11. CONTROLLING OFFICE NAME AND ADDRESS Naval Air Systems Command Washington, DC 20361		12. REPORT DATE Mar 78
		13. NUMBER OF PAGES 114
14. MONITORING AGENCY NAME & ADDRESS (if different from Controlling Office)		15. SECURITY CLASS. (of this report) Unclassified
		15a. DECLASSIFICATION/DOWNGRADING SCHEDULE N/A

16. DISTRIBUTION STATEMENT (of this Report)

Approved for public release; distribution unlimited.

17. DISTRIBUTION STATEMENT (of the abstract entered in Block 20, if different from Report)

18. SUPPLEMENTARY NOTES

19. KEY WORDS (Continue on reverse side if necessary and identify by block number)

Frit-bonded inks	Gold powder sintering
Reactively bonded inks	Liquid-phase sintering
Mixed-bonded inks	Spinel formation

20. ABSTRACT (Continue on reverse side if necessary and identify by block number)

    This report is the fourth and final one in a series pertaining to the identification of factors which influence thick-film metallization adhesion. Prior work was concerned with the characterization of commercial thick-film conductors, i.e., gold, silver, copper, and gold-platinum (-palladium) systems. In addition, the preceding work

over

DD FORM 1473
1 JAN 73

299 000

20.

explored variables, such as firing temperature and time, which influenced the basic processes of metal sintering and interactions with the adhesive agent.

As a result of prior analyses, it became clear that factors which influence adhesion would differ with adhesive agent type, e.g., frit-bonded, mixed-bonded or reactively bonded. The present study addresses this distinction and explores the factors which primarily contribute to adhesion in each class. To simplify the discussion, the experiments in this year's study have been confined to gold films.

For the frit-bonded type, pertinent sintering theories were reviewed, a model gold powder was synthesized and sintering behavior was observed in the presence and absence of glass. From the determination and comparison of activation energies, it is shown that gold powder densification is initially accelerated in the presence of glass. This acceleration is attributed to liquid phase-assisted sintering which is enhanced by gold solubility at $900°C$. Experimental measurements of electrical resistivity showed that prolonged firing does not cause proportionate improvement in conductivity. Indeed, continued sintering in the presence of glass results in pore coarsening via Ostwald ripening which was observed in the fired film microstructures. Adhesion strength degradation is thus related to the initial metal powder particle size distribution and morphology. Recommendations for further study pertaining to these variables are offered.

With regard to reactively bonded and mixed-bonded inks, experimental studies of reaction kinetics indicate that formation of spinels, MAl_2O_4, where M may be Cu, Cd, or Mg is crucial to film adhesion. Incorporation of small amounts of a glassy phase with the reactive bonding agent enhances the growth of the spinel phase and aids in densifying the film.

PREFACE

This final report describes work performed in the Integrated Circuit Technology Center of RCA Laboratories, under Contract No. N00019-77-C-0176. Mr. Joseph H. Scott is the Laboratory Director and Dr. George L. Schnable is the Project Supervisor and Group Head. Dr. Thomas T. Hitch is Project Scientist and, with Kenneth R. Bube, comprises the principal research team. James Willis is the Government Project Monitor.

It is a pleasure to acknowledge the help of R. J. Paff and R. T. Smith who have contributed to this study by their use of x-ray diffraction techniques for phase identification, to B. Seabury for his work in scanning electron microscopy, and to H. H. Whitaker for his work in emission spectroscopic and atomic absorption analyses. We also acknowledge the able assistance of E. J. Conlon and A. Z. Miller in the preparation of samples and the day-to-day pursuit of this study. Discussions throughout the work with Dr. G. L. Schnable, and his reviews of the manuscript were most valuable.

We acknowledge helpful discussions with a number of the scientists studying thick-film technology in several companies and government laboratories. Discussions with members of the Naval Research Laboratories team working in coordination with RCA, including Dr. Jim Murday, Dr. Paul Becher, and Dr. Bill Bascom; with the Project Monitor, Mr. James Willis; and with his supervisor, Dr. Herbert J. Mueller, have been particularly useful.

TABLE OF CONTENTS

TABLE OF CONTENTS (Continued)

LIST OF ILLUSTRATIONS

LIST OF ILLUSTRATIONS (Continued)

LIST OF ILLUSTRATIONS (Continued)

LIST OF TABLES

LIST OF TABLES (Continued)

SECTION I

INTRODUCTION

The microelectronics industry has profited from two diverse technologies, i.e., monolithic silicon and thick-film. By combining components from both fields, the resulting "hybrid" circuits have progressively improved in terms of packaging density, cost and ruggedness. Historically, however, effort in thick-film technology has lagged behind monolithic silicon technology to the detriment of hybrid circuit design and development. The work presented herein is directed toward resolving problems in thick-film technology.

In any hybrid circuit, the basic building block is the insulating ceramic substrate. Onto this ceramic surface are deposited all the active and passive devices which comprise the circuit. A key element to reliable circuit performance is the bond which is established between the ceramic substrate and the first-level metallization. All subsequent devices or components are directly or indirectly connected to this level by screen printing and firing, wire-bonding, soldering or organic adhesive attachment methods. Consequently, the integrity of circuit performance and reliability hinges heavily upon first-level metallization properties, i.e., adhesion, bondability, conductivity, etc. In order to improve circuit performance, reliability and cost objectives, it is necessary to develop a better understanding of the factors which determine metallization properties. This report culminates a four-year program of study designed to identify basic adhesion mechanisms. Work of the preceding years had focused upon evaluation of commercial gold [1], copper and silver [2] and gold-platinum [3] metallizing inks. In addition, ink constituents, notably gold powders and glass frit, were characterized with regard

1. T. T. Hitch and K. R. Bube, "Basic Adhesion Mechanisms in Thick and Thin Films," Final Report, NASC Contract No. N00019-74-C-0270, 31 January 1975.
2. T. T. Hitch and K. R. Bube, "Basic Adhesion Mechanisms in Thick and Thin Films," Final Report, NASC Contract No. N00019-75-C-0145, 30 January 1976.
3. K. R. Bube and T. T. Hitch, "Basic Adhesion Mechanisms in Thick and Thin Films," Final Report, NASC Contract No. N00019-76-C-0256, 31 January 1977.

to sintering kinetics and glass spreading phenomena. The commercial inks were studied to determine the influence of screen printing and firing parameters upon film adhesion, electrical resistivity and morphology. As a result of the data base, a means was provided for classifying the inks according to inorganic binder type, i.e., frit-bonded*, mixed-bonded** and reactively bonded† inks. From the study of commercial inks and metal powder sintering kinetics in the presence and absence of glass, it was obvious that film microstructure development and properties differ with binder class.

Since microstructure development was sensitive to binder type, a universal model would be tenuous and of little use in describing film properties. The plan of the present study divides the effort into two segments; frit-bonded vs mixed- and reactively bonded classes. The physicochemical relationships between inorganic binder type and metal powder are divisible into at least these two sections. Gold thick films, which have the most useful material properties, can suffer from the poorest adhesion of all the metallizations. For these reasons as well as simplicity, the present attempt at modeling film microstructure and/or reaction kinetics in the presence of different binder types is limited to gold films.

---

*Frit-bonded - Made adherent (to the substrate) by including in the paste, particles of glass, bismuth oxide and/or fluxing agents which become somewhat fluid on firing and wet the substrate and the sintering metal.
**Mixed-bonded - Made adherent by the presence of copper oxide (or a suitable copper oxide precursor such as a carbonate), other reactive bonding compounds such as cadmium oxide, and an amount of frit approximately equal to the amount of reactive bonding additives.
†Reactively bonded - Made adherent principally through the presence of discrete chemical compounds which are formed during firing at the film-to-substrate interface, from components of both the thick-film ink and the substrate.

SECTION II

FRIT-BONDED INKS

A. ADHESION AT THE METAL-GLASS INTERFACE

In the normal firing of thick-film inks, the frit or glass constituent is at some point molten and the degree of wetting of the available metal surface is governed by Young's equation [4,5]

$$\gamma_{SL} + \gamma_{LV} \cos \theta = \gamma_{SV}, \tag{1}$$

where θ = metal-glass contact angle

γ_{SL} = solid-liquid interfacial energy

γ_{LV} = liquid-vapor interfacial energy

γ_{SV} = solid-vapor interfacial energy

The work of adhesion, W_A is then

$$W_A = \gamma_{LV} + \gamma_{SV} - \gamma_{SL}, \tag{2}$$

or

$$W_A = \gamma_{LV}(1 + \cos \theta). \tag{3}$$

From the observed surface tension, γ_{LV} (see Appendix A) and contact angle between E1527 glass and gold [1], one can determine the work of adhesion at 900°C to be:

$$W_A = 258 (1 + \cos 10°) = 512 \text{ ergs/cm}^2 \tag{4}$$

Nicholas [6] cites the Au-Al$_2$O$_3$ work of adhesion to be 530 ergs/cm^2 for Au at 1000°C. At the same temperature, he reports for Ni-Al$_2$O$_3$, 645 ergs/cm^2 and for Fe-Al$_2$O$_3$, 810 ergs/cm^2. Therefore, gold has a predictably

---

4. W. D. Kingery, H. K. Bowen, and D. R. Uhlmann, *Introduction to Ceramics*, 2nd ed. (John Wiley & Sons, Inc., New York, 1976), pp. 183, 208.
5. N. K. Adam, "Use of the Term 'Young's Equation' for Contact Angles," Nature 180, October 19, 1957, p. 809.
6. M. Nicholas, "The Strength of Metal/Alumina Interface," J. Mat'ls. Sci. 3, 571-576 (1968).

low adhesion strength to the model glass or to an alumina substrate. This low adhesion strength was corroborated previously where gold foil peel strengths to E1527-glazed alumina showed 56 g/mm of peeled width [2,3]. In comparison, the silver foil peel strength was 267 g/mm [3].

Consequently, improvements in frit-bonded gold thick-film adhesion must flow from a better understanding of the factors which influence the large surface area gold-glass interface or microstructure. The logical place to begin is in the treatment of metal powder sintering kinetics.

B. SINTERING THEORIES RELEVANT TO FRITTED METALLIZATION

A recent review of sintering theories was published by Vest [7] in preparation for a discussion of models pertaining to thick-film resistors. The several theoretical mechanisms which, according to Vest, describe neck growth and shrinkage behavior, are tabulated in Tables 1 and 2, repectively. While the volumetric ratios of conductive and insulating phases differ considerably for thick-film resistors and metallizations, the basic mechanisms are still considered applicable. As shown in Fig. 1, the classical model of sintering phenomena is based on the approach of two spherical particles of radius, r, and growth of the neck radius, x. The relationship between the neck radius, x, and particle radius, r, after sintering isothermally at a temperature, T, for a time, t, can be expressed as

$$\left(\frac{x}{r}\right)^n = F(T) r^{-m} t \tag{5}$$

Appropriate values of $F(T)$, m, and n can be found in Table 1. Similarly, the shrinkage in powder compacts, $\Delta L/L_o$, where ΔL is the change in length,

7. R. W. Vest, "Conduction Mechanisms in Thick-Film Microcircuits," Final Technical Report under ARPA Order No. 1642, Grant Nos. DAHC-15-70-G7 and DAHC-15-73-G8. Grantee: Purdue University Research Foundation, December, 1975.

4

TABLE 1. SUMMARY OF NECK GROWTH RELATIONSHIPS [1]

Mechanism	$F(T)$	$\underline{n}$	$\underline{m}$
Newtonian Viscous Flow	$\dfrac{3}{2}\dfrac{\gamma_{SV}}{\eta}$	2	1
Volume Diffusion	$\dfrac{40\gamma_{SL}\delta_\ell^{\,3}D_V}{KT}$	5	3
Surface Diffusion	$\dfrac{56\gamma_{SL}\delta_\ell^{\,4}D_S}{KT}$	7	4
Grain-Boundary Diffusion	$\dfrac{96\gamma_{SL}\delta_o bD_g}{KT}$	6	4
Evaporation-Condensation	$\dfrac{3\pi M\alpha_1 P_o\gamma_{SL}(M/2\pi RT)^{\frac{1}{2}}}{d_1^{\,2}RT}$	3	2

Solution-Precipitation:

	$F(T)$	$\underline{n}$	$\underline{m}$
A. Kingery's Model			
1. Diffusion-Controlled Process	$\dfrac{48K_1\delta C_o\gamma_{LV}V_o D}{K_2 RT}$	6	4
2. Reaction-Controlled Process	$\dfrac{8K_1 C_o\gamma_{LV}V_o K_T}{K_2 RT}$	4	2
B. Without Shrinkage	$\dfrac{3\pi M\alpha_1 C_o\gamma_{SL}(M/2\pi RT)^{\frac{1}{2}}}{d_1^{\,2}RT}$	3	2

5

TABLE 2. SUMMARY OF SHRINKAGE RELATIONSHIPS [1]

Mechanism	$G(T)$	n'	m'
Newtonian Viscous Flow	$\dfrac{3}{4}\dfrac{\gamma_{SV}}{\eta}$	1	1
Volume Diffusion	$\dfrac{40\gamma_{SL}\delta_\ell^3 D_V}{KT}$	$\dfrac{2}{5}$	$\dfrac{6}{5}$
Grain-Boundary Diffusion	$\dfrac{12\gamma_{SL}\delta_o b D_g}{KT}$	$\dfrac{1}{3}$	$\dfrac{4}{3}$
Solution-Precipitation: Kingery's Model			
1. Diffusion-Controlled Process	$\dfrac{6K_1\delta C_o\gamma_{LV}V_o D}{K_2 RT}$	$\dfrac{1}{3}$	$\dfrac{4}{3}$
2. Reaction-Controlled Process	$\dfrac{2K_1 C_o\gamma_{LV}V_o K_T}{K_2 RT}$	$\dfrac{1}{2}$	1

LEGEND FOR EQUATIONS IN TABLES 1 AND 2

α_1 = sticking coefficient

b = grain boundary thickness

C_o = equilibrium solubility of the solid in the liquid

d_1 = density of solid phase

D = diffusion coefficient of the slowest moving species

D_g = grain boundary diffusion coefficient

D_S = surface diffusion coefficient

D_V = volume diffusion coefficient

δ = thickness of liquid film separating the particles

δ_o = vacancy volume

δ_ℓ = interatomic distance

η = viscosity

δ_{LV} = interfacial energy (liquid vapor)

γ_{SL} = interfacial energy (solid-liquid)

γ_{SV} = interfacial energy (solid-vapor)

K = constant

M = molecular weight

P_o = equilibrium vapor pressure over a flat surface

R = gas constant

T = absolute temperature

6
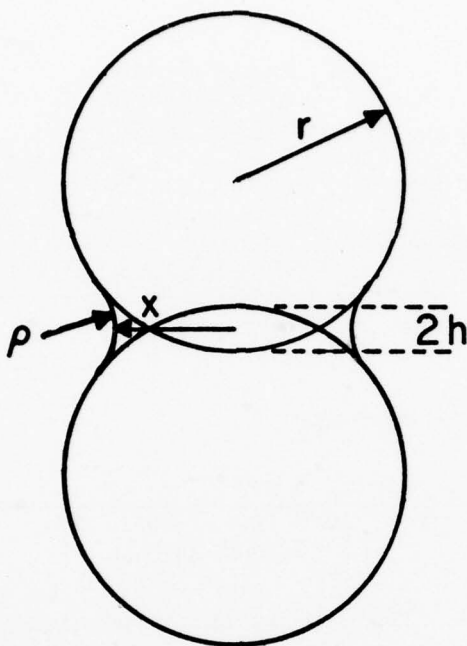
Figure 1. Neck growth during initial stage sintering.

and L_o the original length, is also a function of temperature, particle radius, and time, viz.,

$$\frac{\Delta L}{L_o} = G(T)^{n'} \; r^{-m'} \; t^{n'} \qquad (6)$$

The values for $G(T)$, m', and n' are found in Table 2.

In frit-bearing metallizations, the frit becomes quite fluid with increasing temperature, i.e., the viscosity decreases exponentially. A typical metallization firing profile is shown in Fig. 2. Under this firing profile, organic binders are burned between 100 and 400°C[*]. As shown by Eqs. (5) and (6), neck growth and shrinkage are inversely related to particle size. Hence, at the lower temperature the smaller particles begin to sinter and the film begins to densify. As the temperature continues to rise, glass spreading occurs while

---

[*]See Appendix B for binder combustion rate.

7
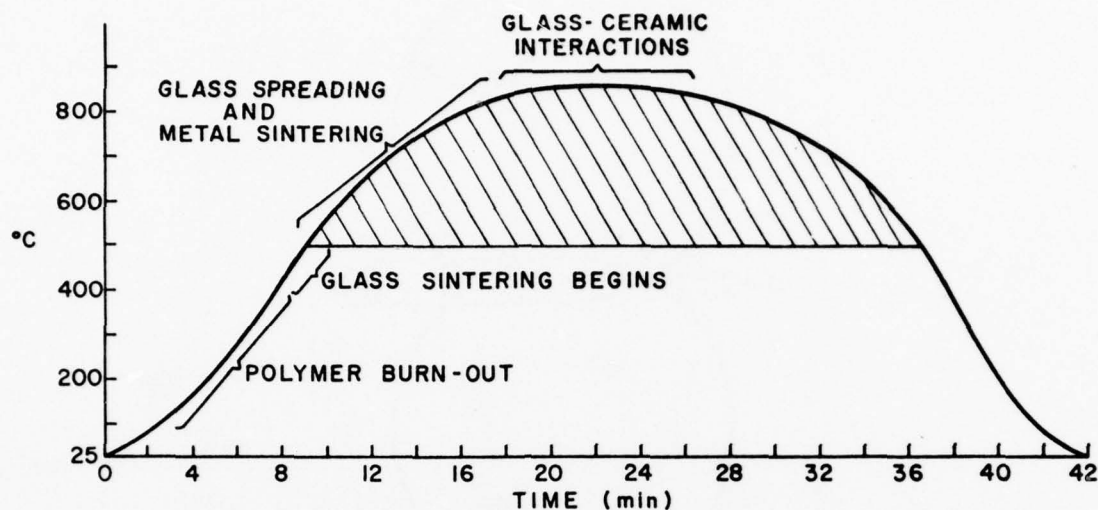
Figure 2. Typical metallization firing profile.

sintering of the metal constituents proceeds. The Drakenfeld E1527[*] glass
used in the model ink work of the contract series has a softening point of
485°C, i.e., the temperature at which the viscosity is $10^{7.6}$ P. Glass spread-
ing is not considered a major factor until the softening point is exceeded.
Above 500°C glass viscosity continues to decrease, and the presence of a fluid
glass requires consideration of the possibility of liquid-phase sintering.

All of the metals examined have shown some solubility in E1527 glass
[2,3][**]. Liquid-phase sintering has been reviewed by Eremenko [8], and Fig. 3
illustrates the three stages. The stages are (a) liquid flow or rearrange-
ment of particles to achieve maximum packing efficiency, (b) solution-
precipitation, in which portions of the solid phase are dissolved in the liquid
phase at areas of high chemical activity and are transported to areas of lower
activity where they precipitate, and (c) solid-state sintering in which pore
closure is completed by solid-state processes, e.g., diffusion by surface,
grain boundary, and bulk lattice paths.

---

*Drakenfeld Div., Hercules, Inc., Wilmington, DE.
**See Appendix C for additional determinations of gold solubility in E1527 glass.

8. V. N. Eremenko, et al., *Liquid-Phase Sintering*, Consultants Bureau, New
    York, 1970, p. 3.

8
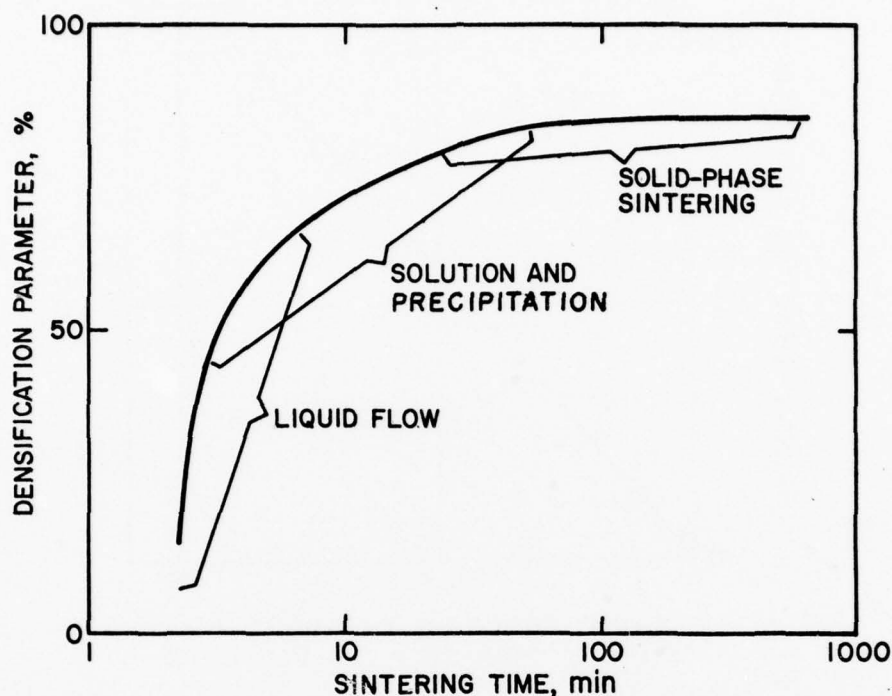
Figure 3. Densification during liquid-phase sintering.
After Huppmann [10].

The volume of pores initially present in a compacted powder, of course,
varies with particle shape and size distribution. For spherical particles,
Kingery's [9] calculations show that a minimum of 35 vol pct of liquid is
needed to fill the pores. Under these conditions, rearrangement processes
alone can account for complete densification (elimination of voids), as shown
in Fig. 4. If the liquid volume is less than 35 vol pct, other processes are
necessary to densify the compact. Eremenko's review [8] suggests that at least
5 vol pct of liquid is needed to facilitate solution-precipitation.

For systems where the solid is insoluble in the liquid phase, Huppmann
[10] has shown that the forces, F, governing particle approach, δ, are a

9. W. D. Kingery, "Densification During Sintering in the Presence of a
    Liquid Phase I Theory," J. Appl. Phys. 30, 301 (1959).
10. W. J. Huppmann, "Sintering in the Presence of Liquid Phase," in G. C.
    Kuczynski, ed., *Sintering and Catalysis* (Plenum Publishing Corp., New
    York, 1975), p. 359.
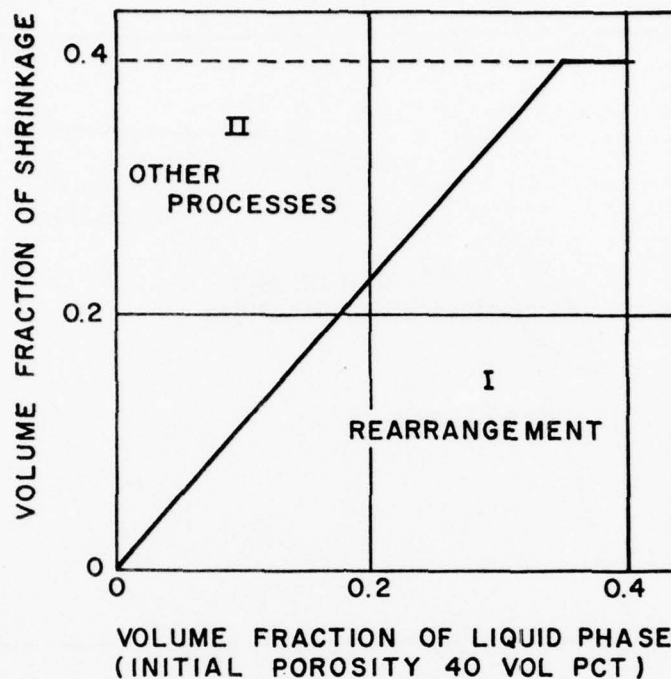
Figure 4.   Shrinkage via rearrangement and other processes vs
volume fraction of liquid phase. After Kingery [9].

function of the interfacial energy, γ, between vapor and liquid and the
capillary pressure, ΔP, as shown in Fig. 5 and expressed as

$$F = 2\pi\rho\gamma \cos \Phi - \pi\rho^2\Delta P \tag{7}$$

where r is the particle radius.

   Huppmann's calculations and observations show that for systems with good
wetting, i.e., $\theta \leq 8°$, a net attractive force increases with increasing volume
of the liquid phase. However, as the interparticle distance decreases below
5 μm, the net attractive force will become progressively greater with lower
volume fractions of the liquid.

   In our work on gold inks [1,2], advancing contact angle measurements of
E1527 on polycrystalline gold were 18.5, 10, and 9°, on heating for 10 min to
800, 875, and 950°C, respectively. The 875 and 950°C values are reasonably
close to the 8° angle observed by Huppmann. In addition, the volume fraction
of liquid observed by Huppmann was up to 10 vol pct. This value is approxi-
mately the same as that found in thick-film metallizations. Therefore, in the
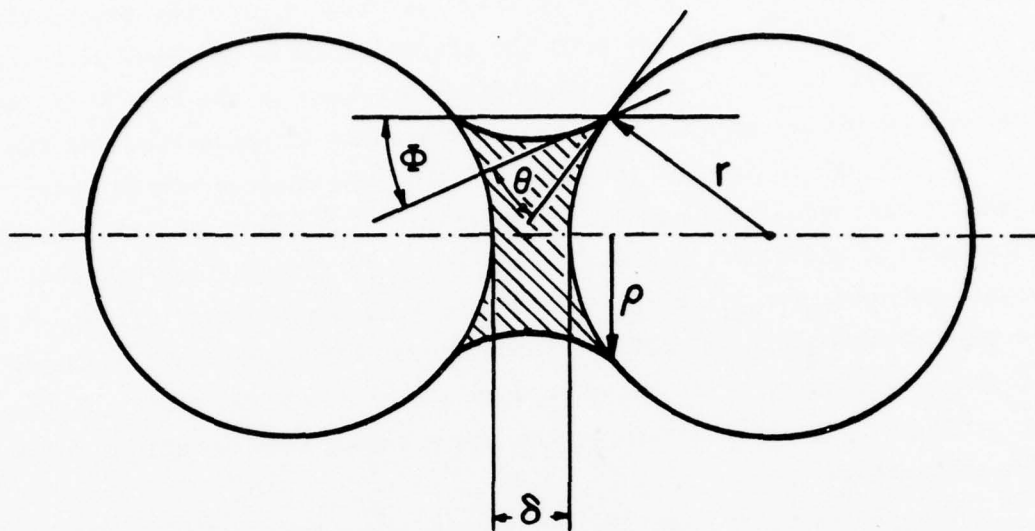
Figure 5. Liquid bridge between particles and resultant force.
After Huppmann [10].

event that the solution-precipitation stage of liquid-phase sintering is not
a major contributor to densification in thick-film metallization, the net
attractive forces prevalent during the rearrangement stage, as described by
Huppmann, may provide the greater contribution to densification.

The ability of the glass phase to enhance densification then depends
upon the degree to which the glass frit liquefies and spreads over adjacent
metal particles. However, while the glass is liquefying, contiguous metal
particles are sintering. The dual phenomena of glass spreading and metal
sintering are represented by the lined area in Fig. 2. For the glass spread
rate Vest [7] utilized a formula based on liquid penetration into small capil-
laries and slits [11]. This formula is

$$\frac{dL}{dt} = \frac{r \, \gamma_{LV} \, \cos \theta}{4 \eta L} \qquad (8)$$

where

L = distance

r = radius of particle

γ_{LV} = liquid-vapor interfacial energy

θ = contact angle between glass and solid

η = viscosity of the glass

11. S. Newman, "Kinetics of Wetting of Surfaces by Polymers; Capillary
Flow," J. Colloid Interface Sci. 26, 209 (1968).

11

Since the spread rate is proportional to the ratio γ_{LV}/η, the penetration between solid particles depends upon the change of these material properties with temperature. The ultimate microstructure then is the result of two simultaneously occurring phenomena. Thus, variations in microstructure can be achieved through changes in the heating rate, the maximum temperature, the time at peak temperature, and material properties. The critical material properties are metal and glass particle sizes and the γ_{LV}/η ratio vs temperature. The surface tension, i.e., interfacial energy, γ_{LV}, for the model glass, E1527, has been shown to have a positive temperature coefficient (see Appendix A) and glass viscosity, η, is known to have a negative temperature coefficient. The ratio, γ_{LV}/η, and, therefore, the glass spread rate should increase rapidly with temperature.

Early sintering studies [2,3] suggested that the powders used were inappropriate for definitive modeling of sintering phenomena. The fine-particle-sized MB-1 mixed-sphere and platelet gold powder sintered extremely rapidly, i.e., at 500°C before glass spreading could occur. Isothermal (900°C) shrinkage curves indicated that powder compact swelling occurred with glass present at extended firing times [2]. Since the times involved were greater than 5 min and most of the shrinkage had already occurred, the swelling was assumed to be in the terminal stage of sintering. The glass effectively retarded pore closure and contributed to expansion of these pores. The volatilization of PbO trapped in the glass may possibly account for this effect. Since the surface of the powder compact was essentially sealed by sintering at much lower temperatures during heating to 900°C, the subsurface glass, which began to volatilize PbO at 900°C, had no means of escape. This resulted in a pressure buildup in the remaining pores, which was relieved by expansion of the compact at 900°C. However, since the vapor pressure of PbO is only 1 mm of mercury at 943°C [12], this phenomenon may not be a significant contributor to the swelling.

Alternatively, the glass could have assisted in the entrapment of air that was present in the compact prior to sintering. When the compact was

---

12. *Handbook of Chemistry and Physics*, 48th ed., The Chemical Rubber Co., Cleveland, Ohio, 1967, p. D-115.

heated, the channels and pores, which were normally open to the surface, were blocked by molten glass. The trapped air created a pressure greater than that derived from the normal sintering forces, i.e., negative capillary pressure [9],

$$P\rho = \frac{-2\gamma_{LV}}{r_\rho} \tag{9}$$

where r_ρ = pore radius. This negative pore pressure increased as the pore size decreased, leading to a greater driving force for pore closure. However, if a sufficient quantity of a gas (e.g., air) that is insoluble in either the solid or liquid is present in the pore, the pressure buildup on heating may exceed the negative capillary pressure and cause pore expansion rather than contraction.

The sintering results with the second powder studied, MJ-2, which was all spherical and larger in particle size, tend to confirm the latter alternative. Swelling, after initial sintering, was observed when no glass was present [2]. In this case only trapped air or reducing agent, absorbed during powder precipitation, can account for the swelling. In both powders, the degree of compaction used in making the powder compact may actually contribute to sealing in air before sintering. Therefore, excessive pressure during compaction and before sintering may hinder ultimate densification.

When glass was added to MJ-2 powder and sintering carried out at 900°C, the shrinkage improved dramatically, in apparent agreement with liquid-phase sintering theory [9]. However, in order to develop a useful model for microstructure formation in thick-film metallization, more definitive experiments need to be conducted. By holding the glass composition and material properties constant and by varying metal powder morphology, one can clarify the role, if any, of liquid-phase sintering in thick-film metallization. This may be accomplished by a series of isothermal sintering studies, at temperatures that encompass those experienced in a normal firing process, e.g., those below, at, and above the temperature where glass spreading and metal sintering begin, as shown in Fig. 2.

C. COMPARISON OF THE SINTERING KINETICS OF VARIOUS GOLD POWDERS

For the purposes of studying gold sintering behavior in the presence
and absence of glass, a new gold powder, designated MK-2 was prepared (see
Appendix D). Since the new powder was not precipitated with gas (SO_2)
or coated with anti-agglomerating agents, it represented a cleaner starting
material for kinetic studies.

The MK-2 powder was compacted in a 0.5-in. (12.5-mm) diameter tungsten
carbide die at 1900-lb (864 kg) force and heated for 2, 20, and 300 min at
900°C. Additional samples were prepared with MK-2 powder plus 10 vol pct of
E1527 frit and were fired under the same conditions as the pure metal compacts.
Figures 6 and 7 show the shrinkage vs time for the pure metal and the metal
plus 10 vol pct of glass, respectively. The newly precipitated powder, MK-2,
exhibits a shrinkage behavior similar to that of the commercially available
MJ-2 powder. If glass is not present, both the MJ-2 and MK-2 show rapid
initial sintering, followed immediately by swelling (Fig. 6). When glass is
added, both powders show considerable improvement in densification (Fig. 7).
In contrast, the fine-particle MB-1 gold densifies less with, than without,
the glass present.
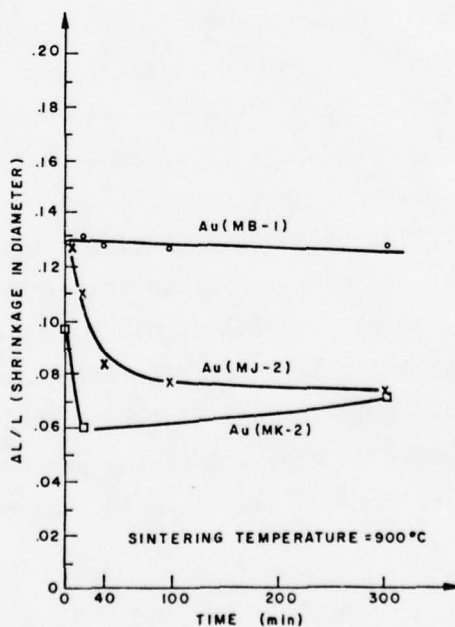
Figure 6. Shrinkage of gold powders at 900°C.
(Compaction force = 1900 lb (864 kg).

14
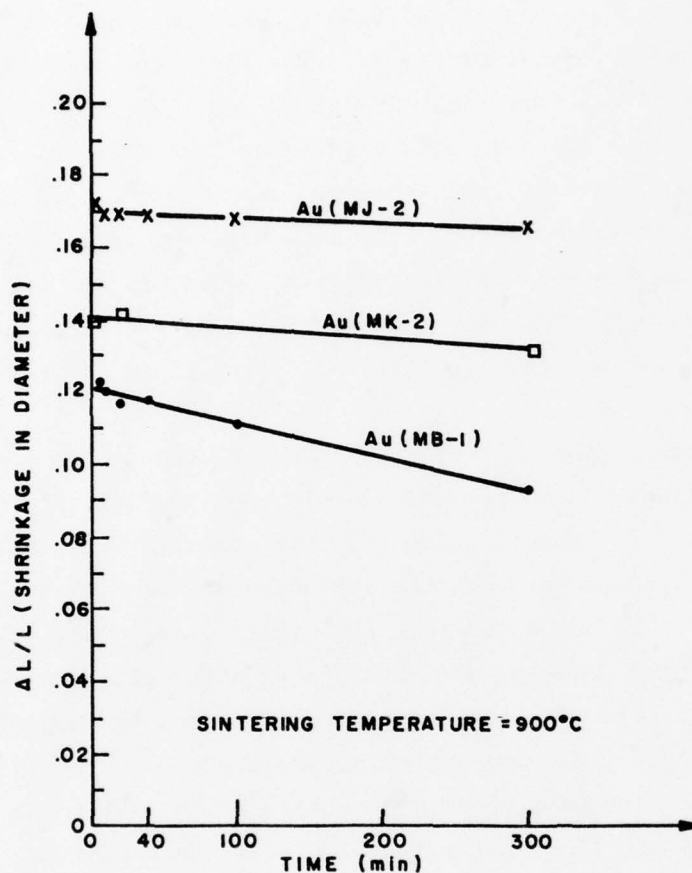
Figure 7. Shrinkage of gold powders plus 10 vol pct of
E1527 glass at 900°C.

If the metal particle size is large enough, liquid-phase-assisted re-
arrangement (first-stage sintering) appears to occur with the glass selected
for this study. This does not necessarily imply that solution-precipitation
(second stage) processes are involved.

D. MK-2 GOLD POWDER SINTERING IN THE PRESENCE AND ABSENCE OF E1527

By increasing the glass volume fraction from 10 to 50 vol pct, it was
anticipated that improvements in gold powder densification should result in
the first or rearrangement stage of sintering. A comparison of densification
results in the first and second stages can confirm the implication found in
Figs. 6 and 7.

15

To illustrate the influence of 10 to 50 vol pct of glass content and temperature on metal densification, 0.5-in. (12.7-mm)-diameter powder compacts pressed at 475 lb (215 kg)[*], and weighing 0.85 g, were heated at 500, 700, 800, and 900°C for 30 and 600 s, respectively. The plots for normalized densification[**], D_n, for 30 and 600 s, appearing in Figs. 8 and 9 show D_n is directly proportional to glass content for 700°C and higher temperatures. At 500°C, which is barely above the glass softening point, glass content does not change D_n in the first 30 s, as shown in Fig. 8, but has a negative effect on D_n for the 600-s samples shown in Fig. 9. Therefore, as a liquid, glass very definitely assists in the first or rearrangement stage of sintering. For temperatures below or slightly above the softening point, increasing glass content retards metal densification.

Theoretically, when $D_n = 100$, the powder compact has completely densified; thus the values above 100 are erroneously high in Figs. 8 and 9. A review of weight loss data in Table 3 indicates fair stability with only minor weight losses for most compacts, with the exception of the higher glass content samples fired at 900°C. It was noted that the higher glass content samples produced glass-encased gold pellets, and that the encasing glass had wet the wire sample support. When the samples were pulled from the supporting wires, ridges were exposed where glass had formed around the wire. The ridges caused errors in compact thickness measurement, and these are probably the major cause for the D_n values which are greater than 100. It was noted that some oxides were transferred to and from the sample pellet and the wire.

When D_n is compared for samples containing no glass and 10 vol pct of glass, for times of 30 to 2400 s, D_n is invariably greater for the glass-bearing samples, as shown in Fig. 10 for 700, 800, and 900°C firings. While linear plots are used for the sake of clarity, it is recognized that the coefficient of determination, r^2, values are low, indicating a poor fit to a

---

[*]See Appendix E for reasons leading to use of lower compaction force.

[**]$D_n = \left(\dfrac{D_f - D_i}{D_t - D_i} \right) \times 100$, where D_f = final density; D_i = initial density; D_t = theoretical density.

See Appendix F for discussion of the use of D_n as well as glass-gold uniformity in powder compacts.
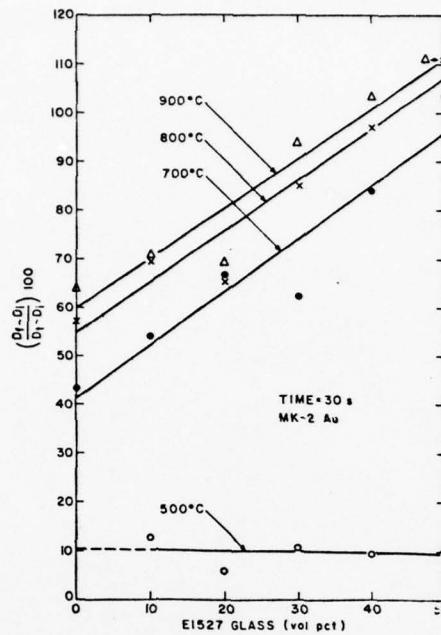
Figure 8. Normalized densification at 30 s vs temperature and glass content.
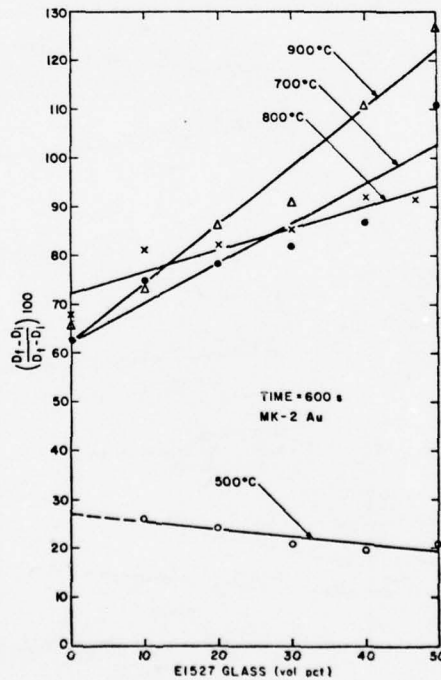
Figure 9. Normalized densification at 600 s vs temperature and glass content.

17

TABLE 3. PERCENT WEIGHT LOSS OF POWDER COMPACTS

Time (s)	Glass (vol pct)	Temperature (°C) 500	700	800	900
30	0	0.04	0.05	0.06	0.08
	10	0.02	0.03	0.03	0.06
	20	0.01	0.03	0.03	0.03
	30	0.01	0.03	0.02	0.01
	40	0.02	0.04	0.02	0.02
	50	0.03	0.04	0.03	0.06
600	0	0.06	0.06	0.06	0.05
	10	0.00	0.04	0.05	0.06
	20	0.02	0.03	0.04	0.06
	30	0.01	0.03	0.03	0.13
	40	0.03	0.02	0.05	0.32
	50	0.03	0.04	0.09	0.49
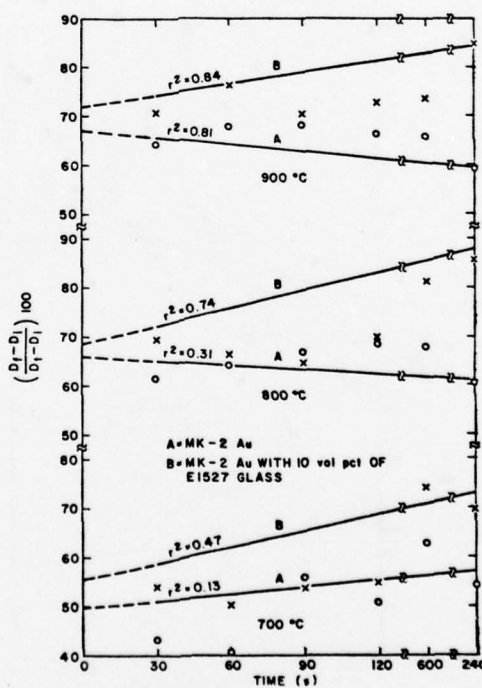
Figure 10. Normalized densification at 10 vol pct of glass vs temperature and time.

18

straight line. This effect is not unexpected since the measured time interval covers the three stages of sintering and densification rates which vary significantly in each stage. Notice, also in Fig. 10, that the glass-free gold compacts exhibit the familiar swelling problem associated with compact sintering, despite the use of the lower compaction force of 475 lb (215 kg). In a screen-printed thick-film metallization, compaction, if any, is due to gravity and surface tension forces. Therefore, it is unlikely that swelling would be prevalent in screened and fired deposits. Furthermore, air bubble escape rate in molten glass is treated in Appendix G.

E. ACTIVATION ENERGIES FOR THE SINTERING OF GOLD IN THE PRESENCE AND ABSENCE OF GLASS

The powder compact diametral changes as a function of time, $t^{0.31}$, (t = 30, 60, 90, 120, 600, and 2400 s) and for sintering temperatures of 700, 800, and 900°C are plotted in Figs. 11 and 12 and tabulated in Tables 4 and 5 for the glass-free and 10 vol pct glass-bearing samples, respectively. In addition, in Tables 4 and 5, the percent of theoretical density, D_t, change in actual density D_a, and normalized density, D_n, are also tabulated.
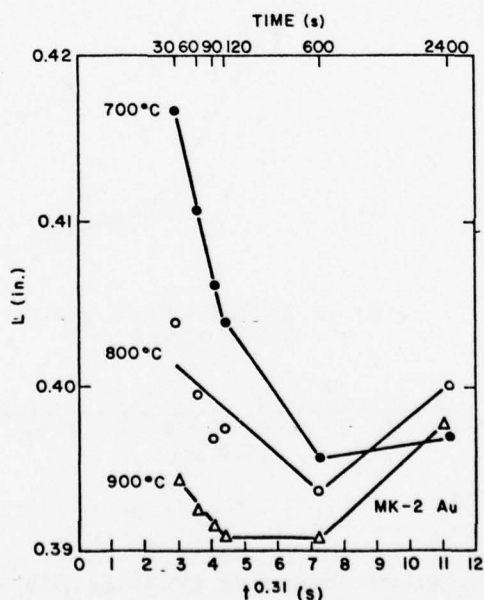
Figure 11. Diametral change vs $t^{0.31}$ at 700, 800, and 900°C for glass-free MK-2 Au.

19
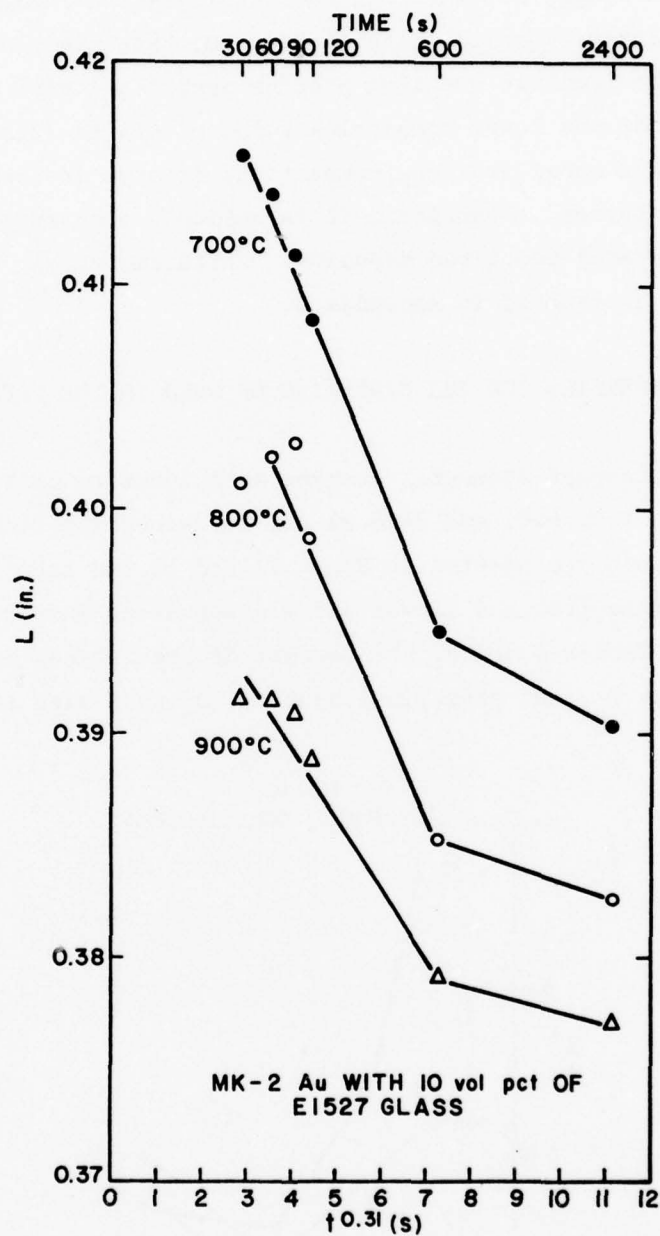
Figure 12. Diametral change vs $t^{0.31}$ at 700, 800, and 900°C for MK-2 Au with 10 vol pct of E1527 glass.

20

TABLE 4. DIAMETRAL AND DENSITY CHANGES OF MK-2 Au

Temp. (°C)	Time (s)	As-Pressed, 475 lb		Sintered			
		Diameter, L (in.)	D_t (1)	Diameter L (in.)	D_t (1)	D_n (2)	D_a (3)
700	30	0.50075	41.1	0.41607	66.6	43.3	62.2
	60	0.50070	41.4	0.40853	65.1	40.5	57.3
	90	0.50010	41.3	0.40537	74.0	55.7	79.2
	120	0.50011	41.6	0.40423	71.3	50.8	71.3
	600	0.50048	41.1	0.39576	78.0	62.7	90.0
	2400	0.50011	43.6	0.40683	74.2	54.3	70.3
800	30	0.50028	40.9	0.40329	77.3	61.6	89.7
	60	0.50020	42.5	0.39871	79.2	69.2	86.7
	90	0.50050	42.5	0.39655	80.9	66.8	90.5
	120	0.50025	43.2	0.39636	82.0	68.3	89.7
	600	0.50010	42.7	0.39367	81.6	67.9	91.3
	2400	0.50018	41.9	0.40010	76.9	60.2	83.3
900	30	0.50031	41.6	0.39421	76.4	64.2	90.1
	60	0.50046	41.6	0.39242	79.6	67.6	94.9
	90	0.50021	41.7	0.39162	76.1	68.2	95.5
	120	0.50028	41.3	0.39097	77.6	66.1	94.0
	600	0.50021	41.2	0.39088	78.0	65.6	93.6
	2400	0.50022	41.5	0.39777	84.0	59.0	83.2

(1) D_t (%) = $\dfrac{\text{observed density}}{\text{theoretical density}}$ x 100

(2) D_n (%) = $\left(\dfrac{D_f - D_i}{D_t - D_i}\right)$ x 100, where D_f = final density, D_i = initial density

(3) D_a (%) = $(D_f - D_i)/D_i$ x 100

TABLE 5.   DIAMETRAL AND DENSITY CHANGES OF MK-2 Au
WITH 10 vol pct of E1527 GLASS

Temp. (°C)	Time (s)	Diameter L(in.)	D_t (1)	Diameter L(in.)	D_t (1)	D_n (2)	D_a (3)
700	30	0.50088	43.7	0.41577	74.1	54.0	69.4
	60	0.50052	43.2	0.41398	71.7	50.2	65.9
	90	0.50069	43.1	0.41133	73.6	53.7	70.8
	120	0.50041	42.8	0.40833	74.0	54.6	73.1
	600	0.50068	42.7	0.39449	85.2	74.2	99.5
	2400	0.50061	42.4	0.39033	82.5	69.6	94.4
800	30	0.50063	43.5	0.40076	82.8	69.6	90.3
	60	0.50050	42.7	0.40060	80.8	66.4	89.5
	90	0.50078	41.9	0.40063	79.5	64.7	90.1
	120	0.50064	42.2	0.39658	82.4	69.5	95.2
	600	0.50069	42.2	0.38529	89.1	81.2	111.3
	2400	0.50070	42.8	0.38264	91.8	85.7	114.6
900	30	0.50053	41.4	0.39154	82.9	70.8	100.1
	60	0.50041	42.8	0.39142	86.4	76.2	102.0
	90	0.50068	41.5	0.39085	82.7	70.4	99.3
	120	0.50055	42.3	0.38876	84.3	72.7	99.3
	600	0.50037	42.1	0.37914	84.7	73.5	101.1
	2400	0.50051	41.6	0.37708	91.2	85.0	119.3

(1) D_t (%) = $\dfrac{\text{observed density}}{\text{theoretical density}}$ x 100

(2) D_n (%) = $\left(\dfrac{D_f - D_i}{D_t - D_i}\right)$ x 100, where D_f = final density, D_i = initial density

(3) D_a (%) = $(D_f - D_i)/D_i$ x 100

22

Following the work of Johnson and Cutler [13,14], the fractional shrinkage, $\Delta L/L_o$, varies according to

$$\frac{\Delta L}{L_o} = \left(\frac{K'D_B}{T}\right)^m t^m \tag{10}$$

where K' = constant

D_B grain boundary diffusion coefficient

T = absolute temperature

t = time.

The value of m for grain boundary diffusion controlled sintering is 0.31. Other values range from 0.25 to 0.50 depending upon which particular diffusion path is invoked. To eliminate the effect of shrinkage errors, ΔL can be replaced by $L_o - L$ in Eq. (10) and expressed as [13,14]

$$L = (L_o - \delta L) \left[1 - \left(\frac{K'D_B}{T}\right)^m t^m\right] \tag{11}$$

where δL is a correction for thermal expansion.

Because the powder compacts were heated for given periods of time, cooled, and then measured in a manner similar to Cole [15], the correction for thermal expansion is no longer required and Eq. (11) can be written:

$$L = L' - L'\left(\frac{K'D_B}{T}\right)^m t^m \tag{12}$$

where $L' = L_o - \delta L$. \tag{13}

Similarly, errors in time measurement are reduced, since sintering time was begun only when the compact reached the sintering temperature of interest.

13.   D. L. Johnson and I. B. Cutler, "Diffusion Sintering: I, Initial Stage Sintering Models and Their Application to Shrinkage of Powder Compacts," J. Am. Ceram. Soc. 46, 541 (1963).
14.   D. L. Johnson and I. B. Cutler, "Diffusion Sintering: Initial Sintering Kinetics of Alumina," J. Am. Ceram. Soc. 46, 545 (1963).
15.   S. S. Cole, "Sintering of Ag-Pd in the Presence of a Reactive Glass," J. Am. Ceram. Soc. 55, 296 (1972).

Equation (12) fits the straight line form, if L is plotted vs t^m. Log $K'D_B$ can then be extracted from the slope and plotted against $1/T$ to determine the activation energy for each stage of sintering. We have arbitrarily set $t = 30$ s as the limit to the first stage of sintering and found the activation energy for glass-free gold to be 7.3 to 12.4 kcal/mole as shown for various values of t^m in Table 6. These values are sufficiently close to 15 kcal/mole recently reported by Nordstrum [16] to suggest that the first stage of sintering is completed in about 30 s. With regard to the second stage, scatter in the 800°C data and the onset of compact swelling at higher temperature and longer time caused us to examine both 120 and 600 s limits. The most credible activation energy value for the glass-free compact sintering is 42.4 kcal/mole where $t^{0.31}$ is used. This value is in very good agreement with the 41.7 kcal/mole reported by Makin, et al. [17]. The corresponding first-stage activation energy is 10.4 kcal/mole, slightly lower than Nordstrum's observation [16]. The third-stage activation energies are not reported for the glass-free compacts because of the presence of swelling in this time regime.

Second-stage sintering in the presence of glass produces the best fit if values of t for 30 to 600 s are used as shown in Table 6. Values for activation energy range from 7.4 to 17.1 kcal/mole. The third-stage values for activation energy appear to be higher in the glass-bearing samples, but these values must be suspect because of the general propensity for swelling at extended sintering time.

If $K'D_B/T$ is replaced by K_o in Eq. (12), the respective slopes of the glass-free and glass-bearing compacts can be compared at constant temperature. Solution-precipitation controlled sintering can be considered to be operating if K_o-(glass-free) $< K_o$-(glass-bearing) in Stage II. From Table 7 it can be seen that a progressive decrease in the ratio K_o-(glass-free)/K_o-(glass-bearing) occurs with increasing temperature. It thus appears that the contribution to sintering by the solution-precipitation process predominates at high temperatures, while grain-boundary diffusion prevails at lower temperatures. The

16. T. V. Nordstrum, "Sintering Kinetics of Reactively Bonded Thick-Film Gold," presented at Fall Meeting, Am. Ceram. Soc. Electron. Div., Sept. 18-21, 1977, Montreal, Quebec, Canada.

17. S. M. Makin, et al., "Self-Diffusion in Gold," Proc. Phys. Soc. 70B, 545 (1957).

24

TABLE 6. SUMMARY OF ACTIVATION ENERGIES

Glass (vol pct)	Stage	Time (s)	700°C	$t^{0.31}$ r^{2*} 800°C	900°C	Q (kcal/mole)	r^{2*}
0	I	0–30	1.0	1.0	1.0	10.4	0.998
	II	30–120	0.952	0.930	0.987	42.4	0.960
	II	30–600	0.884	0.718	0.543	65.1	0.977
	III	600–2400	–	–	–	–	–
10	I	0.–30	1.0	1.0	1.0	11.2	0.992
	II	30–120	0.940	0.511	0.682	34.9	0.960
	II	30–600	0.993	0.943	0.957	13.4	0.999
	III	600–2400	1.0	1.0	1.0	21.9	0.985
				$t^{0.33}$			
0	I	0–30	1.0	1.0	1.0	9.9	0.998
	II	30–120	0.950	0.928	0.986	39.7	0.960
	II	30–600	0.879	0.711	0.535	61.2	0.978
	III	600–2400	–	–	–	–	–
10	I	0–30	1.0	1.0	1.0	10.7	0.993
	II	30–120	0.942	0.514	0.685	32.6	0.960
	II	30–600	0.993	0.946	0.960	12.4	0.999
	III	600–2400	1.0	1.0	1.0	20.5	0.985
				$t^{0.25}$			
0	I	0–30	1.0	1.0	1.0	12.4	0.998
	II	30–120	0.957	0.936	0.989	52.6	0.959
	II	30–600	0.900	0.740	0.568	80.1	0.977
	III	600–2400	–	–	–	–	–

$*r^2$ = coefficient of determination

25

TABLE 6. SUMMARY OF ACTIVATION ENERGIES (continued)

Glass (vol pct)	Stage	Time (s)	700°C	$t^{0.25}$ 800°C	900°C	Q (kcal/mole)	r^{2*}
10	I	0–30	1.0	1.0	1.0	13.4	0.992
	II	30–120	0.934	0.501	0.671	43.7	0.960
	II	30–600	0.991	0.934	0.948	17.1	0.999
	III	600–2400	1.0	1.0	1.0	27.6	0.986
				$t^{0.5}$			
0	I	0–30	1.0	1.0	1.0	7.3	0.999
	II	30–120	0.934	0.909	0.977	25.8	0.960
	II	30–600	0.836	0.653	0.471	40.9	0.978
	III	600–2400	–	–	–	–	–
10	I	0–30	1.0	1.0	1.0	7.8	0.994
	II	30–120	0.957	0.542	0.714	20.7	0.962
	II	30–600	0.992	0.962	0.978	7.4	0.999
	III	600–2400	1.0	1.0	1.0	12.9	0.982

$*r^2$ = coefficient of determination

TABLE 7. SUMMARY OF SINTERING KINETICS OF POWDER COMPACTS

Temp. (°C)	Glass (vol pct)	$L'(K_o)^{0.31}$	L (in.)	$K_o \times 10^8$	$\dfrac{K_o \text{ (glass-free)}}{K_o \text{ (glass-bearing)}}$
700	0*	−0.00783	0.43766	230.74	4.04
	10**	−0.00500	0.43093	57.16	
800	0*	−0.00468	0.41612	51.50	1.87
	10**	−0.00383	0.41374	27.60	
900	0*	−0.00209	0.40009	4.38	0.30
	10**	−0.00305	0.40186	14.56	
700	0**	−0.00410	0.42414	31.64	0.55
	10**	−0.00500	0.43093	57.16	
800	0**	−0.00180	0.40571	2.59	0.09
	10**	−0.00383	0.41374	27.60	
900	0**	−0.00060	0.39467	0.08	0.01
	10**	−0.00305	0.40186	14.56	

*Data from t = 30, 60, 90, 120 s
**Data from t = 30, 60, 90, 120, 600 s

increasing solubility of gold in E1527 glass at higher temperatures, as noted in Appendix C, corroborates this finding.

F. ELECTRICAL RESISTIVITY OF SINTERED GOLD FILMS AS A FUNCTION OF GLASS CONTENT, TEMPERATURE, AND TIME

In order to confirm that glass enhances gold powder densification in a gold film on a ceramic substrate, gold inks were prepared which had a solids content of 82 wt pct. Prior to blending the MK-2 gold powder, E1527 glass frit and organic vehicle[*], the gold powder was coated with a suitable surface active agent[**] to eliminate "cold welding" and particle agglomeration.

---

[*]Partilok "C" obtained by special arrangement from Thick Film Systems, Inc. Santa Barbara, CA.
[**]Dow Corning Z-5456 Silane, Dow Corning Corp. Midland, MI.

27

Emission spectroscopic analysis showed that cation impurities in the coated powder remained at the trace level and therefore could not materially alter the sintering kinetics. A surface active agent on the gold powder is needed to ensure adequate dispersion in the organic vehicle.

An ink, containing a gold-glass solids ratio of 9, was used to screen print terminal electrodes on 25.4-mm x 25.4-mm x 0.64-mm (1-in x 1-in x 0.025-in.) - square 96 wt pct - alumina substrates[+]. These electrodes were fired at 900°C for two minutes. A second pattern, designed to overlap the electrodes, consisted of a 0.38-mm (0.015-in.)-wide serpentine line containing 1874 squares. Both electrode and serpentine line patterns utilized a 325-mesh screen with a 0.03-mm (0.001-in.) emulsion buildup. Four gold inks were formulated so that the fired films contained 0, 10, 20 and 30 vol pct of E1527 glass. Sufficient samples of the inks were screen printed on the pre-fired electrodes and subsequently fired at 700, 800 and 900°C for 30, 60, 90, 120, 600, 2400, 10,000 and 30,000 s, respectively. Electrical resistance measurements were taken with a four-wire (Kelvin) connection and the resistivity computed after microscopically measuring line thickness and width. The electrical resistivity-temperature-time graphs for the 0, 10, 20 and 30 vol pct of glass inks are presented in Figs. 13, 14, 15, and 16, respectively. Since the cross-sectional areas are presumed to be rectangular, when in fact, they are more nearly bell-shaped, the electrical resistivities presented in the figures are apparent values. The actual resistivities are estimated to be about 20 to 30% less than the plotted resistivities.

From a comparison of Figs. 13 and 14, it is obvious that the addition of 10 vol pct of glass causes a dramatic and quick reduction in electrical resistivity, confirming the influence of liquid-phase assisted sintering. Greater additions of glass, e.g., 20 and 30 vol pct, as shown in Figs. 15 and 16, respectively, cause further reduction in the resistivity. However, the reduction is not linear. Most of the improvement occurs in the first (rearrangement) stage of sintering, i.e., within about the first 30 s. After 600 s, all glass concentrations produce about the same reduction in electrical resistivity. As expected, at a given time, higher temperatures produce greater

---

+AlSi Mag 614, American Lava Corp., Chattanooga, TN.
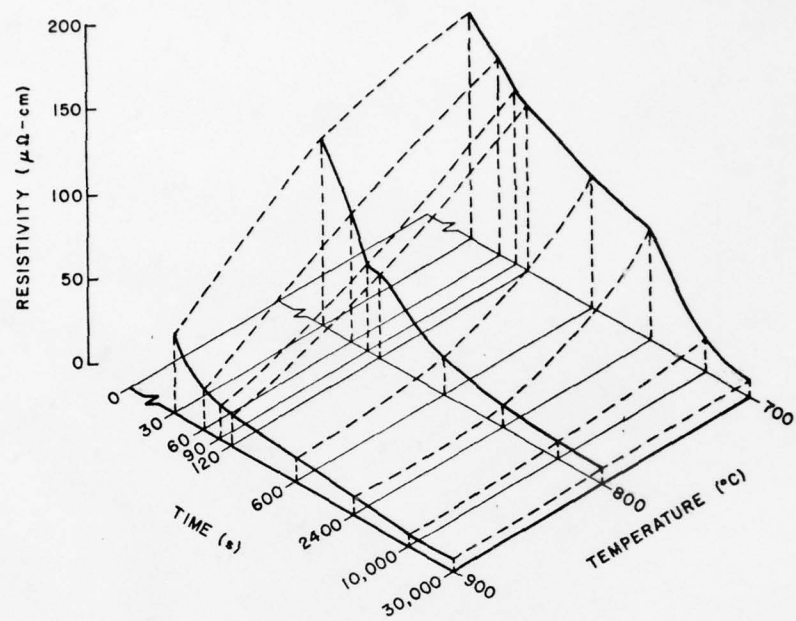
Figure 13. Resistivity-temperature-time graph for MK-2 Au.
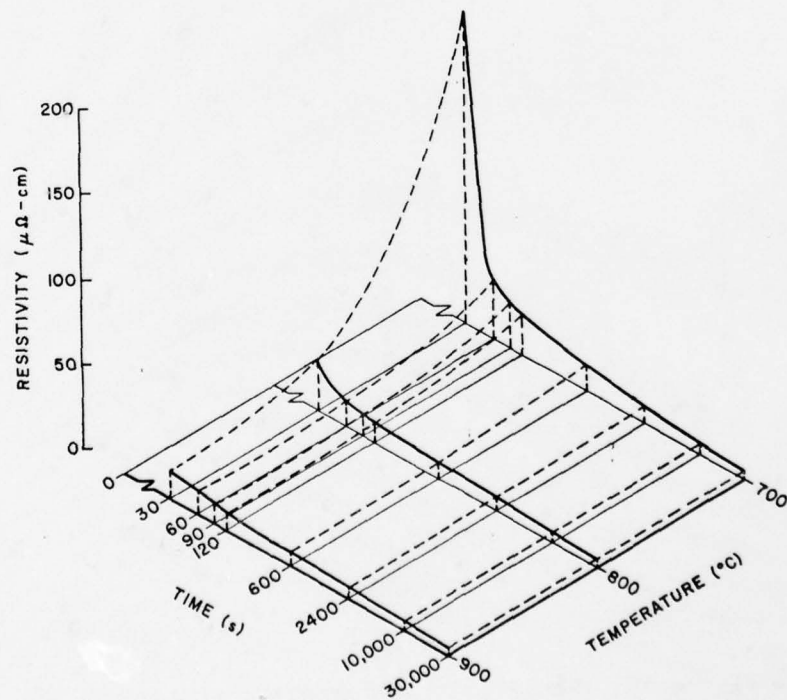
Figure 14. Resistivity-temperature-time graph for MK-2 Au + 10 vol pct
of E1527 glass.

29
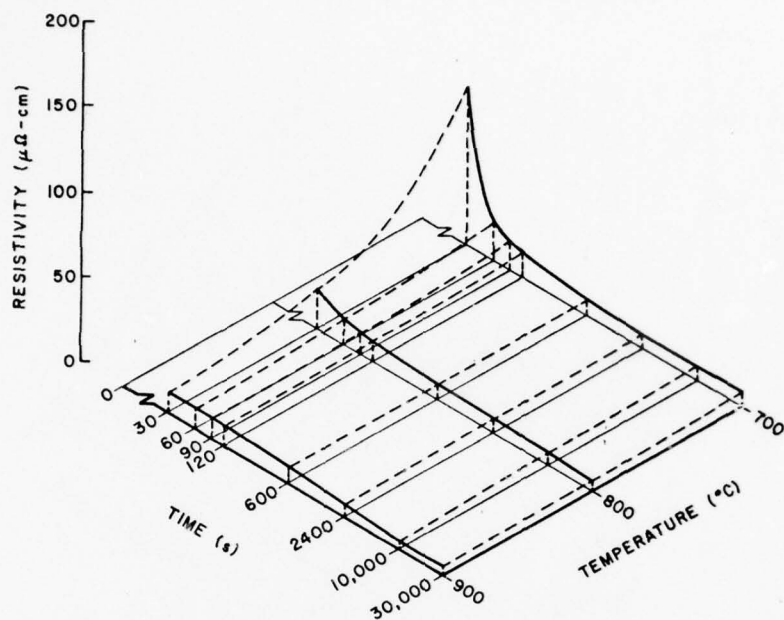
Figure 15.   Resistivity-temperature-time graph for
MK-2 Au + 20 vol pct of E1527 glass.
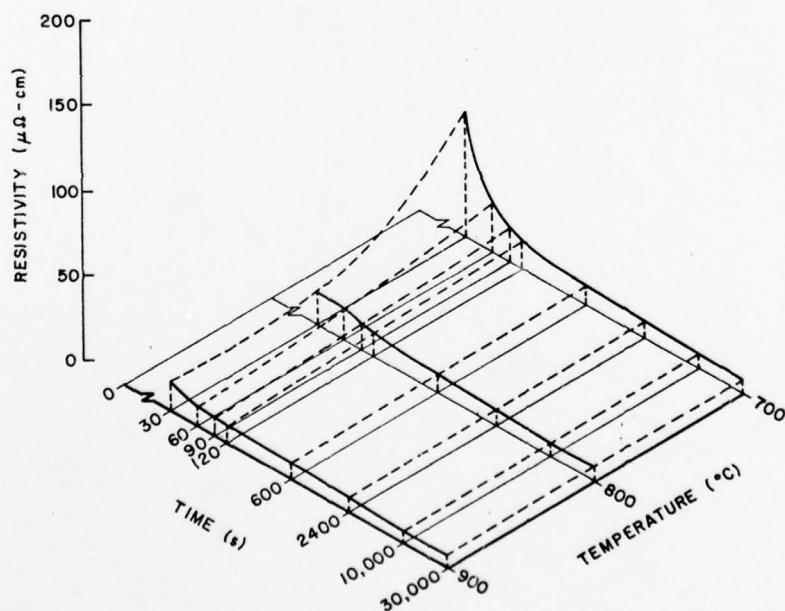
Figure 16.   Resistivity-temperature-time graph for
MK-2 Au + 30 vol pct of E1527 glass.

reduction in resistivity. At 900°C and 30 s, the reduction attributed to glass additions is still evident but much less significant than that at 700 and 800°C.

In practical terms little reduction in resitivity is gained by extending firing time. For example, for the 900°C-firing, resistivity of a gold – 10 vol pct of glass film can be reduced only about 60% by increasing the firing time from 600 to 30,000 s, i.e,. by a factor of 50.

G. MICROSTRUCTURAL COARSENING OF SINTERED GOLD FILMS

In Figs. 17 and 18, transmitted light photomicrographs illustrate the degree of porosity for the gold films fired at 900°C for 30 and 30,000 s, respectively. In the case of the pure gold film only slight porosity is seen after 30 s at 900°C (Fig. 17). However, after 30,000 s (Fig. 18), considerable porosity is present and is the result of continued neck growth and coalescence between contiguous gold particles. Furthermore, the porosity increases with glass volume fraction and time as the gold surface area to volume ratio rapidly decreases.

The greater porosity, observable in the glass-bearing gold films, results basically from the increased solubility of the smaller gold particles in the liquid glass. From the Kelvin equation [18]

$$\frac{\ln p}{P_o} = \frac{2 \, V_m}{RTr} \tag{14}$$

where p = vapor pressure over curved surface of particle

p_o = vapor pressure over flat surface of particle

V_m = molar volume

r = particle radius

Since activity, a, can be substituted for pressure, particle solubility increases with decreasing particle size. A concentration gradient of dissolved gold in glass is established between large and small gold particles. This gradient results in the transfer of material from the smaller to the larger

---

18. W. J. Moore, *Physical Chemistry* (Prentice-Hall, Englewood Cliffs, NJ, 1962) 3rd ed., p. 734.
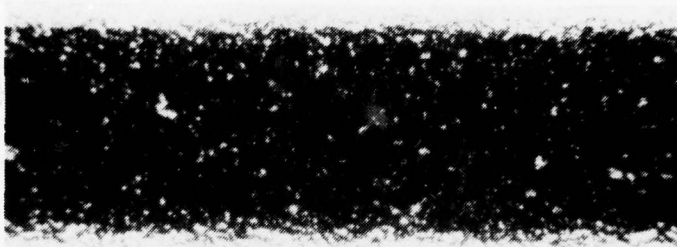
31

(a) MK-2 Au

(b) MK-2 Au + 10 vol pct of E1527 glass

(c) MK-2 Au + 20 vol pct of E1527 glass
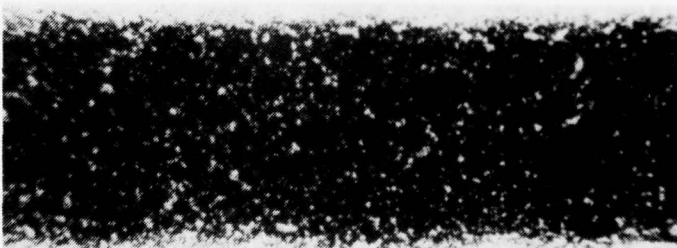
(d) MK-2 Au + 30 vol pct of E1527 glass

Figure 17. MK-2 gold films fired at 900°C for 30 s (Mag. 100X).
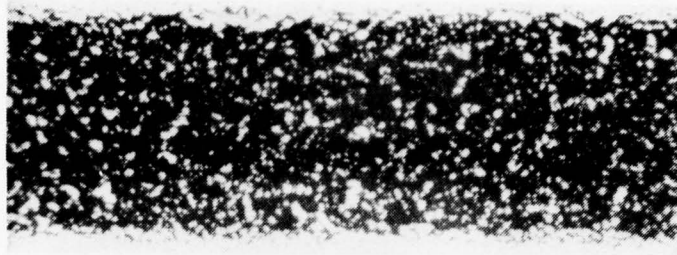
(a) MK-2 Au
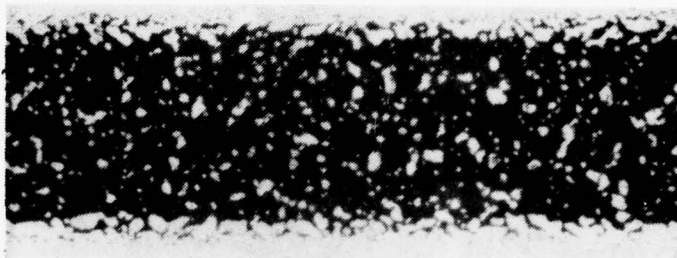
(b) MK-2 Au + 10 vol pct of E1527 glass
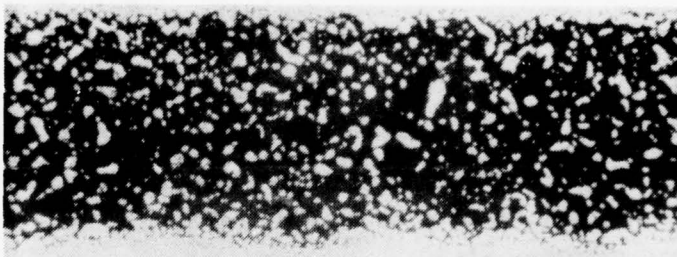
(c) MK-2 Au + 20 vol pct of E1527 glass
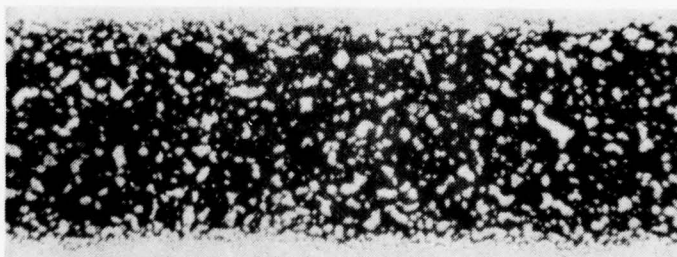
(d) MK-2 Au + 30 vol pct of E1527 glass

Figure 18. MK-2 gold films fired at 900°C for 30,000 s (Mag. 100X).

33

particles. Commonly known as Ostwald ripening, the phenomenon has been found in metal [19], ceramic [20] and glass [7] systems and to some extent quantified, i.e., rate law equations have been proposed which follow the generic form [21]

$$\bar{r}(t)^n - \bar{r}(0)^n = kt \tag{15}$$

where $\bar{r}(t)$ = average particle size at time t
$\bar{r}(0)$ = average particle size at time zero
t = time
n = rate limiting constant

If the diffusion of atoms between the particles is the slowest step in material transfer, $n = 3$ in Eq. (15); if solution and/or precipitation is the slowest step, $n = 2$. In both cases, particle growth is proportional to surface tension, γ_{SL} and molar volume of the solid phase.

H. DISCUSSION

From the foregoing comparison of gold powder sintering in the presence and absence of glass, it is clear that glass dramatically influences metal densification rates. A liquid glass phase accelerates densification during the re-arrangement stage of sintering and this favorably decreases the total processing time necessary to provide an electrically conductive and useful film. If the sintering temperature is high enough, e.g., 900°C, sufficient gold is taken into solution by the glass to further densify the film. However, as shown in Figs. 17 and 18, an excessively high glass volume fraction or long sintering time can be deleterious to film densification. The combination of particle

19. G. H. S. Price, et al., "Sintered Alloys, Part I, Copper-Nickel-Tungsten Alloys Sintered with a Liquid Phase Present," J. Inst. Metals, 62, 39 (1938).
20. W. D. Kingery, H. K. Bowen, and D. R. Uhlmann, *Introduction to Ceramics,* 2nd ed. (John Wiley & Sons, Inc., New York, 1976), p. 425.
21. H. Fischmeister and G. Grimvall, "Ostwald Ripening – A Survey," in Ed. G. C. Kuczynski, *Sintering and Related Phenomena* (Plenum Publishing Corp., New York, (1973), p. 119.

coalescence by solid state processes and Ostwald ripening causes more porosity
to develop, not less. As a result of pore coarsening, the number of microscopic
pores per unit area will decrease. Since adequate film adhesion depends upon
a uniform distribution of microscopic pores, excessive pore coarsening can only
lead to a reduction in film adhesion strength.

In general, predicting the relative rates of neck growth, coalescence,
and Ostwald ripening, to model the ultimate microstructure development is
extremely difficult. However, recent work by Courtney [22,23,24] has shown
that some progress is being made in this area. From his work it is clear that
as the distribution in particle sizes increases, i.e., as $\sigma/\overline{r}^*$ increases,
Ostwald ripening increases and there is less chance for particles to come
into contact [23]. The result is a more "isolated" rather than "skeletal"
microstructure. Early models of Ostwald ripening, based on the precipitation
of solutes from supersaturated solutions [25], assumed independence from time
and the initial particle size distribution. A more recent treatment illustrates
that the average particle size achieved during ripening is heavily dependent
upon the initial particle size distribution [26].

Intuitively, there is a critical particle size above which Ostwald ripening
will be reduced to a negligible level in terms of normal thick-film firing tem-
peratures and times. A better understanding of the optimum particle size dis-
tribution and particle morphology is needed to improve film properties. To
enhance adhesion in gold films, some porosity in the microstructure is neces-
sary. Excessive porosity, or pore coarsening, resulting from the combined
effects of coalescence and Ostwald ripening, degrades not only film adhesion
but also film surface quality and subsequent wire bond reliability.

22. T. H. Courtney, "A Reanalysis of the Kinetics of Neck Growth During
    Liquid Phase Sintering," Met. Trans. A 8A, 671 (May 1977).
23. T. H. Courtney, "Microstructural Evolution During Liquid Phase Sintering:
    Part I, Development of Microstructure," Met. Trans. A 8A, 679 (May 1977).
24. T. H. Courtney, "Microstructural Evolution During Liquid Phase Sintering:
    Part II, Microstructural Coarsening," Met. Trans. A, 8A, 685 (May 1977).
25. J. M. Lifshitz and V. V. Slyozov, "The Kinetics of Precipitation from
    Supersaturated Solid Solutions," J. Phys. Chem. Solids 19, 35 (1961).
26. D. B. Dadyburjor and E. Ruckenstein, "Kinetics of Ostwald Ripening,"
    J. Cryst. Growth 40, 279 (1977).

$*\sigma/\overline{r}$ = standard deviation $\div$ mean particle size.

I. CONCLUSIONS

It has been shown that gold powder sintering in the presence of as little as 10 vol pct of an appropriate glass results in the initial acceleration of film densification. Furthermore, from the determination and comparison of activation energies for the sintering processes, it was shown that the solution-precipitation process is certainly active at the highest firing temperatures studied, i.e., 900°C.

From evaluations of electrical resistivity of the fired gold films, containing variable amounts of glass, it is evident that prolonged firing does not increase electrical conductivity proportionately with firing time. Indeed prolonged firing time, excess glass, and excessive numbers of smaller metal particles cause normal solid-state and ripening processes to produce pore coarsening. Since pore coarsening implies a reduced number of micro-scopic pores, which are normally required to form a micromechanical interlock with the sintered metal film, adhesion strength must decrease. In addition, a film with pore coarsening does not represent the ideal bonding surface, which is free from pores, surface glass, and irregularities.

SECTION III

REACTIVELY BONDED AND MIXED-BONDED FILMS

A. INTRODUCTION

1. General

The investigation of adhesion strength development in inks containing
copper in their binder phase has been concentrated throughout the contract
series on identifying the character of the materials at the metal-ceramic in-
terface. It was anticipated that by identifying the interfacial structure,
the mechanism would be elucidated by which the adhesion strength of noble
metals to the alumina phase is improved over that of frit-bonded inks.

In the earlier contract studies [1-3] three techniques were used to study
these materials: low-angle electron diffraction, Auger electron spectrometry,
and SEM. All were performed on surfaces which had been mercury-vapor-leached
and vacuum-baked. No crystallinity was detected by means of low-angle elec-
tron diffraction on samples of two mixed-bonded and one reactively bonded
gold inks. Auger spectrometry was successful in determining the concentra-
tions of binder phase elements in the binder layers, in making a first-order
correlation of the adhesion with copper concentration, and in profiling the
binder element concentrations versus depth. Results obtained with SEM in-
dicated that no appreciable part of the adhesion strength of these materials
could be attributed to a physical interlocking of the metal and the binder
phases. SEM also made it possible to observe the formation of a crystalline
phase (or phases) in the interface between the metal phase and the alumina
substrate. In the 1977 contract study more detailed investigations were under-
taken to identify the crystalline phases at the interface and to study the
kinetics of their formation. About one third of the way through the contract
we became aware of a study [27] that was so pertinent to the field of mixed-
bonded and reactively bonded thick-film conductor adhesion that it required

---

27. R. J. Lisauskas, "Characterization of the Reaction between Thick-Film
     Reactive-Bonded Gold Pastes and Alumina Substrates," Master's Thesis,
     Massachusetts Institute of Technology, June 1976.

37

a reconsideration of some of our planned experiments. Because the work is not generally available we have prepared a synopsis of the work and presented it as Appendix H.

2. A Critique of Lisauskas's Thesis

Lisauskas clearly proved that CdO and CuO can react with 96 wt pct Al_2O_3 substrate surfaces to form spinels(s) by one or more thermally activated mechanisms. It is also clear from his work that in reactively bonded ink films, the adhesion strength increases along with the amount of spinel for firings of increasing temperature. On the other hand, we believe that Lisauskas's contention that the gold film in reactively bonded inks adheres principally to a metal oxide layer which in turn adheres to the spinel has not been proven satisfactorily. In earlier work we had found, but had not identified, a layer which appeared loosely adherent by SEMography of specimens after mercury-vapor leaching on more poorly adherent firings of reactively bonded films. Compare Ref. [1], Fig. 23, and Ref. [27], Fig. 15.

Mercury-vapor leaching should not attack cadmium or copper oxides (although it could lift them free of the substrate if the mercury condensed rapidly under the metal oxide layer). Thus mercury-vapor leaching, used with the low mercury-vapor flux rates we have normally employed should reveal approximately the same structures as Lisauskas's $KI-I_2$ etch. When strongly adherent, reactively bonded thick films have been mercury-vapor leached at RCA, structures that we and Lisauskas regard as spinels have been revealed, but no metal oxide films are usually seen. Compare Figs. 21 and 26 of Ref. [1], with Fig. 9 from Lisauskas [27].

Whether the gold adheres principally to spinel, to a metal oxide layer or in some other phase in reactively bonded inks is an important question. There is substantial evidence in the SEMographs reviewed above and in the following argument that the gold sticks preferentially to the spinel: Because Lisauskas normalized all his weight gain data to his 850°C samples, it is not possible for the reader to obtain an accurate picture of how the weight of metal oxide decreased in the high-temperature-fired, reactively bonded samples. It is, however, clear that it did decrease since the normalized weight of binder additive (CuO and CdO, as oxides or combined into spinel) remained constant

38

at the gold-ceramic interface for increasing firing temperatures, and since the amount in spinel form increased. Thus, the reduction in the amount of metal oxides in the interface correlates directly with the increase in adhesion strength. Even if some metal oxide were always present at the interface, the principal adhesion mechanism could still be adhesion of the gold to the spinel through holes in the oxide.

The activation energy data for spinel formation shown in Table H-1 (Appendix H) were explained sensibly only in the case of the copper paste ink. Conclusion C in Appendix H was made on the basis of a moderately good fit* of the ionic radius of Cu^{2+} and the activation energy for the formation of $CuAl_2O_4$ with a series of data pairs for the ionic radii of Ni^{2+}, Zn^{2+}, and the activation energies for the bulk diffusion of these ions through their respective spinels. The point for cadmium does not fit at all with the rest of the data, as shown in Fig. 19. Hence, Conclusion C of Appendix H is invalid for the formation of $CdAl_2O_4$.
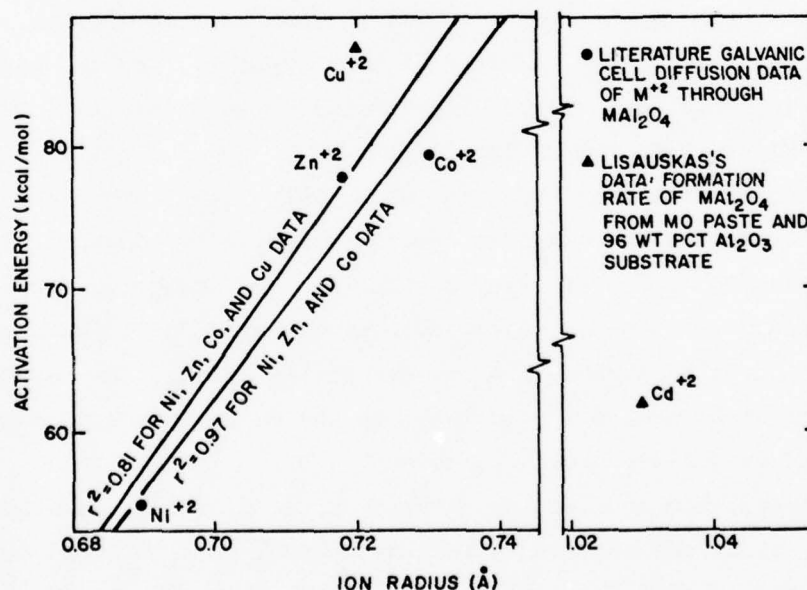
Figure 19. Comparison of the activation energies for spinel formation with the divalent cation radii.

---

*The coefficient of determination, r^2, of the straight line calculated by a least-squares fit of the data was reduced substantially by the addition of the copper data point, as shown in Fig. 19.

For the reactively bonded gold inks, surface, interfacial, grain boundary, or bulk atomic diffusion models may prove useful. The presence of a metal oxide layer could have influence on the kinetics of spinel formation. A surface diffusion or vapor transport model for the spread of CdO over Al_2O_4 to form spinel may be required to explain this phenomenon, but literature data on $CdAl_2O_4$ formation have not proved readily available.

Several comments are appropriate concerning Lisauskas's mixed-bonded ink studies. With these materials Lisauskas found a strongly different activation energy for spinel formation from that of the reactively bonded inks. A review of the applicable phase diagrams noted in the Appendix I – particularly Bi_2O_3-CuO and Al_2O_3-Bi_2O_3- strongly indicates that a liquid phase must form. Material transport should be strongly influenced by the presence of a liquid phase as discussed in Section II of this report and in our earlier work [2,3]. The amount of the liquid phase, its solubility for CuO, CdO, and Al_2O_3, and its viscosity as a function of temperature are expected to be critical properties of the liquid. The time during which the limited amount of Bi_2O_3 can dissolve other species before solidifying, the chemical species it deposits during solidification, the location of such deposits, and the way the molten frit phase is absorbed into the polycrystalline substrate will also strongly affect the kinetics of spinel formation.

The part of Lisauskas's Conclusion H, which states that the adhesion strength of the mixed-bonded inks remains essentially constant, is based on adhesion strength data containing a great deal of scatter. Figure 20 compares the data from a reactively bonded and a mixed-bonded gold ink studied by Lisauskas with data taken by RCA on very similar inks. The reported compositions of all of Lisauskas's gold inks and the compositions of comparable gold inks studied by RCA are shown in Table 8.

To compare such adhesion data taken in two different laboratories may be questioned, since the soldered-wire tensile peel test is known to be sensitive to the assembly techniques and handling of test specimens. RCA has, however, recently developed the test to a high degree of precision [28]. To plot

---

28. T. T. Hitch, "Reproducible Adhesion Test for Soldered Thick-Film Conductors," Final Report on Naval Avionics Facility, Indianapolis, Contract No. N00163-76-C-0287, released March 1978.

40

ADHESION FAILURE LOAD (lb)

15

LISAUSKAS'S DATA
SCATTER AVERAGED
~± 50 PCT OF THE
FAILURE LOAD VALUES.
IT WAS A GREATER
FRACTION OF THE
HIGHER LOAD
VALUES.

□----- Au NO.2
△----- Au NO.3
■----- Au H-1
●----- Au D-2
▣----- Au C-1

10

NO "A"
FAILURE
MODES

5

0

700   800   900   1000   1100
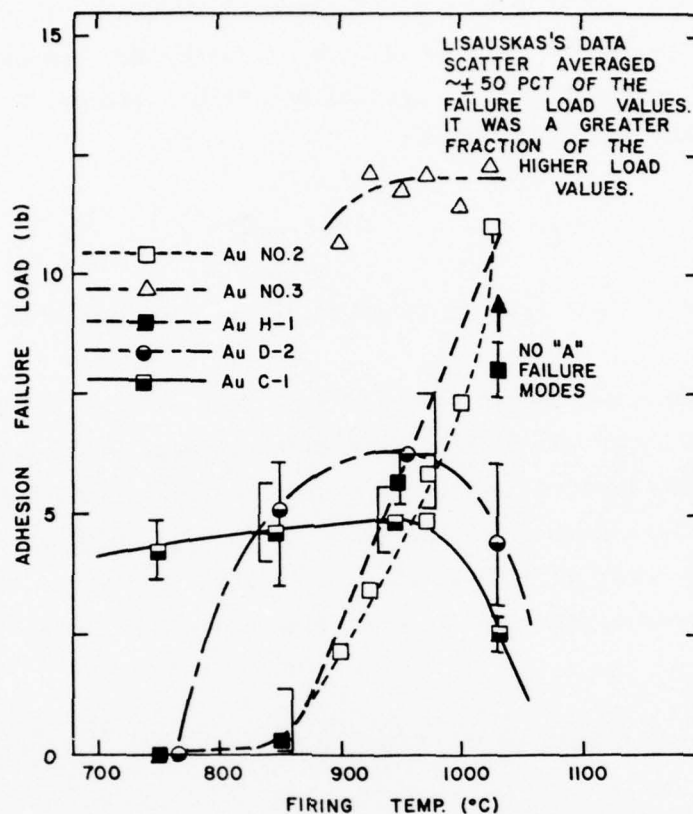
FIRING TEMP. (°C)

Figure 20.   The adhesion strength of reactively bonded
and mixed-bonded gold conductors as a
function of firing temperature.

TABLE 8.   THE COMPOSITIONS OF THE BINDER PHASES OF INK
MATERIALS STUDIED BY LISAUSKAS AND BY RCA

Gold Ink Designation	Binder Type	Binder Composition (wt pct)*						
		CuO	CdO	Bi_2O_3	ZnO	PbO	SiO_2	B_2O_3
RCA [1] Code H-1	Reactively bonded	0.88	0.23				0.06	
RCA [1] Code D-2	Mixed-bonded	0.25	0.93	2.0				
RCA [1] Code C-1	Mixed-bonded	0.5			1.0	2.5	0.2	0.5
Lisauskas No. 1	Reactively bonded	2.25	0.63					
Lisauskas No. 2	Reactively bonded	0.99	0.26					
Lisauskas No. 3	Mixed-bonded	0.29	1.63	1.23				
Lisauskas No. 4	Mixed-bonded	0.65	0.69	0.78				

*The binder compositions have all been calculated as if they were present as the most likely
oxide at 1000°C. The compositions are expressed as wt pct of the total inorganic material
in the inks.

41

Lisauskas's data, which report his failure strengths as load per unit area, for comparison with RCA's data, we chose to normalize the data. Lisauskas most probably obtained each of his failure stress values, S, in psi values according to the standard formula

$$S = \frac{F}{A}$$

where F is the failure load in lb and A is the test-pad area (0.080 in. x 0.080 in.).

The soon-to-be-released study of this test method [28] indicates that a linear dependence of the failure load with test-pad width holds in such tests. Accordingly, we converted Lisauskas's data to the failure load values shown in Table H-1 and have further normalized them in Fig. 20 to be comparable to our data that were taken with (0.10-in. x 0.10-in.) metallized test pads. The following conversion was used to normalize Lisauskas's data for presentation in Fig. 20.

$$F \text{ plotted} = \left[S(\text{psi}) \right] \times \left[0.08 \text{ in.} \right]^2 \left[x \frac{0.10 \text{ in.}}{0.08 \text{ in.}} \right]$$

$$= \left[S \times 0.008 \quad (\text{lb}) \right]$$

The good agreement of data between the two very similar reactively bonded inks, H-1 and No. 2 in Fig. 20 gives credence to the comparison. Furthermore, except for the test-pad areas, the tests run by both groups were similar. The solder was 12In-70Sn-18Pb (in wt pct), and the Instron loading rate was 0.5 in./min in both test procedures. The difference in wire diameters − 0.032 in. for RCA and 0.022 in. for Lisauskas − should not affect the data significantly as long as "A" failure modes are observed [28].

An "A" or adhesive failure mode is one in which the pad solder and wire are pulled clearly off the substrate during testing. Lisauskas does not describe failure modes in detail but does mention a transition to failure modes other than our "A" mode for the higher-strength reactively and mixed-bonded

films. His constant failure load data may be the result of a failure mode that no longer reflects the film-to-substrate adhesion strength, but instead shows the strength of the solder, the wire, or the bulk gold film.

On the basis of our study of the data, we believe it is not advisable to conclude that adhesion strengths of mixed-bonded inks are constant with firing temperature. However, a conclusion that there is a reduced sensitivity to firing temperature in the mixed-bonded inks compared with reactively bonded inks may certainly be drawn from Lisauskas's data and is in agreement with our own. Why Lisauskas's adhesion strengths for his mixed-bonded Au ink No. 3 is much higher than our data for the similar ink D-2 is not clear.

Lisauskas's Conclusion I indicates that the Bi_2O_3 glassy phase covers the spinel and that the adhesion of the gold is principally to the glassy layer. It could be argued that the gold is adhering to the spinel through holes in the Bi_2O_3 frit phase. This appears possible from Lisauskas's and RCA's SEMographs and from our Auger studies. However, Lisauskas's conclusion is supported by our data and model for the adhesion of mixed-bonded inks [2].

Lisauskas did not report $MgAl_2O_4$ on the surface of his as-received sub-strates. Analysis by x-ray diffraction at RCA of the surfaces of Coors ADS96F substrates, to be described below, (and of a great many other 96 and 99.5 wt pct alumina substrate surfaces[*]) indicates that most contain significant amounts of $MgAl_2O_4$ spinel. Moreover, instead of the minor impurity Lisauskas states it to be, MgO was present in our ADS96F at ∿1.0 wt pct, i.e., ∿25% of the binder-phase additions to the alumina substrate body. Indeed, Lisauskas's EDAX surface analyses of the substrate clearly indicated the presence of magnesium, despite the reduced sensitivity of EDAX for elements with low atomic numbers.

B. EXPERIMENTAL WORK

1. Analysis of Reactively and Mixed-Bonding Interface Compounds

One of the most powerful techniques for the identification of crystal phases is by x-ray diffraction of a powdered sample using the Debye-Scherrer

---

[*]Private communication, Dr. Eric Hockings, RCA Laboratories, July 1977.

43

camera method. To obtain a sufficient quantity of sample for the test, 1-in. x 1-in. x 0.025-in. alumina substrates were printed with conductor inks over a 0.075-in. x 0.075-in. area, dried, and fired at temperatures which had produced high adhesion strength in our earlier studies [1,2]. The metal phase was leached away by mercury vapor, and the reacted substrate surface was low-temperature baked in vacuum to remove residual mercury and scraped with a polycrystalline diamond tool No. SP-10.*

The scrapings were collected and studied by the Debye-Scherrer method. The x-ray source was copper with a nickel filter (i.e., Cu $K\alpha$ radiation was used).

Some chipping of the diamond tool was evident, due, in part, to the tool holder design. Because of this, control samples were prepared of the diamond tool chips as well as from scrapings of as-received substrates from the two lots on which thick films had been prepared for the study.

The results are shown in Table 9. The carbon and silicon carbide lines are attributed to the scraper and may be disregarded in the thick-film binder data. A comparison of the data for each sample with that for the appropriate control substrate gives a clear indication that changes in the surface crystal-linity were caused by the thick-film bonding agents present in several of the samples. For gold ink H-1, the amount of sample studied was apparently too small to obtain a good pattern. In silver ink B-3, the detection of a spinel phase, not seen in an equally strong pattern from the substrate, is taken as an indication of the importance of the spinel phase to the high adhesion strength in this material. In the extremely high adhesion silver ink C-7 fired onto substrate D, the spinel phase was still more prominent than in the sample from silver ink B-3.

In the control sample of substrate A, a very weak spinel-phase pattern was detected and a silicate phase identified as *high cordierite* was detected more strongly. In silver ink C-7 fired on substrate A, the intensities from cordierite and the spinel are reversed, suggesting the possible transformation of some of the high cordierite components into spinel.

---

*Megadiamond Industries, New York, NY.

44

TABLE 9. PHASE IDENTIFICATION BY X-RAY POWDER DIFFRACTION

| | | | | | | | | X-Ray Data | | | | |
| | Sample Description | | | | | | | | Relative Strength of Phase Patterns Within a Film | | Carbon | SiC |
Ink	Bond Type	Substrate*	Firing Temperature (°C)	Peel Adhesion Strength (g)	Color of Scraped Area	New Crystalline Phase Seen in SEM	General Intensity of Patterns on a Film	α-Al_2O_3 α-Alumina	$Mg_2Al_4Si_5O_{18}$ High Cordierite	$CuAl_2O_4$ and $MgAl_2O_4$ Spinel	Diamond	Silicon Carbide
Au H-1	reactive	A (96% Al_2O_3)	1030	~225	light tan	believed seen	weak	medium	~	-	medium	very weak
Ag B-3	mixed	D (99.5% Al_2O_3)	950	~270	brown	seen	strong	strong	-	very weak	very weak	-
Ag C-7	mixed	D	950	>370	grey	prominent	strong	strong	-	weak	very weak	-
Ag C-7	mixed	A	950	~300	grey-green	unsure	medium	strong	very weak	medium	-	-
		A**			white		strong	strong	very weak	-	very weak	-
		D**			white		strong	strong	weak	very weak	-	-
		diamond fragments†					weak	-	-	-	strong	weak

*Unless otherwise indicated.
**Control sample (as-received substrate). Substrate A is American Lava Corp. (Chattanooga, TN) AlSiMag 614. Substrate D is Coors Porcelain (Golden, Co) ADS995.
†Control sample from scraper material.

45

It will be noted in Table 9 that the spinels $CuAl_2O_4$ and $MgAl_2O_4$ are shown together. These two materials are isostructural and their lattice spacing is so nearly the same that it was difficult to determine which one was present. Furthermore, only medium-to-weak front reflection lines were found. Some differences in intensity between the lines for these two compounds are indicated by the ASTM card file of x-ray diffraction data. These results from the differences in the atomic scattering factors of the copper and magnesium occupying the same spinel lattice sites. However, we could not distinguish between the spinel phases in the three samples in this experiment. We believed, however, that the spinel was not pure and has a formula such as $Cu_xMg_{1-x}Al_2O_4$. Additional experiments which clarify this point are described later in this report.

A copper-containing aluminum silicon oxide similar to $Mg_2Al_4Si_5O_{18}$ was searched for, but is not listed in the ASTM card file. The likelihood of the formation of such a material is believed high.

All the data found are shown in Table 9; no lines remained unaccounted for. The patterns of the two forms of copper-aluminum oxide, $CuAlO_2$, were searched for specifically, but were not found.

The indications that may be drawn from the scraping and x-ray-diffraction work are more meaningful when considered in the light of equilibrium phase diagrams found in the literature. Of several available, Fig. 21 appears to describe the system most thoroughly. It shows that only $CuAlO_2$ may be expected as a product of the reaction of CuO and Al_2O_3 above a temperature of 1170°C. Between 612 and 1000°C, $CuAl_2O_4$ is the only expected product [29]. Between 1000 and 1170°C both $CuAl_2O_4$ and $CuAlO_2$ are found. Of course, the presence of an isostructural spinel of very similar lattice size, e.g., $MgAl_2O_4$, and the depletion of oxygen under a sintering metal film could influence the equilibrium between CuO, Al_2O_3, and their products.

At RCA, mixtures of copper oxide with both pure alumina powder and ground 96-wt pct alumina (substrate A) were fired for 1 h at 1075°C. Copper aluminum

29. K. T. Jacob and C. B. Alcock, "Thermodynamics of $CuAlO_2$ and $CuAl_2O_4$ and Phase Equilibria in the System $Cu_2O-CuO-Al_2O_3$," J. Am. Ceram. Soc. 58, 192 (1975).
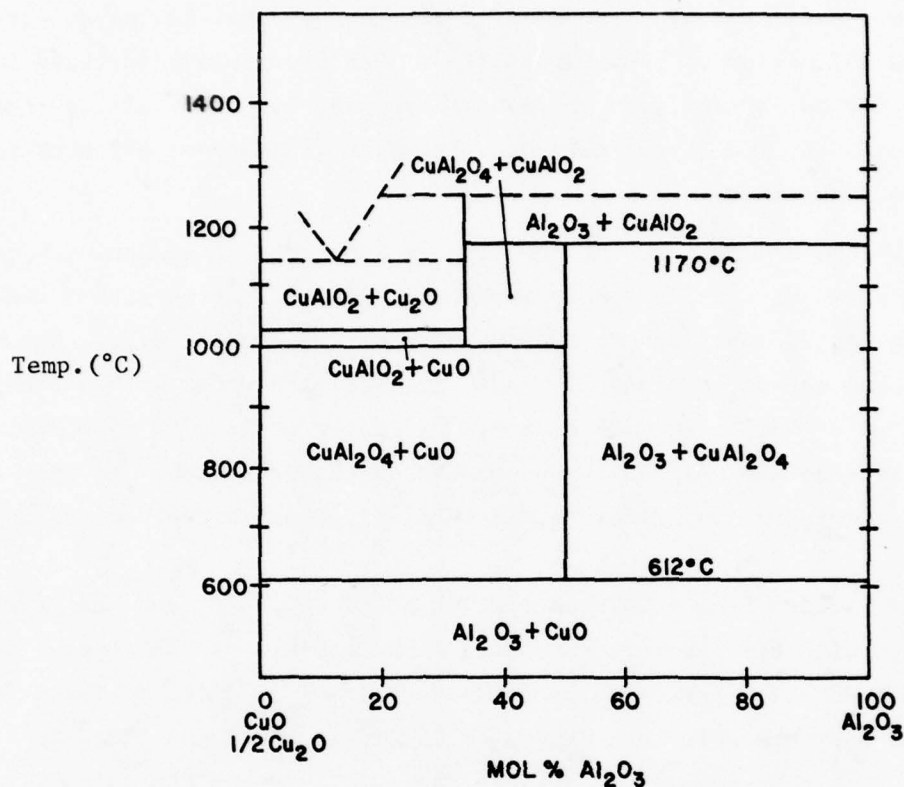
Figure 21. The phase diagram $Cu_2O-CuO-Al_2O_3$ at an
oxygen pressure of 0.21 atm. after
Jacob and Alcock [29].

spinel $CuAl_2O_4$ and $CuAlO_2$ were formed in both cases [2]. Note that a higher
ratio of $Cu_2O:Al_2O_3$ than is present in reactively bonded thick films, as well
as a high reaction temperature, would promote the formation of $CuAlO_2$, accord-
ing to Fig. 21.

Although the systems we have studied are more complicated than the
$Al_2O_3-Cu_2O-O_2$ ternary and our experiments probably do not bring the samples
fully to equilibrium, the formation of copper-containing spinel and of $CuAlO_2$
in our samples appears to be predicted by Fig. 21.

2. Interface Compound Formation As a Function of Film
    Composition and Reaction Temperature

The object of this group of experiments was to study the kinetics of
spinel formation. The method used was modeled after one of Lisauskas's
experiments where oxide films were fired onto the substrates, etched to remove

unreacted oxide, and the weight increase of reaction product on the substrate was studied as a function of temperature [27]. Our experiments included CuO and CdO films for comparison with those of Lisauskas, but study of the reaction of 3:1 and 1:3 CdO to CuO (by weight) mixtures with alumina was our principal reason for the experiment.

a. Procedure - Coors ADS96F[*] 96 wt pct alumina substrates, the same substrate material that Lisauskas studied, were marked for identification with a red EMCA[**] marking pencil and fired at 1000°C to react the pencil marks. The substrates were then washed in ethanol, rinsed in distilled water with ultrasonic agitation, dried at 150°C, and baked at 600°C. After cooling to room temperature, each substrate was weighed in succession to the nearest 10^{-5}g; then each substrate was reweighed two or more times until agreement between weighings was apparent.

Inks were blended from -400 mesh reagent grade CuO, CdO, and the mixtures of these oxides with CV-9 vehicle purchased from Cermalloy[†]. The pastes were screened with a 200-mesh screen in patterns 0.73 in. x 0.73 in. on the tared substrates. The prints were then dried for 15 min at 150°C and fired at 600°C in a belt kiln to remove the organic phases. To react the oxide films with the substrates, firing was performed in a tube furnace equipped with a system to pull the quartz boat semiautomatically into the furnace, to allow a 30-min soak at peak temperature, and to pull the boat from the furnace. The total time in the furnace was 36 min. Nominal soak temperatures of 900, 950, 975, 1000, and 1025°C were used. Each soak temperature was measured with a precision calibrated thermocouple and recorder system immediately before or after the specimens were fired.

The specimens were thoroughly etched in concentrated hydrochloric acid to remove the unreacted oxides, and then were washed, dried at 150°C, refired at 600°C to drive off residual moisture, and reweighed after cooling to room temperature.

---

[*]Coors Porcelain Co., Golden, CO.
[**]Electro Materials Corporation of America, Mamaroneck, NY.
[†]Division of Bala Electronics, West Conshohocken, PA.

b. *Results* – The data points in Figs. 22, 23 and 24 are each the natural logarithm of the average weight gain (in grams) of four substrates. The higher-temperature-fired CdO substrates showed substantial weight losses, in contrast to the data of Lisauskas. Those data are shown in Fig. 25, and the process is clearly a thermally activated one.

It was clear from the weight gains and the appearances of the substrate after etching (see Table 10) that the mixed-oxide films had strongly reacted on the substrates. There were indications that the mixed-oxide films formed liquid phase at the two higher temperatures. The larger weight gains (see Figs. 20-25) were correlated with the appearance of more strongly colored (mixed-oxide) films remaining in the printed areas after etching.

Activation energies were computed from the slopes of the least-square-fit straight line through the data of Figs. 20-23 and are compared with Lisauskas's activation energies in Table 11. The CdO values are in fair agreement, except that one is a weight gain and the other a weight loss. The two CuO values are substantially different, but there are several differences between the experimental techniques which could have influenced the values.

It should also be noted that our weight gain data has a precision of $\sim$2 x 10^{-5}g. Accordingly, values of W_{int} below -10.5 are shown in Figs. 22 through 25, but were omitted in computing the best straight line through and the Q's from the data.

We caution anyone attempting experiments to react CdO with alumina at high temperatures to beware of cadmium vapor poisoning. We used a 4-ft^3/h flow rate of dry air through the 2 1/8-in. inside diameter furnace tube and exhausted the furnace atmosphere into a fume hood duct. We believe this is a fairly safe approach to the experiment, since most of the cadmium appeared to have condensed in the unheated exhaust end of the furnace tube. Chemical analysis was performed to determine what other species besides cadmium were removed from the substrates to cause the weight losses, but the results were inconclusive.

Table 12 describes the appearance of the reacted and etched film substrates under ultraviolet (uv) light. The sources for the long and short wavelength uv light were, respectively, Models UVL-56 and R-52 lamps.[*] The samples which had large weight gains showed little luminescence, but a strong

---

[*]Ultra-Violet Products, Inc. (San Gabriel, CA).
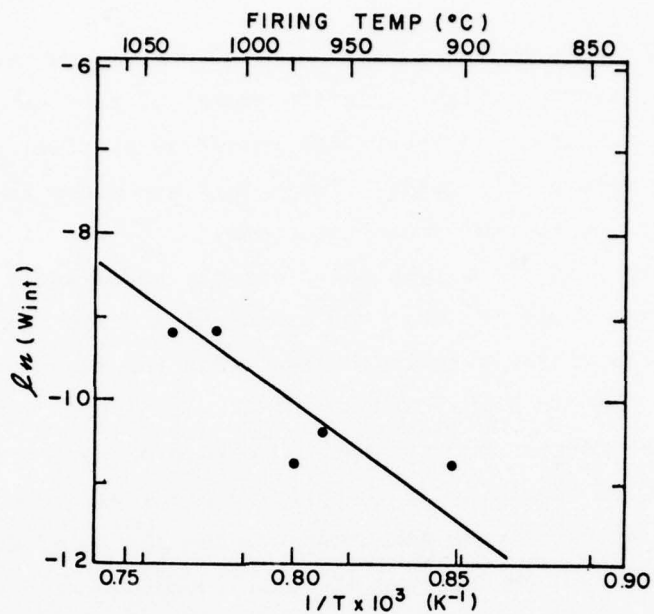
Figure 22. The reaction of CuO films with 96 wt pct
alumina substrates as a function of tem-
perature (weight gain).
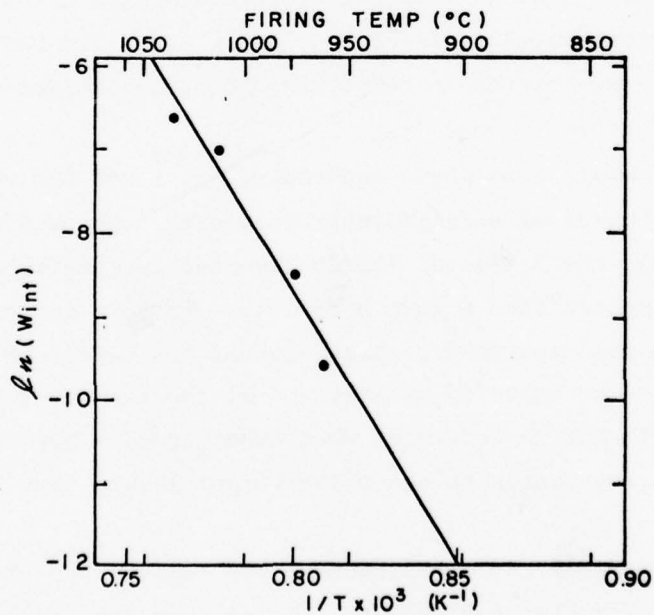
Figure 23. The reaction of 3CuO:1CdO weight mixture
films with 96 wt pct alumina substrates
as a function of temperature (weight gain).

50
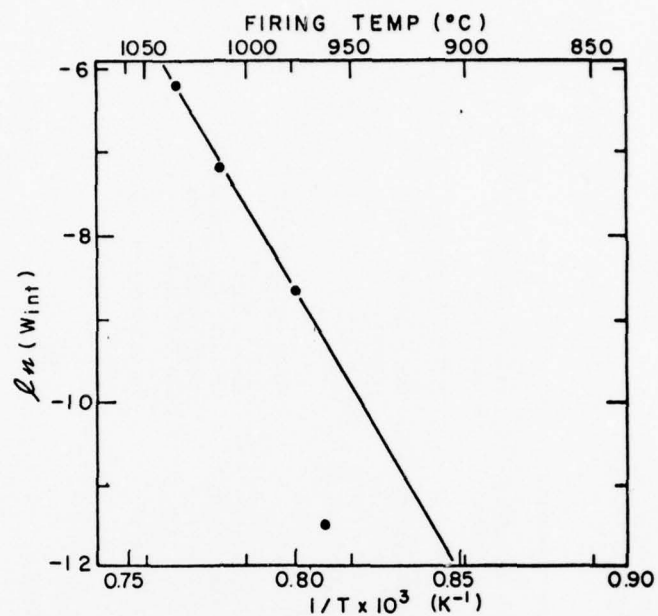
Figure 24. The reaction of 3CdO:1CuO weight mixture films with 96 wt pct alumina substrate as a function of temperature (weight gain).
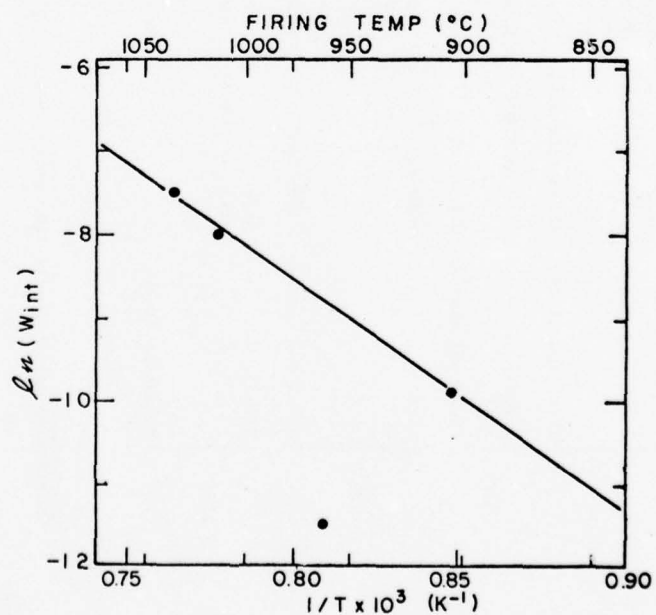
Figure 25. The reaction of CdO films with 96 wt pct alumina substrates as a function of temperature (weight loss).

TABLE 10. THE CHARACTER AND APPEARANCE OF THERMALLY REACTED OXIDE FILMS ON COORS ADS96F SUBSTRATES

Firing Temp. (°C)	Condition	Oxide Paste Composition (by wt.)			
		CuO	3CuO:1CdO	3CdO:1CuO	CdO
900°	Fired	Grey-black; easily scratched*	Grey-black with brownish tinge; some evidence of sintering; easily scratched	Lighter brown than CdO 900°C; easily scratched	Medium brown; some sintering
	Fired and etched	Clean substrate	Clean substrate	Clean substrate	Clean substrate
950°	Fired	Same as 900°C	Same as 900°C	Same as 900°C, except harder	Vaporization loss detectable
	Fired and etched	Trace color	Very light tan	Very light tan	Clean substrate
1000°	Fired	Same as 900°C	Dark greenish brown; can be scratched but film not completely removed	Pattern yellow with brown speckles; brown; can be scratched	Vaporization loss apparent
	Fired and etched	Light tan	Yellow-brown	Yellow-tan	White square visible
1025°	Fired	Dark grey; slightly harder	Medium brown; cannot scratch	Smooth, dark mustard color; cannot scratch	Pattern barely visible; weak brownish color irregular over one-half pattern area
	Fired and etched	Tan	Brown-yellow	Yellow-brown	White square visible

*Scratching was done with the corner of a polystyrene drafting triangle.

52

TABLE 11. THERMAL ACTIVATION COEFFICIENTS FOR WEIGHT CHANGES DUE TO
OXIDE FILM REACTIONS WITH 96 wt pct ALUMINA SUBSTRATES

Composition (by wt)	This Study Q (kcal/mole)*	r^2 of Plotted Line	Lisauakas's Thesis [7] Q (kcal/mole)	r^2 of Plotted Line
CuO	57 wt gain	0.92	87	0.99
3CuO:1CdO	130 wt gain	0.96	no data	–
1CuO:3CdO	137 wt gain	1.00	no data	–
CdO	56 wt loss	1.00	62 wt gain	0.99

*These data were taken ignoring the graphed points where $\ln(W_{int})$ was $\leq - 10.5$.

effect was seen from CuO and CdO samples for which W_{int} had been almost un-detectable.

The strong overall luminescence (see Table 12) of the CdO-1025°C specimen may be a significant clue to the discrepancy between Lisauskas's and our weight changes after etching such samples. Cadmium oxide has a significant vapor pressure (1 mm of Hg [30]) at 1000°C). With a continuous flow of air through a tube furnace, much of the CdO vapor will be carried away from the parts. This could have limited the reaction to a much lower level than would occur in a stagnant atmosphere such as Lisauskas may have used. Even so, it appears that the overall luminescence of the RCA CdO-1025°C specimen under long wavelength uv light (see Table 12) could only be due to reaction of the substrate surface with the CdO vapor.

A value for thp heat of vaporization, ΔH_{vap}, was calculated from vapor pressure-temperature data of Stull [30]. The ΔH_{vap} value found was 54.8 kcal/mole for CdO, which is rather close to the activation energies for weight loss from our CdO samples in Table 11. It also correlates reasonably well with Lisauskas's value for weight gains in his CdO samples. If the growth of $CdAl_2O_4$ spinel is controlled by the partial pressure of CdO vapor, ΔH_{vap} for CdO could be the activation energy for spinel formation from a CdO film on alumina in a furnace with a stagnant atmosphere. The activation energy for vaporization of CdO does not match with the activation energies of the other CdO-containing films (see Table 11). The vaporization of cadmium oxide could still be important

30. D. R. Stull, "Vapor Pressure of Pure Substances," Ind. and Eng. Chem., 39, 517 (1947).

TABLE 12. RESULTS OF THE ULTRAVIOLET INSPECTION OF THERMALLY REACTED OXIDE FILMS ON COORS ADS96F SUBSTRATES AFTER ETCHING IN HYDROCHLORIC ACID

Firing Temp. (°C)	Ultraviolet Source - Relative Wavelength	CuO	3CuO:1CdO	3Cdo:1CuO	CdO
950	long	very weakly luminous	same as CuO–950°C	no luminescence	no luminescence
950	short	clearly luminous, greenish white glow	same as CuO–950°C	slightly brighter than CuO–950°C	no luminescence
1000	long	clearly luminous	no luminescence	luminous border around dark printed pattern	~ same as CuO–950°C
1000	short	strong greenish white luminescence	no luminescence	luminous border around dark printed pattern	no luminescence
1025	long	luminous, but weaker than CuO–1000°C	no luminescence	luminous border around dark printed pattern	printed pattern ~ same as CuO–1000°C substrate glowed bright cherry red.
1025	short	~ same as CuO–950°C	no luminescence	slightly stronger luminescence than CuO–950°C	no luminescence

Note: All comparisons pertain to inspection of the two compared samples under the same ultraviolet source.

54

to those reactions, however. The presence of CdO vapor could initiate the reaction between the substrate and other spinel formers. It is also likely that the apparent ΔH_{vap} would be changed in the presence of other materials besides alumina. For instance, this would be so if the other material was a metal with a substantial solubility for cadmium, or a material with which cadmium oxide strongly reacted. Then the vapor pressure of the cadmium oxide would be reduced for any given temperature.

3. Experiment to Study the Growth Mechanism of Spinel

Lisauskas concluded that $CuAl_2O_4$ grew between 96 wt pct alumina and his Cu_2O film by bulk diffusion on the basis of the fit of his activation energy for copper-aluminum spinel growth and the known ionic radius of Cu^{+2} (see Fig. H-1). Even using our activation energy value, this could be argued.

In a single system of two bulk phases between which and from which a third phase is growing, if the growth kinetics are controlled by the bulk diffusion of a single component through the new phase, the rate of phase formation will be proportional to the square root of reaction time [31]. Accordingly, we performed a series of experiments similar to those described in III.B.2 but in which the time of reaction was varied while the temperature was held constant at 1000°C. Films of CuO, 3CuO:1CdO, and 3CdO:1CuO (by wt) on Coors ADS96F substrates were studied. The data are shown in Fig. 26 in a log-log plot. None of the data taken fit a slope of 0.5, which the model requires. If the theoretical bulk diffusion model is obeyed in these systems, it must be at short reaction times. Further data for shorter reaction times for those studied would be instructive.

The linearity of the data for the CdO-CuO mixtures for reaction times greater than 36 min and the similarity of the slopes of those lines with slope of the line through the CuO data for times greater than 81 min are interesting, but are not yet understood. It does appear, however, that there is a change in the spinel formation mechanism within the duration of the experiments.

---

31. W. D. Kingery, *Introduction to Ceramics* (John Wiley & Sons, Inc., New York, 1960), p. 335.
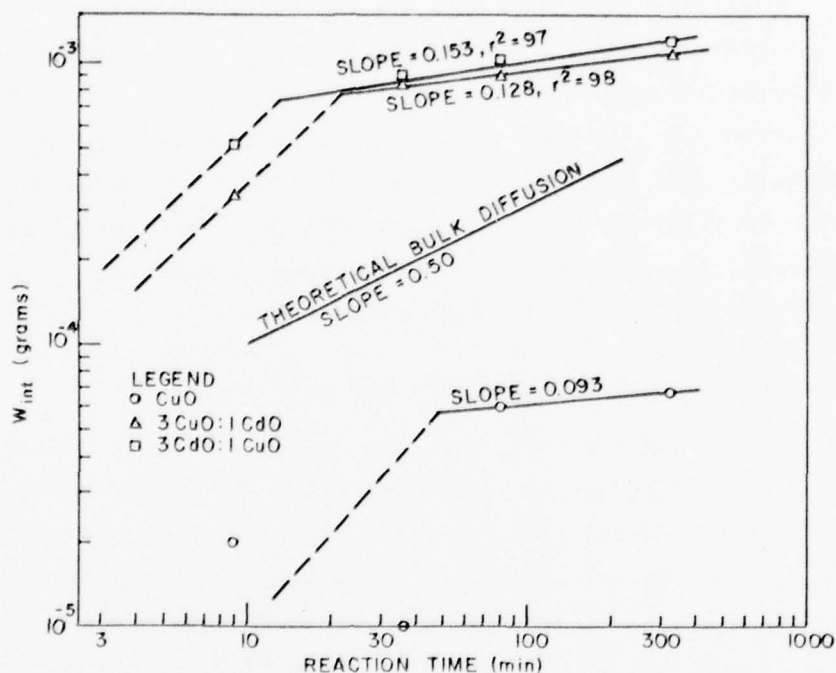
Figure 26. Log-log plot of reaction time vs the weight of
HCl-insoluble interface reaction products formed.

4.   Further Study of Spinel Growth By X-ray Diffraction

Because of the weakness of the spinel patterns studied in the x-ray work
described in III.B.1, an x-ray diffractometer method was chosen for the further
study of spinel structures and their growth.

Samples of Coors ADS96F alumina substrates that had been reacted with
CuO, 3CuO:1CdO, 1CuO:3CdO (by wt) or CdO films for 30 min at 950, 1000, or
1025°C were prepared by etching with HCl as for the weight gain experiments
described in III.B.2. The x-ray data corresponding to the spinel structure
found in these experiments and in studies of as-received substrates are compared
in Table 13 with data taken by Lisauskas. ASTM x-ray diffraction standard data
for spinels are also presented for comparison. The agreement between most of
the lattice parameter and relative intensity data taken by Lisauskas and by
RCA is good.

In general, the increase in spinel x-ray pattern strength (relative
strength of (311)) correlates with the increase in firing temperature for each
film type. Where this did not occur, preferred orientation is believed to be

56

TABLE 13. X-RAY DATA ON SPINEL FORMATION

Spinel or Reacted Film (Proportional by Weight)	Source	Reaction Temp. (°C)	Reaction Time (min)	Miller Indices of Spinel Plane							Relative Strength of (311)**	Spinel Lattice Parameter (Å) †	Comments
				(111)	(220)	(311)	(400)	(422)	(511)	(440)			
CuO	RCA	1025	30	36*	36	100	45	---	23	45	17	8.08 ± 0.01	
CuO	RCA	1000	30	50	50	100	40	---	45	65	7	8.08 ± 0.01	
CuO	RCA	950	30	18	13	35	100	---	---	20	10	8.07 ± 0.01	
CuO	Lisauskas[27]	1100	120	not sought	45	100	15	10	25	10	----	8.07	
CuAl$_2$O$_4$	ASTM	not given		not given	40	90	70	80	90	100	----	8.64	
MgAl$_2$O$_4$	ASTM	not given		35	40	100	65	10	45	55	100	8.0831	
MgAl$_2$O$_4$	RCA	----	----	0	70	100	0	0	30	0	----	not calculated	Highly preferred orientation of irregularly distributed spinel. Sample oriented for maximum signal.
3CuO:1CdO	RCA	1025	30	11	61	100	18	10	17	88	100	8.09 ± 0.02	
3CuO:1CdO	RCA	1000	30	8	53	100	12	7	12	16	75	8.11 ± 0.005	
3CuO:1CdO	RCA	950	30	0	50	100	0	0	0	10	8	8.10 ± 0.03	
Reactively bonded Au#1	Lisauskas	1015	15	not sought	25	100	20	---	5	10	not given	8.12	
Relatively bonded Au#2	Lisauskas	1000	15	"	25	25	5	---	10	100	not given	8.08	
Mixed-bonded Au#3	Lisauskas	1025	15	"	60	100	5	---	40	40	not given	8.08	
Mixed-bonded Au#4	Lisauskas	1000	15	"	40	100	25	---	40	40	not given	8.08	
1CuO:3CdO	RCA	1025	30	----	84	100	13	15	21	23	75	8.12 & 8.18 ± .03	Peaks were broad and not well shaped
1CuO:3CdO	RCA	1000	30	18	94	100	18	13	22	26	35	8.10 & 8.20 ± .02	
CdO	RCA	1025	30	----	63	100	47	---	39	29	11	8.11 ± 0.01	
CdO	RCA	1000	30	----	32	57	24	---	22	36	9	8.10 ± 0.02	
CdO	RCA	950	30	none	none	none	none	none	none	none	0	8.10 ± 0.05	A spinel phase appeared to be present but the peaks were very, very weak.
CdO	Lisauskas	1050	15	not sought	80	100	10	---	10	20	not given	8.12	
CdAl$_2$O$_4$	Lisauskas's Calculations	----		not calculated	40	90	70	80	90	100	----	8.08	

*For a sample, the strengths of x-ray diffraction peaks are expressed (in percent) relative to the strongest peak from that sample.

**The strength comparisons made between x-ray data from different samples were made relative to the strongest (311) peak seen in the study, which was from the 3CuO:1CdO specimen fired at 1025°C.

†Alpha aluminum oxide lines on the x-ray diffractometer data were used to calibrate the data for calculation of the lattice parameter values.

57

the reason. The increase in spinel pattern strength also correlates with the increase in weight gains of the interfacial materials in Figs. 20-23.

One of the most interesting findings is that two spinel patterns were found to be superimposed in data from the 3CdO:1CuO specimens. The lattice parameter of the larger spinel unit cell is clearly larger than any seen in the other experiments. Because of the lattice expansion due to distortion, which is likely to be present when a structure incorporates substitutional atoms, this finding is taken as a first-order proof that a mixed spinel of the form $Cu_xCd_{1-x}Al_2O_4$ is being formed. A strong, specific relationship between the position of the copper and cadmium in the structure is also suspected. Accordingly, the range of the relative amounts of Cu and Cd in this spinel, which is designated by the value of x, may be quite limited. Clearly, additional work will be required to further understand this newly discovered material.

It must be noted that the diffractometer method used in this study detects only planes which lie parallel to the substrate surface. If any preferred orientation exists it will shift the relative intensities of the peaks away from that of randomly oriented samples such as the ASTM standards. In samples where the (440) or (111) spinel planes give stronger x-ray peaks than the (311) planes, preferred orientation is likely (Table 13).

Table 14 shows data for x-ray diffraction peaks which were seen repeatedly in the analyses of the spinel peaks but could not be identified. ASTM file patterns of copper and cadmium oxide patterns, α- and γ- alumina patterns, silicate patterns of the cordierite type, and both forms of $CuAlO_2$ were compared with the Table 14 lattice spacings without finding a sensible match. At least two phases are suspected to be present, and one of these is believed to be a compound containing both copper and cadmium. These were detected in addition to the spinel which we identified as having a lattice parameter of ~ 8.19 Å.

The strengths of the patterns from a given oxide film type generally increased with the reaction temperature. It also should be noted that the strengths of the various x-ray diffraction peaks in Table 14 are given relative to each other but were generally weaker than those described by Table 13. A very strong peak in Table 14 is approximately equivalent to a relative intensity

TABLE 14. LATTICE SPACINGS FROM UNIDENTIFIED PHASES FOUND
AFTER OXIDE FILM REACTION AND ETCHING ON COORS
ADS96F ALUMINA SUBSTRATES

Oxide Film	Lattice Spacings ($\mathring{A}$)* and relative x-ray peak strengths								
CuO	3.98 very weak	-	3.90 very weak	-	3.21 strong	-	1.96 very weak	-	1.42 weak
CdO	-	-	-	-	3.19 weak	-	1.96 weak	-	1.43 medium
3CuO:1CdO	3.98 very weak	3.88 weak	3.74 medium	3.59 weak	3.18 very strong	2.94 medium	1.96 very weak	1.54 weak	1.44 weak
3CdO:1CuO	-	-	3.74 medium	3.59 weak	3.18 strong	-	1.96 weak	-	~1.43 obscured by another peak

*These values assume an order number of one in the Bragg equation for x-ray diffraction.

of 10 on the scale of (311) intensities in Table 13. Weak peaks on Table 14 were separated from the background only by their repetition in the same locations on diffractometer recorder charts from several samples.

5. Binder Layer/Overlay Adhesion Experiments

The last series of experiments were attempts to differentiate between the adhesion strength of overlay gold films to various reactive bonding binder layer materials. Specimens were prepared by firing layers of copper oxide, cadmium oxide, and mixtures of CdO and CuO at various temperatures onto ADS96F substrates and etching them in hydrochloric acid as described in Section III.B.1.

An overlay gold ink made from Metz 708* gold powder and CV-9 was then printed in an adhesion test pattern and fired at 900 or 1020°C in air onto the previously prepared binder layer area of the substrate. The adhesion strength samples were Scotch-tape adherence tested. Those which passed were subjected to the recently developed, and more vigorous, soldered wire peel test [28]. The solder used was Indalloy No. 9.** None of the samples were sufficiently adherent to allow soldered-wire peel test strength values to be measured, however. Table 15 indicates the adhesion of the samples.

*Metz Metallurgical Company, South Plainfield, NJ.
**Indium Corporation of America, Utica, NY.

TABLE 15. RESULTS OF SCOTCH-TAPE ADHESION STRENGTH TESTS ON OVERLAY GOLD FILMS FIRED ONTO THERMALLY REACTED OXIDE LAYERS ON COORS ADS96F SUBSTRATE

Oxide Layer Firing Temp. (°C)	Overlay Gold Firing Temp. (°C)	CuO	3CuO:1CdO	1CuO:3CdO	CdO
900	900	Failed	Failed	Failed	Failed
	1025	Nearly passed	Nearly passed	Partially passed	Partially passed
950	900	Failed	Failed	Failed	Failed
	1025	Nearly passed	Partially passed	Nearly passed	Failed
1000	900	Failed	Failed	Failed	Partially passed
	1025	Passed	Passed	Nearly passed	Failed
1025	900	Failed	Failed	Partially passed	Nearly passed
	1025	Passed	Passed	Passed	Failed

Note: In the order of increasing adhesion strength, the classifications are: failed, partially passed, nearly passed, and passed.

Clearly, increasing the firing temperature of the overlay gold improved the adhesion except on the substrates which had been reacted with CdO or 3CdO:1CuO at the higher temperatures. With those parts, adhesion decreased with an increase of the firing temperature of the gold film.

In further experiments, 2 wt pct CuO was added to the Metz gold powder, blended into an ink, and fired onto the reacted and etched substrates at 1025°C. Adding copper oxide to the gold improved the metal film adhesion. All of the parts passed Scotch-tape testing, but none of the materials demonstrated sufficient adhesion strength to allow its use as a conductor in most hybrid circuits. It was noted that in several instances where heavy layers of reacted material had remained after etching, some melting of the gold 2 wt pct CuO film with the binder layer material occurred during the 1020°C firing.

C. DISCUSSION

At the beginning of the 1977 contract year there was strong evidence that the aluminate $CuAlO_2$ might be important to the adhesion mechanism of reactively bonded thick-film conductors. Phase diagrams [32,33], another worker [34], and our own experiment reacting equal quantities of Cu_2O and Al_2O_3 at 1075°C [2] had suggested that $CuAlO_2$ might be forming in the interface between the alumina substrate and the noble metal phase. Compelling evidence has now been produced to support our earlier theory [35] that it is the formation of copper-aluminum-based spinel phase(s) on which the optimum adhesion strength of silver- and gold-based reactively bonded and mixed-bonded conductors depends.

Clear x-ray identification was made of copper-aluminum spinels by Lisauskas [27], RCA, and in allied systems [36]. The absence of the $CuAlO_2$ phase was established in these studies of binder layer compounds. A phase diagram study [29] more advanced than the others, which had been consulted, supported the formation of $CuAl_2O_4$ spinel and the presence or absence of the $CuAlO_2$ phase in the reaction products of all the RCA experiments - despite the facts that our alumina was only 96 wt pct pure and that our spinels sometimes contained cadmium additions.

The kinetics of spinel formation have been elucidated by our study this year. In particular it is now clear that the addition of cadmium oxide to copper oxide makes a very strong change in the activation energy for spinel formation. The amounts of spinel which formed in our experiments correlate well with our knowledge of adhesion strength in reactively bonded conductor

32. S. K. Misra and A. C. D. Chaklader, "The System Copper Oxide-Alumina," J. A. Ceram. Soc. 46, 509 (1963).
33. A. Gadalla and J. White, "Equilibrium Relationships in the System $CuO-Cu_2O-Al_2O_3$," J. Brit. Ceram. Soc. 63(1), 39 (1964).
34. R. G. Loasby, N. Davey, and H. Barlow, "Enhanced Property Thick-Film Conductor Pastes," Solid-State Technology 15(5), 46 (1972).
35. T. T. Hitch, "Phase Morphology and Bondability of Reactively Bonded and Frit-Bonded Gold and Silver Thick-Film Conductors," J. Electron. Mat. 3 553 (1974).
36. G. Katz, "Adhesion of Copper Films to Aluminum Oxide Using a Spinel Structure Interface," Thin Solid Films 33, 99 (1976).

inks, e.g., the gain in adhesion strength for a modest increase in firing temperature from 950 to 1000°C of cadmium-containing, reactively bonded inks than for those containing only copper oxide. Furthermore, for the same reaction time at 950°C, a binder containing a cadmium oxide-copper oxide mixture will form more spinel than a plain copper oxide binder, and the corresponding cadmium-containing conductor ink will be more adherent. Just how the reaction rate is increased is not fully understood. However, the pre-existent spinel, $MgAl_2O_4$, and silicates such as high cordierite $Mg_2Al_4Si_5O_{18}$, which are present in the substrate together with glassy phase additives to the ink binder phases, are believed to accelerate the spinel formation in all cases. The $MgAl_2O_4$ may act as an epitaxial site for spinel growth. The silicates and glasses may dissolve the copper oxide, cadmium oxide, and perhaps alumina, to transport them to spinel surfaces and to precipitate them there where they are in-corporated into the spinel structure. It is known that higher temperatures are required to develop optimum adhesion strength on 99.5 wt pct than on 96 wt pct alumina substrates [1,2]. The amounts of silicates and magnesium-aluminum spinels in the 99.5 aluminas are greatly reduced from those in 96 aluminas. If a eutectic liquid phase forms directly from CdO, CuO, and possibly other constituents on the substrate surface, that should, of course accelerate spinel growth rates.

The mechanism of spinel growth has not been uniquely determined. Lisauskas concluded that the bulk diffusion of copper through the spinel controlled its growth rate. If that model were correct the gain in weight of interfacial compound should be proportional to the square root of the reaction time for a fixed firing temperature [31]. While our data on the formation of spinel from a copper oxide film on 96 wt pct alumina substrate could not preclude that mechanism, the growth of spinel from films of mixed cadmium oxide and copper oxide is not controlled by bulk diffusion during the time of our experiments. There is some indication that once a continuous layer of spinel forms on the substrate surface, the further growth of spinel into the bulk of the alumina is severely limited. The limited dependence of spinel formation on further reaction time after ∿10 min in our experiments is one such indication. It also has been noted that the erosion rate of fire clay crucibles (which contain

a high proportion of alumina) by high lead oxide content glasses is drastically reduced by the addition of ∿2 wt pct copper oxide to the glass.*

The bonding mechanism in mixed-bonded conductors has been discussed above only insofar as the liquid glassy phase could be important in increasing the formation rate of spinel. At least two phases must be considered to be important binder materials which cause the alumina substrate and the noble metal film to adhere. If we accept that the spinel grows directly on the surface of the alumina, the glassy phase must then lie between the metal phase and the spinel. If this is so, why should the adhesion strength of mixed-bonded conductors so greatly exceed that of frit-bonded conductors? The primary reason must be a reduced free energy of the interface between the glass and metal phases, γ_{gm}. A reduction in γ_{gm}, which is caused by dissolving copper oxide in the glass, is indicated by the results of the glass spreading experiments [2]. The reduction in γ_{gm} is expected to result in a more than proportionate increase in the adhesion strength for the following reasons:

1. It is the nature of plastic work in an adherend that it distributes the applied load over a greater area of bond interface. Thus, if the interfacial adhesion strength is increased and the metal phase is ductile, it is likely that the failure load will be increased by an amount more than proportional to the interfacial adhesion strength increase, simply due to the larger area which will be bearing the load.

2. The adhering area will be increased because the glassy phase will wet more strongly and eliminate voids at the interface. Once voids are eliminated by being filled with glass to create new voids within the interface, they must be nucleated and grow to a stable size. For these materials this is believed to be so disfavored energetically that if some of the glassy phase were slowly drawn out of the interface a soft gold or silver metal phase would plastically flow (creep) at the firing temperature to prevent void formation. Accordingly, elimination of voids between metal and ceramic by an advancing front of glassy phase might be likened to the action of a zipper, i.e., once the front passes, separation of surfaces linked by the glass becomes more difficult.

---

*Private communication with E. Conlon, July 1975.

63

It may also be important in mixed-bonded inks that formation of the spinel phase occurs and limits the amount of glassy phase that can be absorbed into the substrate. The self-limiting spinel formation model has pertinence to mixed-bonded inks in another way: If spinel growth continues indefinitely, the copper oxide in the dissolved glassy phase would be depleted, then γ_{gm} would approach that of frit-bonded inks, and adhesion strength would be reduced. This is one mechanism for the strength loss on overfiring mixed-bonded inks, which was reported by RCA [1,2] but was not seen by Lisauskas [27].

The model which states that in mixed-bonded inks the metal phase adheres directly to a glassy phase containing dissolved copper is in agreement with the conclusions of Lisauskas and with our low angle electron diffraction data on mercury-vapor-leached, mixed-bonded layers [2] in which we detected no crystallinity at the binder phase surface. It is also in agreement with our empirical theory of adhesion which was based on the Auger spectrometric analyses of mercury-vapor leached reactively bonded and mixed-bonded binder layers [2].

D. CONCLUSIONS

1. The formation of spinels is an important part of the bonding mechanism of both mixed-bonded and reactively bonded noble-metal-bond conductor inks. Generally, the spinels adhere directly to the alumina.

2. According to the best data available at present, the metal phase in reactively bonded inks that contain no frit phase and that are fired on alumina substrates containing no interfering glassy phase, adheres to the spinel phase(s).

3. In addition to verifying Lisauskas's lattice parameters for spinels grown on Coors ADS96F alumina from films of CdO or CuO, RCA has identified a spinel with a lattice parameter of $\sim$8.19 Å that was grown from films of mixed CuO and CdO on Coors ADS96F.

4. The presence of a glassy phase from the substrate or incorporated in smaller amounts in the composition of a reactively bonded, or in greater amounts in a mixed-bonded ink, accelerates the growth of spinel and aids in the elimination of voids in the binder phase-metal phase interface.

5. A void-free interface is crucial to the highest adhesion strength in thick-film conductors.

6. In mixed-bonded inks with optimum adhesion strength, the metal phase adheres to a glassy phase containing ~ 5 wt pct of dissolved copper at the interface.

7. The thermodynamic work of adhesion between the metal phase and the binder phase surface of a mixed-bonded or reactively bonded one is estimated to reach values as high as three times that of a good thick-film frit which contains no copper, e.g., Bi_2O_3 or a lead borosilicate glass such as E-1527.

SECTION IV

RECOMMENDATIONS FOR FUTURE WORK

A. FRIT-BONDED INKS

In frit-bonded films, the most important variables appear to be the particle size distribution and morphology of the metal constituents. Gold-film film adhesion is primarily dependent upon mechanical interlock with the frit. The stability of the sintered gold microstructure is, in turn, dependent upon the relative amounts of small and large particles. Since the ripening process favors the growth of large particles at the expense of small ones, improvements in microstructural stability can predictably result from controlling the relative amounts of small and large particles, i.e., the particle size distribution. Future work should address this key variable as well as the influence of particle morphology upon overall sintered microstructural stability as a function of frit content, sintering time, and temperature. In conjunction with these variables, it is necessary to adequately describe the critical glass parameters, e.g., surface tension, viscosity, metal and ceramic solubility in the glass, and thermal coefficient of expansion. Identifying useful ranges of the glass parameters is required, since they directly affect the ripening kinetics and resultant microstructure.

B. REACTIVELY BONDED AND MIXED-BONDED INKS

The importance of spinel to the adhesion of reactively bonded and mixed-bonded inks has been established empirically, but a full understanding of the growth mechanism, particularly for such binders in the presence of a sintering conductor film, does not yet exist. Experiments to define the critical areas of the phase diagram $CdO-CuO-Al_2O_3$ at 0.2 atmospheres oxygen pressure and perhaps with the addition of minor amounts of SiO_2 are needed to understand whether liquid phases are being formed. If present, liquid phases probably control spinel growth kinetics in these materials.

Further experiments with CdO films are required. One object of such experiments should be to resolve the differences in the data of Lisauskas and RCA by finding a value for the activation energy of formation for W_{int} from

66

CdO films in a confined CdO atmosphere. A second set of experiments are required to determine whether CdO vapor transport does indeed cause $CdAl_2O_4$ to form far from the printed areas and whether the vapor can accelerate the growth of copper-containing spinels where no CdO was present in the printed film.

The dependence of the growth of other spinels on their epitaxiality with $MgAl_2O_4$ in the substrate surface should be addressed. Experiments can be conceived in which $MgAl_2O_4$ particles are located in an alumina substrate surface, the surface is reacted with CuO and/or CdO films at temperature where the growth of these spinels is slow, the substrate is etched to remove unreacted oxide, the original $MgAl_2O_4$ spinel grains are located again, and the growth of the new spinel phase is studied relative to such growth in $MgAl_2O_4$-free areas on the substrate surface. High lateral resolution Auger spectrometry together with SEM and an electron or x-ray diffraction technique are required for such an experiment.

The role of unreacted metal oxide, which was credited as the adhesive link between the spinel and the metal phase by Lisauskas, needs further study. Analytical techniques should be employed to examine fracture interfaces using Auger spectrometry and SEM. Similar experiments should be carried out on mixed-bonded films to test the spinel-surface-seal hypothesis as a part of a study of the mechanism for adhesion degradation, which can be caused by over-firing these materials. Comparison of the effects of mercury-vapor and $KI-I_2$ etching should be performed.

A test of the void-filled-interface hypothesis used to explain the overlay gold ink study would be useful. A critical experiment would be to fire overlay gold films onto various spinel surfaces while pressing the films onto the spinels isostatically or otherwise, and then to test the bond adhesion strengths.

The work of adhesion of typical thick-film frits such as E1527 and Bi_2O_3 with and without additions of CuO and CdO, on surfaces of sapphire, debased alumina, gold, and silver should be measured. The NRL/Purdue University subcontract to study pertinent glass systems under the NASC program, "Basic Adhesion Mechanisms in Thick and Thin Films," together with RCA work in this contract series should form a good basis for design of those experiments.

67

REFERENCES

1. T. T. Hitch and K. R. Bube, "Basic Adhesion Mechanisms in Thick and Thin Films," Final Report, NASC Contract No. N00019-74-C-0270, 31 January 1975.

2. T. T. Hitch and K. R. Bube, "Basic Adhesion Mechanisms in Thick and Thin Films," Final Report, NASC Contract No. N00019-75-C-0145, 30 January 1976.

3. K. R. Bube and T. T. Hitch, "Basic Adhesion Mechanisms in Thick and Thin Films," Final Report, NASC Contract No. N00019-76-C-0256, 31 January 1977.

4. W. D. Kingery, H. K. Bowen, and D. R. Uhlmann, *Introduction to Ceramics,* 2nd ed. (John Wiley & Sons, Inc., New York, 1976), pp. 183, 208.

5. N. K. Adam, "Use of the Term 'Young's Equation' for Contact Angles," Nature $\underline{180}$, October 19, 1957, p. 809.

6. M. Nicholas, "The Strength of Metal/Alumina Interfaces," J. Mat'ls. Sci. $\underline{3}$, 571-576 (1968).

7. R. W. West, "Conduction Mechanisms in Thick-Film Microcircuits," Final Technical Report under ARPA Order No. 1642, Grant Nos. DAHC-15-70-G7 and DAHC-15-73-G8; Grantee: Purdue University Research Foundation, December 1975.

8. V. N. Eremenko, et al., *Liquid-Phase Sintering*, Consultants Bureau, New York (1970), p. 3.

9. W. D. Kingery, "Densification During Sintering in the Presence of a Liquid Phase I Theory," J. Appl. Phys. $\underline{30}$, 301, (1959).

10. W. J. Huppmann, "Sintering in the Presence of Liquid Phase," in G. C. Kuczynski, ed., *Sintering and Catalysis* (Plenum Publishing Corp., New York, 1975), p. 359.

11. S. Newman, "Kinetics of Wetting of Surfaces by Polymers; Capillary Flow," J. Colloid Interface Sci. $\underline{26}$, 209 (1968).

12. *Handbook of Chemistry and Physics,* 48th ed., The Chemical Rubber Co., Cleveland, Ohio (1967), p. D-115.

13. D. L. Johnson and I. B. Cutler, "Diffusion Sintering: I, Initial Stage Sintering Models and Their Applications to Shrinkage of Powder Compacts," J. Am. Ceram. Soc. $\underline{46}$, 541 (1963).

14. D. L. Johnson and I. B. Cutler "Diffusion Sintering: Initial Sintering Kinetics of Alumina," J. Am. Ceram. Soc. $\underline{46}$, 545 (1963).

15. S. S. Cole, "Sintering of Ag-Pd in the Presence of a Reactive Glass," J. Am. Ceram. Soc. $\underline{55}$, 296 (1972).

16. T. V. Nordstrum, "Sintering Kinetics of Reactively Bonded Thick-Film Gold," presented at Fall Meeting, Am. Ceram. Soc. Electron. Div., Sept. 18-21, 1977, Montreal, Quebec, Canada.

REFERENCES (Continued)

17. S. M. Makin, et al., "Self-Diffusion in Gold," Proc. Phys. Soc. 70B, 545 (1957).

18. W. J. Moore, *Physical Chemistry* (Prentice-Hall, Englewood Cliffs, NJ, 1962), 3rd ed., p. 734.

19. G. H. S. Price, et al., "Sintered Alloys, Part I, Copper-Nickel-Tungsten Alloys Sintered with a Liquid Phase Present," J. Inst. Metals, 62, 39 (1938).

20. W. D. Kingery, H. K. Bowen, and D. R. Uhlmann, *Introduction to Ceramics* 2nd ed. (John Wiley & Sons, Inc., New York, 1976), p. 425.

21. H. Fischmeister and G. Grimvall, "Ostwald Ripening - A Survey," in Ed. G. C. Kuczynski, *Sintering and Related Phenomena* (Plenum Publishing Corp., New York, 1973), p. 119.

22. T. H. Courtney, "A Reanalysis of the Kinetics of Neck Growth During Liquid Phase Sintering," Met. Trans. A 8A, 671 (May 1977).

23. T. H. Courtney, "Microstructural Evolution During Liquid Phase Sintering: Part I, Development of Microstructure," Met. Trans. A 8A, 679 (May 1977).

24. T. H. Courtney, "Microstructural Evolution During Liquid Phase Sintering: Part II, Microstructural Coarsening," Met. Trans. A, 8A, 685 (May 1977).

25. J. M. Lifshitz and V. V. Slyozov, "The Kinetics of Precipitation from Supersaturated Solid Solutions," J. Phys. Chem. Solids 19, 35 (1961).

26. D. B. Dadyburjor and E. Ruckenstein, "Kinetics of Ostwald Ripening," J. Cryst. Growth 40, 279 (1977).

27. R. J. Lisauskas, "Characterization of the Reaction Between Thick-Film Reactive-Bonded Gold Pastes and Alumina Substrates," Master's Thesis, Massachussetts Institute of Technology, June 1976.

28. T. T. Hitch, "Reproducible Adhesion Test For Soldered Thick-Film Conductors," Final Report, on Naval Avionics Facility, Indianapolis, Contract No. N00163-76-C-0287, released March 1978.

29. K. T. Jacob and C. B. Alcock, "Thermodynamics of $CuAlO_2$ and $CuAl_2O_4$ and Phase Equilibria in the System $Cu_2O-CuO-Al_2O_3$," J. Am. Ceram. Soc. 58, 192 (1975).

30. D. R. Stull, "Vapor Pressure of Pure Substances," Ind. and Eng. Chem. 39, 517 (1947).

31. W. D. Kingery *Introduction to Ceramics* (John Wiley & Sons, Inc. New York, 1960), p. 335.

32. S. K. Misra and A. C. D. Chaklader, "The System Copper Oxide-Alumina," J. Am. Ceram. Soc. 46, 509 (1963).

33. A. Gadalla and J. White, "Equilibrium Relationships in the System $CuO-Cu_2O-Al_2O_3$," J. Brit. Ceram. Soc. 63(1), 39 (1964).

REFERENCES (Continued)

34. R. G. Loasby, N. Davey and H. Barlow, "Enhanced Property Thick-Film Conductor Pastes," Solid State Technology $\underline{15}$(5), 46 (1972).

35. T. T. Hitch, "Phase Morphology and Bondability of Reactively Bonded and Frit-Bonded Gold and Silver Thick-Film Conductors," J. Electron. Mat. $\underline{3}$, 553 (1974).

36. G. Katz, "Adhesion of Copper Films to Aluminum Oxide Using a Spinel Structure Interface," Thin Solid Films $\underline{33}$, 99 (1976).

A-1. G. W. Morey, *The Properties of Glass* (Reinhold Pub. Co., New York, 1954) pp. 202-203.

A-2. E. Matijevic, Ed., *Surface and Colloid Science* (1) (Wiley-Interscience, New York, 1969), pp. 129-134.

I-1. E. M. Levin, et al., *Phase Diagrams for Ceramists*, The American Ceramic Society, Columbus, OH (1964).

I-2. E. M. Levin, et al., *Phase Diagrams for Ceramists 1969 Supplement*, The American Ceramic Society, Columbus, OH (1969).

I-3. E. M. Levin and H.F. McMurdie, *Phase Diagrams for Ceramists 1975 Supplement*, The American Ceramic Society, Columbus, OH (1975).

APPENDICES

APPENDIX A

DETERMINATION OF THE SURFACE TENSION OF E1527 GLASS

A sample of E1527 glass in a Pt crucible was heated at 800°C until all
the bubbles escaped and a clear glass was obtained. The surface tension was
measured by using a Pt-Ir DuNoüy ring which was suspended from a Pt wire and
attached to an Instron Tensile Machine "A" cell. The ring was immersed in
and withdrawn from the glass at 0.005 in (0.13 mm)/min. The maximum observed
force of separation is shown in Fig. A-1 and indicates a positive temperature
coefficient, i.e., the surface tension increases with temperature. Morey [A-1]
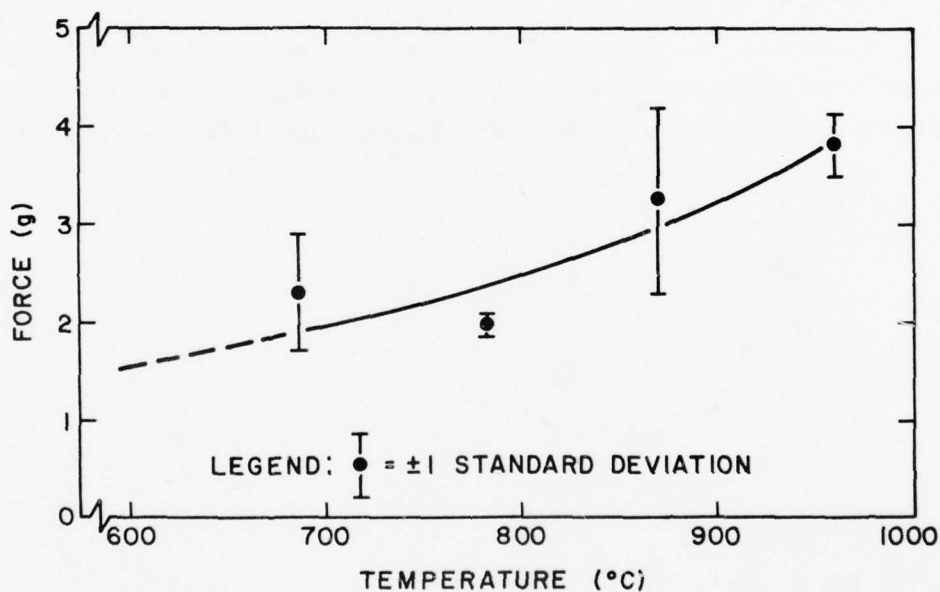
Figure A-1. Separation force vs temperature for
E1527 glass from DuNoüy ring.

A-1. G. W. Morey, *The Properties of Glass* (Reinhold Pub. Co., New York,
1954), pp. 202-203.

71

has shown that high PbO binary glasses of SiO_2 and B_2O_3 also exhibit positive temperature coefficients. The actual surface tension, γ_{LV}, is computed from [A-2]

$$\gamma_{LV} = \left(\frac{fg}{4\pi R}\right) F$$

where f = force in grams
g = acceleration due to gravity
R = ring radius
F = correction factor

The correction factor, F, is dependent upon the molten glass density. Since we do not know the exact density at the test temperatures, two values for F have been computed based on a wide enough range of densities to encompass the actual densities. Table A-1 summarizes the computed surface tensions determined from the force vs temperature plot, in Fig. A-1, and the assigned values of density, as well as the statistical significance of the data.

A-2. E. Matijevic, Ed., *Surface and Colloid Science (1)* (Wiley-Interscience, New York, 1969), pp. 129-134.

TABLE A-1. SURFACE TENSION OF E1527 GLASS[*]

Temp.	Assumed density = 3.5 g/cm^3		Assumed density = 2.03 g/cm^3	
	Correction	Surface Tension	Correction	Surface Tension
°C	factor,F	γ, dynes/cm	factor,F	γ, dynes/cm
600	0.89	117	0.93	122
700	0.90	144	0.94	150
800	0.92	185	0.96	193
900	0.94	251	0.99	264

Surface Tension Statistics

Temp. °C	Force, Grams	Standard Deviation	Coefficient of Determination V in pct	Sample Size n
691	2.30	0.58	25.1	10
784	1.96	0.09	4.7	8
871	3.27	0.94	28.7	10
960	3.83	0.33	8.7	10

Ratio Test[**]

Temp. Pair, °C	Ratio	Significance
691-784	1.8	not significant
691-871	2.8	probably significant
691-960	7.3	definitely significant
784-871	4.4	definitely significant
784-960	5.5	definitely significant
871-960	1.8	not significant

*Based on DuNoüy ring radius = 0.950 cm, wire radius = 0.018 cm

**Ratio = $(\bar{x}_1 - \bar{x}_2) \div (\sigma_1^2/n_1 + \sigma_2^2/n_2)^{1/2}$.

73

APPENDIX B

ORGANIC BINDER COMBUSTION TEST

In all thick-film ink systems, the metal powder and glass frit are suspended in an organic vehicle. To enhance durability in the dried but unfired state, the inks contain organic polymer or resin which remains in the dried deposit prior to high-temperature firing. With a view to examining sintering kinetics and the interreactions of frit and metal, as well as achieving a dense deposit, the organic polymer should be thoroughly burned before significant sintering occurs. A typical polymeric additive is ethylcellulose dispersed in an appropriate solvent.

To assess the burnout rate of the polymer a quantity of high-molecular-weight, N-300 grade[*] ethylcellulose was dissolved in a mixture of Carbitol[**] [2-(2-ethoxyethoxy)ethanol] and butyl Carbitol [2-(2-butoxyethoxy)ethanol] to yield 10 wt pct polymer in a solution containing 25 wt pct Carbitol and 75 wt pct butyl Carbitol. For tares, polished alumina substrates measuring 1 in. x 1 in. x 0.005 in. were used. Onto the tares, the solution was doctor-bladed into a 0.75-in.-diameter hole in a 0.064-in.-thick Teflon (polytetra-fluoroethylene) stencil[†]. After drying at 125°C for 45 min, the dried polymer film weighing 0.040 - 0.045 g was exposed to 300, 400, and 500°C, respectively, in air flowing at 10 ft^3/h. The percent-weight-loss curves for these temperatures are plotted as a function of time in seconds in Fig. B-1. From Fig. B-1, it can be seen that only 3 s at 500°C or 17 s at 400°C suffices to burn the polymer completely. At 300°C the weight loss is still incomplete after 2 min. However, with reference to the sintering of fine particle size Au, for example MK-2, 17 s at 400°C shows only a small percentage of total densification (Fig. E-1, Appendix E). The 0.040-g polymer test print covered a

*Hercules Corp., Wilmington, DE.
**Union Carbide Corp., New York, NY.
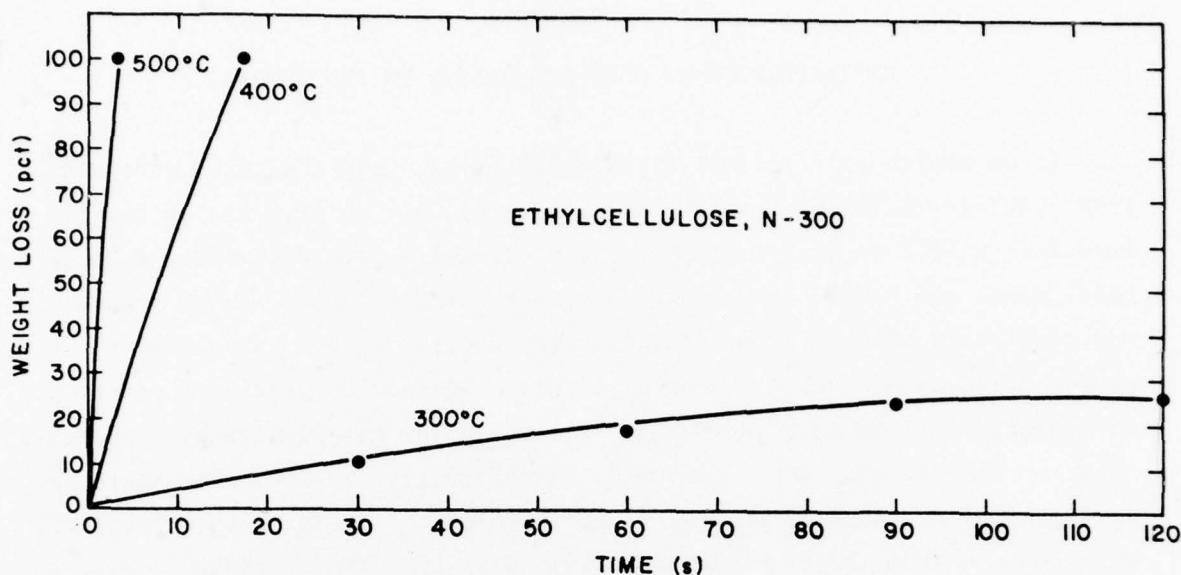†E. I. DuPont de Nemours & Co., Inc., Wilmington, DE.

74

WEIGHT LOSS (pct)

100 ● 500°C ●
90
80 400°C
70
60   ETHYLCELLULOSE, N-300
50
40
30
20   300°C
10
0
0 10 20 30 40 50 60 70 80 90 100 110 120

TIME (s)

Figure B-1. Polymer combustion rate.

0.75-in.-diameter circle; this corresponds to 1.4×10^{-2} g/cm^2. If a thick-film gold ink contains 3 wt pct polymer, corresponding to approximately 30 wt pct vehicle, the polymer would cover 250 in^2. (1613 cm^2) per troy ounce (31.1 g). Then the polymer weight per unit area is 6×10^{-4} g/cm^2 and is 10 vol pct of the conductor film thickness. On the basis of this example it appears highly improbable that the polymer combustion curve would seriously overlap with a metal sintering curve. If the glass sinters at a lower tempera-ture than the metal constituents, exit paths for the polymer combustion products still exist in the unsintered metal network which typically comprises 90 vol pct of the film. Consequently, organic polymer burnout is expected to be complete before the major sintering reactions occur.

APPENDIX C

DETERMINATION OF GOLD SOLUBILITY IN E1527 GLASS

To determine gold solubility in E1527 glass, gold crucibles were made from 0.002-mm (0.005-in.) thick foil measuring 25.4 mm (1.0 in.) x 25.4 mm (1.0 in.) x 12.7 mm (0.5 in.) high. The crucibles were repeatedly filled with E1527 glass and heated at 900°C to outgas the molten glass. When outgassing was completed, after 3.75 h, the glass was cooled to room temperature. Gold powder MK-2 was sprinkled on the solid glass surface to provide 1 wt pct Au, in a highly divided form and readily available for dissolution by the glass. After heating at 700, 800, and 900°C, respectively, for the times specified in Table C-1 the samples were quenched in deionized water. Glass fragments were removed from the crucible and examined at 50X magnification to ensure that no Au particles were present. The samples were then analyzed by the atomic absorption technique with appropriate calibration standards made with E1527 glass.

From Table C-1 it is apparent that Au solubility increases with temperature, approaching 0.02 wt pct after 10 min at 900°C.

TABLE C-1. GOLD SOLUBILITY IN E1527 GLASS

Temp,°C	700	800			900	
Time, min.	240	5	10	40	5	10
Au, wt pct	0.0004	0.0015	0.0009	0.00046	0.007	0.016

76

APPENDIX D

GOLD POWDER PREPARATION

It was desired to make gold powders with controlled particle size and spherical shape. The Au was dissolved in aqua regia, and the pH adjusted to 2.5 by addition of NaOH. The solution was kept below 50°C during this period and cooled to room temperature prior to the addition of Na_2SO_3 solution. The specific amounts involved were:

Au	19.9 g
37% HCl	85 ml
70% HNO_3	30 ml
50% NaOH	48 ml
Na_2SO_3	25 g in 175 ml of water

The Na_2SO_3 solution was added with stirring in about 30 s. The precipitated gold was rinsed in deionized water and oven-dried for 40 min at 70-95°C, followed by 30 min at 95-125°C. The yield was 98 wt pct.

Additional 20-g lots of MK-2 gold powder were prepared. Scanning electron micrographs (SEMs) of powder samples from the five lots, labeled 8-12, are shown in Figs. D-1 through D-5. With the exception of occasional large clusters, the individual particles are generally in the 1-2-μm range. Whether clusters or individual particles, the shapes are roughly spherical. This morphological form is believed to result from the rather fast nucleation and growth. Under the conditions used, i.e., rapid addition of concentrated reducing agent, little opportunity is given for slower, anisotropic growth on the relatively faster growing crystal planes. Only one hexagonal-shaped particle, indicative of slower particle growth, is visible in lot 12 (Fig. D-5). Subsequently, the five lots were combined into one lot by the use of isopropyl alcohol to prevent cold welding between particles, rinsing with methyl alcohol, drying at less than 125°C, and cooling in a dessicator.
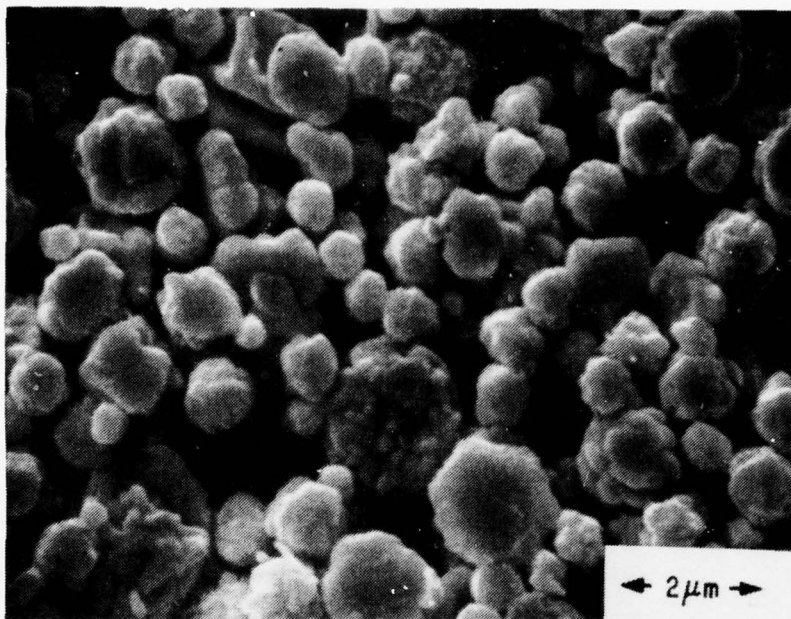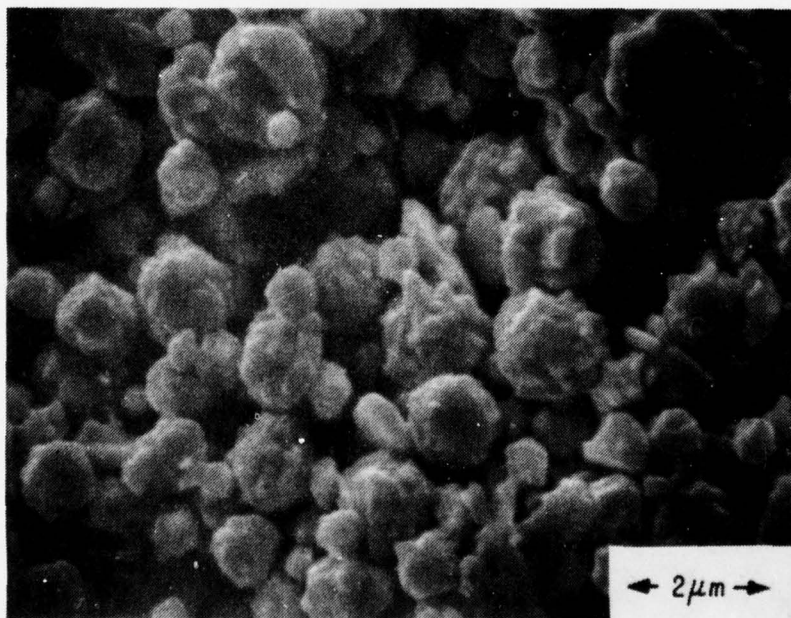
Figure D-1.   Gold powder MK-2, lot 8.

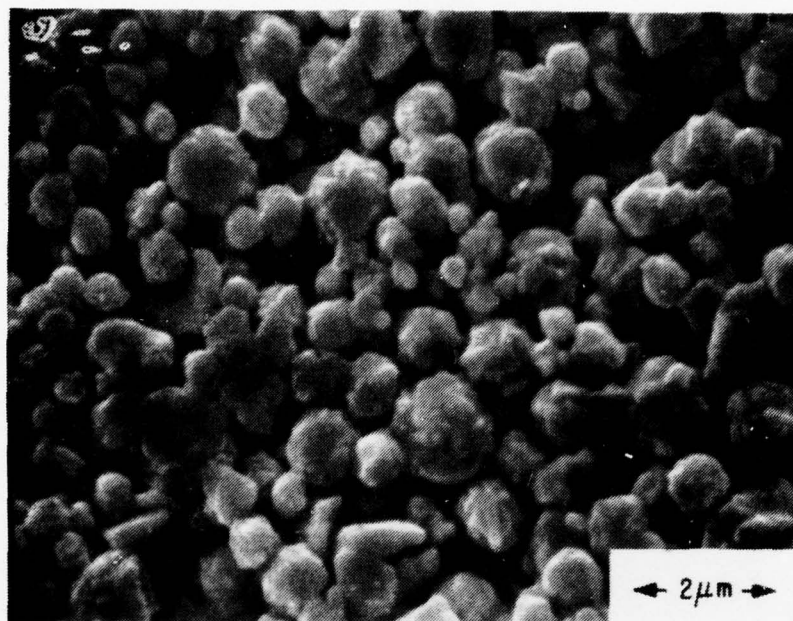

Figure D-2.   Gold powder MK-2, lot 9.

78

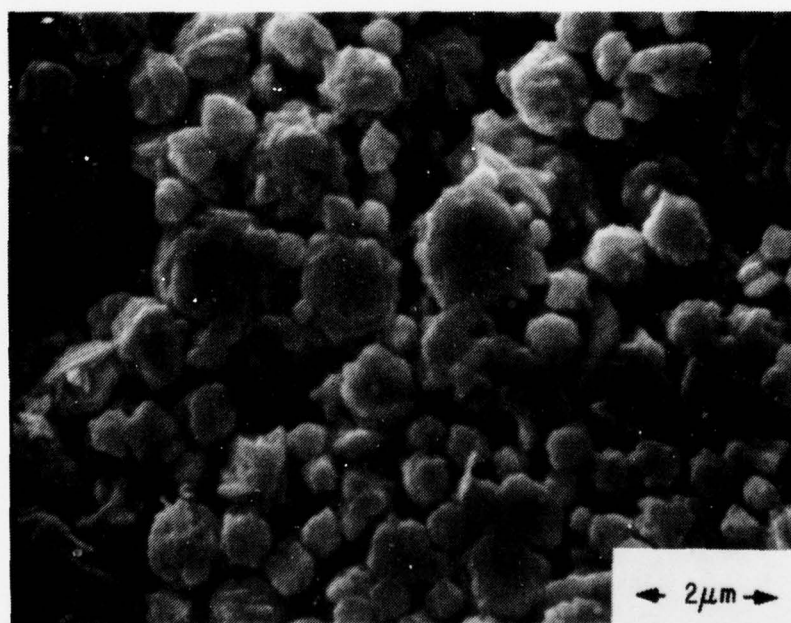Figure D-3. Gold powder MK-2, lot 10.

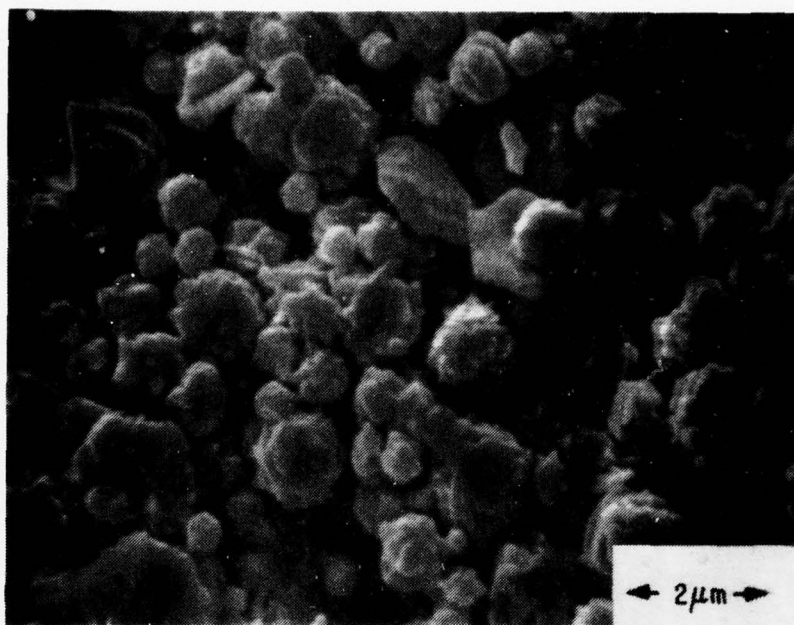Figure D-4. Gold powder MK-2, lot 11.

Figure D-5. Gold powder MK-2, lot 12.

APPENDIX E

SINTERING BEHAVIOR OF GOLD POWDER COMPACTS

Because the MK-2 Au powder exhibited swelling under isothermal (900°C) sintering conditions, (Figs. E-1 and 2), it was necessary to determine the cause prior to undertaking sintering comparisons with glass added to the gold. Samples of the MK-2 Au powder weighing 0.85 g were compacted in a carbide die of 0.5-in. (12.5-mm)-diameter, as usual, at a force of 1900 lb (864 kg), and heated isothermally at 400-900°C for time periods of 30-2400 s. The diametral swelling of the sample shown in Fig. E-1 occurs at 600°C after isothermally heating for 2400 s. At higher temperatures the swelling becomes evident in less than 600 s. When the sintering data are expressed as percent change in actual density, as shown in Table E-1, the swelling at the higher temperatures becomes more evident. Since foreign contaminants were kept to a minimum in preparing the powder, and the average weight loss on heating was only 0.07 wt pct, it did not seem plausible that the outgassing of adsorbed material could have caused the swelling. A possible cause, however, was the sealing of air in the powder compact by a compaction force that was excessively high. When the temperature of the compact is raised during sintering, the tensile strength of gold decreases, while the trapped-air pressure increases. In an effort to achieve equilibrium, the internal pressure was increased; this resulted in some plastic flow (expansion) of the sintered gold compact. On cooling, the air pressure in the expanded pores decreased. However, the increase in the strength of the gold at room temperature prevents the greater atmospheric pressure from collapsing the sealed pores.

To confirm the above hypothesis, samples of MK-2 Au powder were compressed at 475 lb (215 kg) and 950 lb (431 kg), respectively, and were fired isothermally at 700°C; at this temperature swelling was observed in the case of the samples compressed at 1900 lb (862 kg). Figure E-2 shows that the swelling decreases with compaction force and is virtually eliminated when 475 lb (215 kg) or 2419 lb/in.^{2} (1.7 kg/mm^2) is used. Further experiments therefore utilized the 475 lb (215-kg) compaction force.
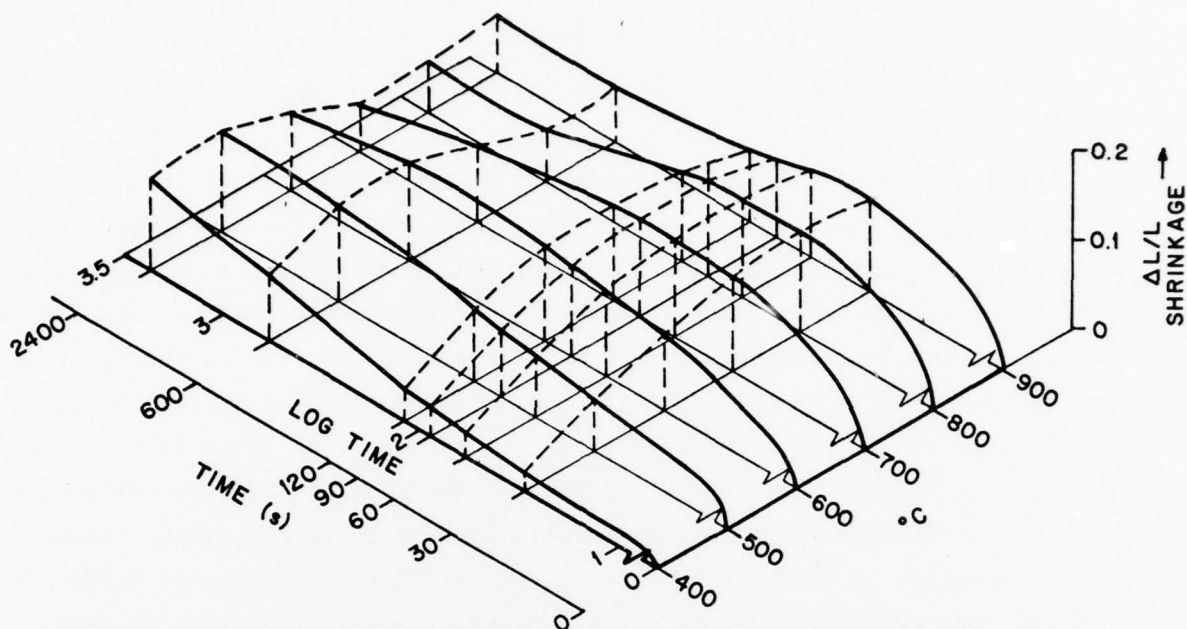
GOLD   POWDER   MK-2   COMPACTION   FORCE = 1900 lb   (862 kg)

Figure E-1.   Isothermal densification rates for MK-2 Au powder.

TABLE E-1.   PERCENT CHANGE IN ACTUAL DENSITY OF SINTERED
MK-2 GOLD (1900-1b (862 kg) COMPACTION FORCE)

Pct Change at Temperature (°C)

Time (s)	400	500	600	700	800	900
30	4.7	7.4	28.6	35.1	36.6	34.5
60	3.2	21.2	30.6	33.5	35.3	30.0
90	8.6	17.3	28.4	33.1	32.7	24.5
120	16.4	26.3	32.8	32.2	32.9	23.8
600	16.4	38.2	35.4	20.9	13.8	16.9
2400	32.6	35.6	26.2	12.9	13.6	20.0

82
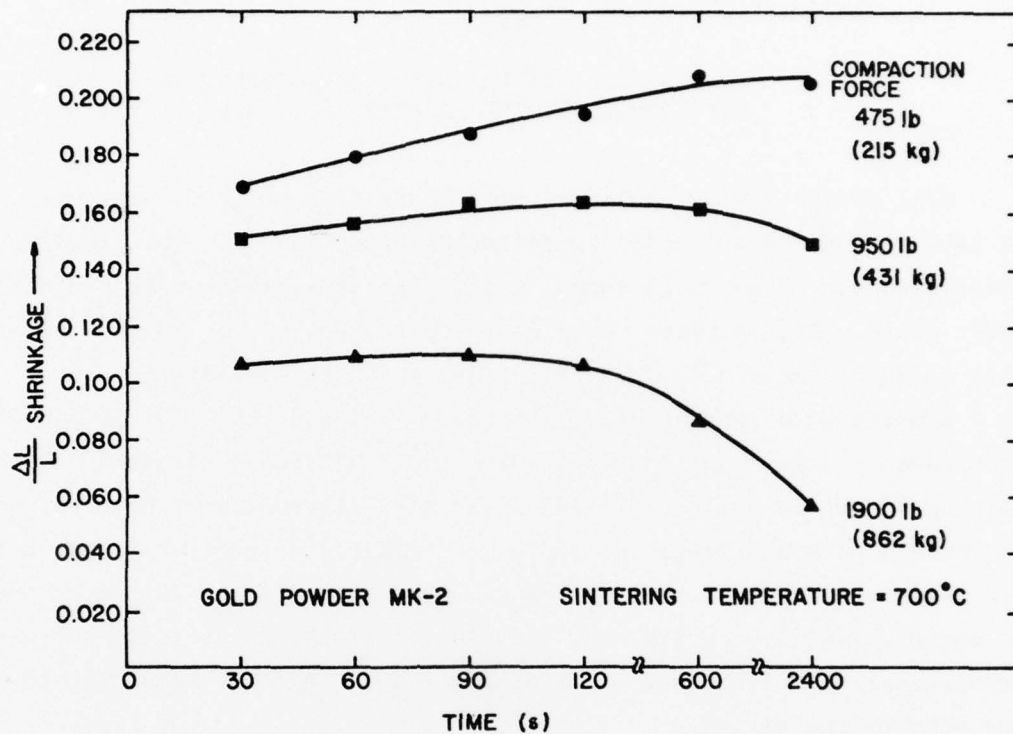
Figure E-2. Isothermal densification rates for MK-2 Au powder
at 700°C vs powder compaction force.

APPENDIX F

GOLD POWDER SINTERING AND MICROSTRUCTURE
DEVELOPMENT IN THE PRESENCE OF GLASS

Gold powder MK-2 was blended with quantities of E1527 glass necessary
to make up individual powder compacts weighting 0.85 g. The blending was ac-
complished for these small quantitites by careful mixing with a spatula on a
glass plate. All samples, containing 10, 20, 30, 40, or 50 vol pct of glass
were compacted at 475 lb (215 kg) as described in Appendix E.

Samples were isothermally sintered at 700 and 800°C for 30 and 600 s in
both cases. Samples of the 700°C-30-s and 700°C-600-s sintered compacts con-
taining 10 and 50 vol pct of glass were metallographically mounted, polished,
and etched with aqua regia at 50°C. A similar treatment was given to the
800°C-sintered samples. Figs. F-1 to F-8 illustrate the degree of phase ag-
glomeration which occurred as a function of temperature, time, and glass con-
centration. In each case, phase dispersion is uniform, attesting to the
adequacy of the mixing.

At the lowest time (30 s) and temperature (700°C) the glass phase (dark)
in the 10-vol pct sample is very finely and uniformly dispersed, as shown in
Fig. F-1. Heating for 600 s at 700°C produces considerable coarsening in the
microstructure, as shown in Fig. F-2. The glass becomes isolated into fewer
but larger pockets as gold sintering progresses. At 50 vol pct, the glass
pockets are still adequately dispersed but are correspondingly larger than
those in the 10-vol pct samples as shown in Figs. F-3 and F-4 for the sintering
times of 30 and 600 s, respectively, at 700°C.

When the samples containing 10 and 50 vol pct of glass are fired at 800°C,
the results differ only in degree (see Figs. F-5 to F-8). The dispersion is
again quite uniform, but the extent of phase agglomeration is somewhat greater
for the 800°C-sintered samples. Compare Figs. F-1 and F-5 for 30 s, 10 vol pct
of glass, F-2 and F-6 for 600 s, 10 vol pct of glass, F-3 and F-7 for 30 s,
50 vol pct of glass, and F-4 and F-8 for 600 s, 50 vol pct of glass. Therefore,
at temperatures where the glass is fairly fluid (700 and 800°C), i.e., well
above its 485°C softening point, the two phases begin to separate with sintering
time. As gold particle neck growth occurs, the more fluid glass phase is ex-
truded into the few remaining voids in the structure. Where the glass phase

84

1.0

4.5
5.0
5.5
6.3
7.1
8.0

2.8

2.5

3.2

2.2

3.6

4.0

1.1

2.0

1.8

1.25

1.4

1.6
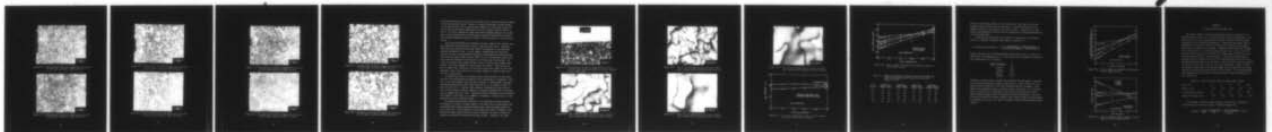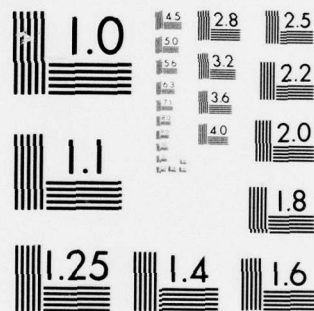
MICROCOPY RESOLUTION TEST CHART
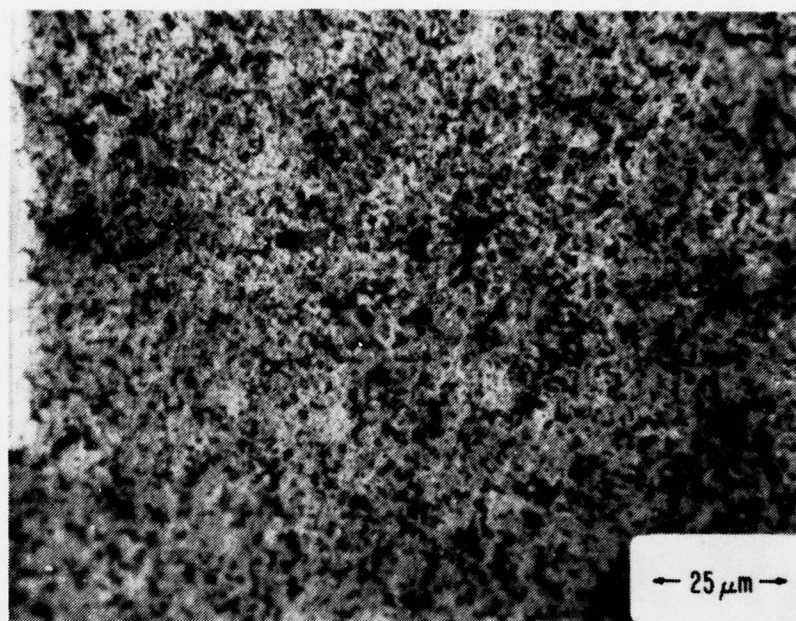NATIONAL BUREAU OF STANDARDS-1963-A

Figure F-1. Microstructure of MK-2 Au powder with 10 vol pct of E1527 glass sintered at 700°C for 30 s.
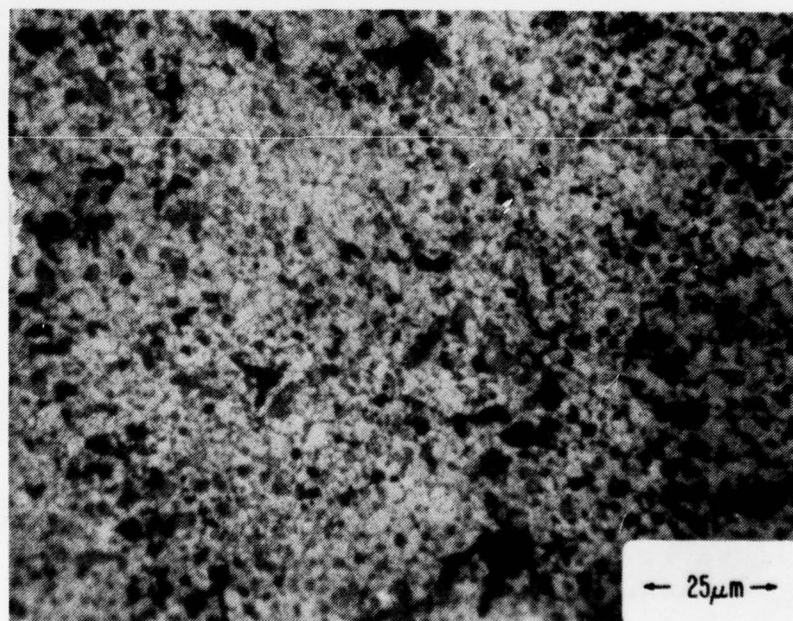

Figure F-2. Microstructure of MK-2 Au powder with 10 vol pct of E1527 glass sintered at 700°C for 600 s.
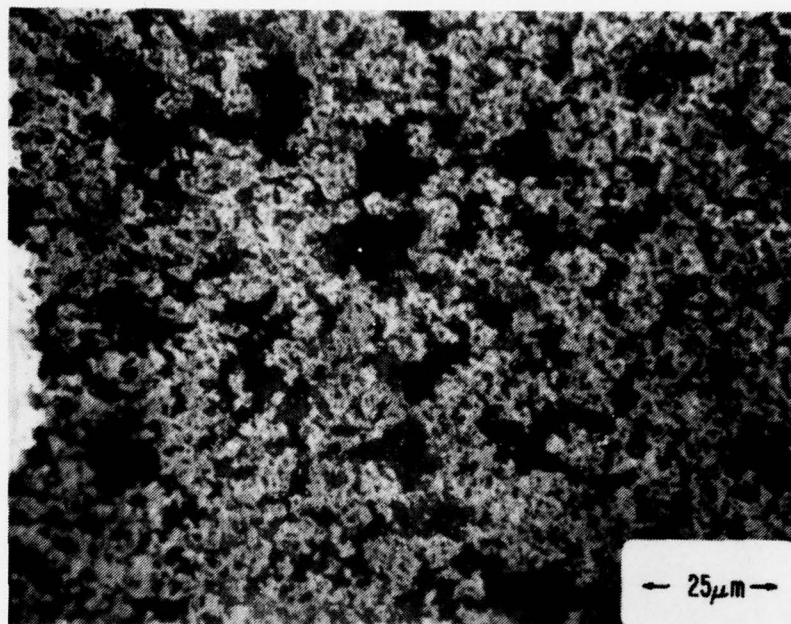
Figure F-3. Microstructure of MK-2 Au powder with 50 vol pct
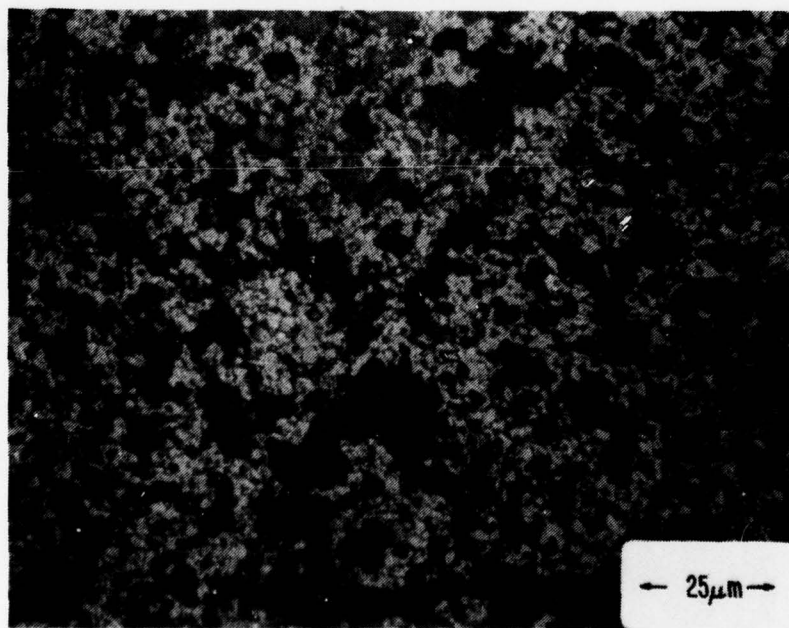of E1527 glass sintered at 700°C for 30 s.

Figure F-4. Microstructure of MK-2 Au powder with 50 vol pct
of E1527 glass sintered at 700°C for 600 s.

Figure F-5. Microstructure of MK-2 Au powder with 10 vol pct
            of E1527 glass sintered at 800°C for 30 s.

Figure F-6. Microstructure of MK-2 Au powder with 10 vol pct
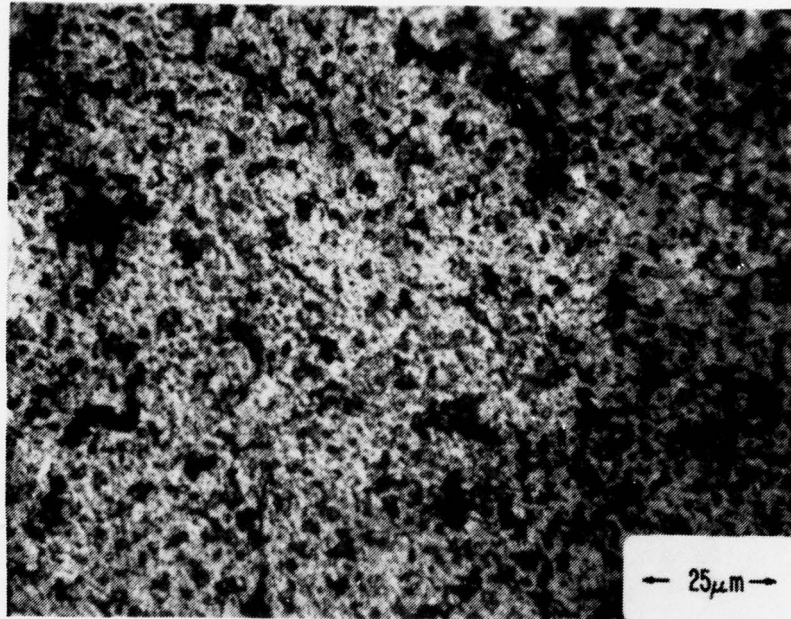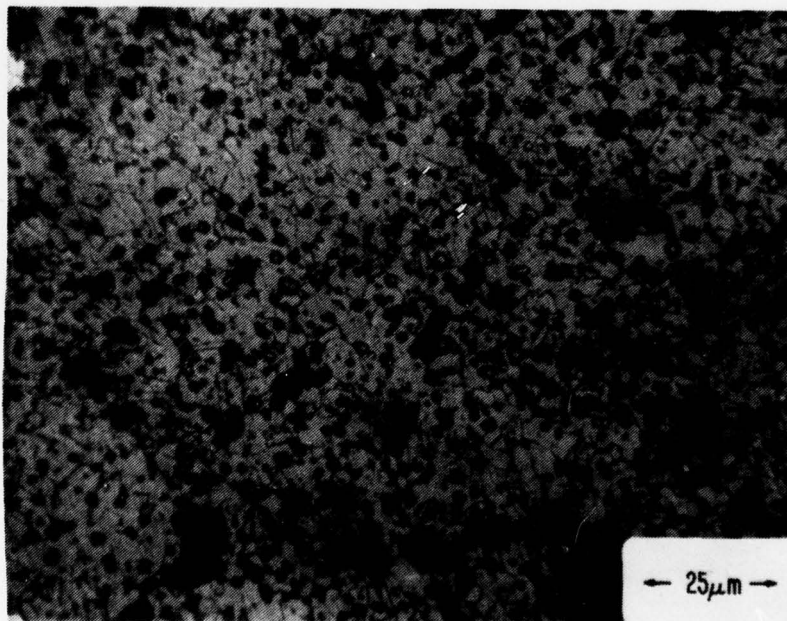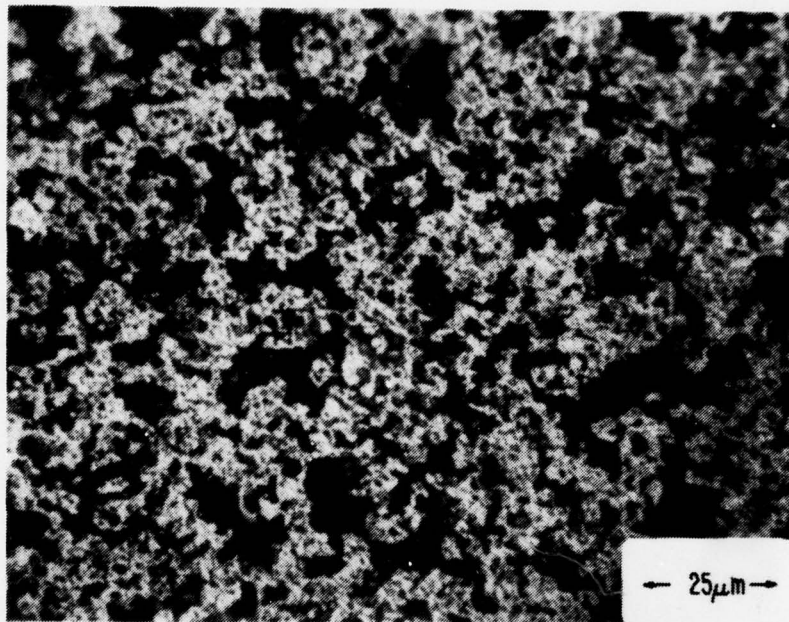   of E1527 glass sintered at 800°C for 600 s.

87

Figure F-7. Microstructure of MK-2 Au powder with 50 vol pct
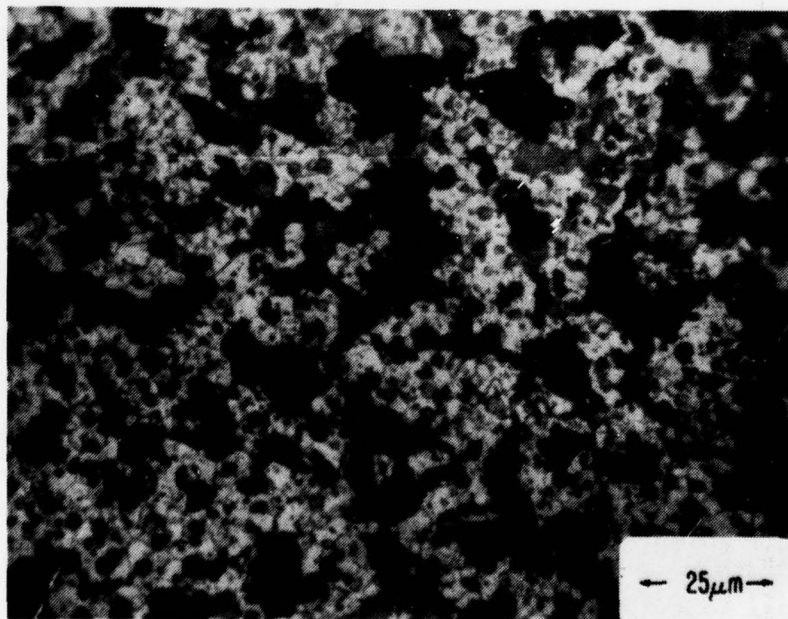   of E1527 glass sintered at 800°C for 30 s.

Figure F-8. Microstructure of MK-2 Au powder with 50 vol pct
            of E1527 glass sintered at 800°C for 600 s.

is already isolated from contact with adjacent pores, the glass remains trapped in the sintered gold matrix. However, a sizable percentage of glass escapes to the outer surface of the sintered gold compact, as can be seen in Fig. F-9 in the case of the sample containing 50 vol pct of glass, fired at 800°C for 600 s. It is this interfacial glass layer which enhances adhesion of the gold layer to the ceramic body in screen-printed conductor applications and which also retards subsequent attempts to bond to the free surface of the film after firing.

After photomicrography was completed, the gold compacts were removed from the epoxy mount by dissolving the epoxy in glacial acetic acid. The glass phase was then removed from the gold compact by immersion in ultrasonically agitated hydrofluoric acid. In this manner, scanning electron microscopy was able to depict the labyrinthian network of interconnecting gold particles. The 10 vol pct glass sample fired at 700°C for 30 s, illustrated in Fig. F-10, shows numerous examples of grain growth, the final stage of sintering. Because of a smaller gold volume fraction in the 50 vol pct glass sample shown in Fig. F-11, fewer examples of grain growth are obvious. After firing for 600 s at 800°C this distinction is less clear since grain growth is quite well advanced in both the 10 and 50 vol pct glass samples, as shown in Figs. F-12 and F-13, respectively.

To compare the effect of different glass volume fractions on gold densification, two characteristics observed in the system must be recognized. From Fig. F-14, which compares ΔL/L with glass content, it would appear that glass improves densification at 700°C when fired for 30 s, but begins to retard it when fired for 600 s. However, when thickness variations are taken into account so that densities may be compared, a monotonic densification is observed for all samples (see Fig. F-15). Apparently powder shrinkage can be anisotropic with regard to direction, i.e., diameter vs thickness. At this time it is not understood why this condition exists.

The second characteristic pertains to the variations in density before sintering as a function of glass content. From Fig. F-15 it would appear that increasing glass content enhances densification, since the higher glass contents result in a closer approach to the theoretical density. However, a comparison of powder compact densities *before* sintering, as shown in Table F-1, indicates that density increases with glass content. Therefore, the glass
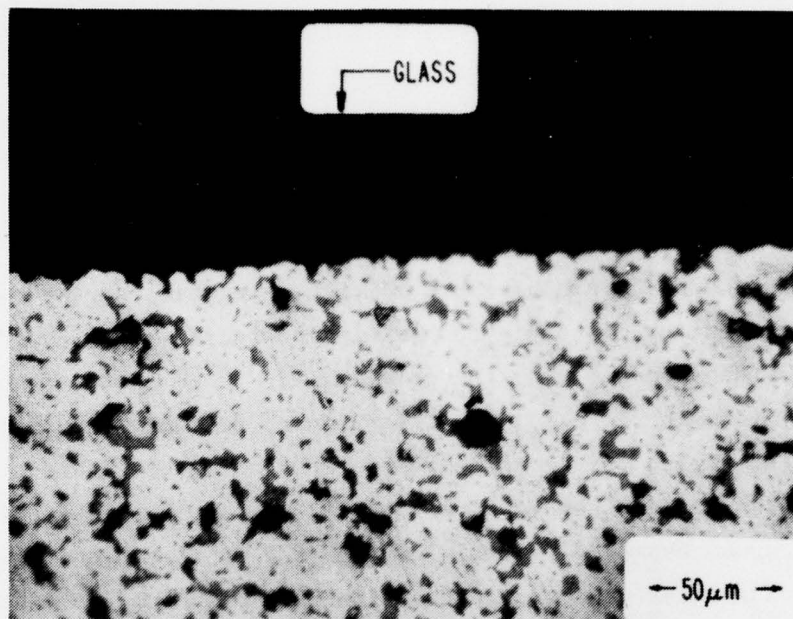
89

Figure F-9.   Microstructure of MK-2 Au powder with 50 vol pct
of E1527 glass sintered at 800°C for 600 s, showing
surface glass layer.

Figure F-10.   SEM of MK-2 Au powder with 10 vol pct of E1527
glass removed after sintering at 700°C for 30 s.

Figure F-11. SEM of MK-2 Au powder with 50 vol pct of E1527
             glass removed after sintering at 700°C for 30 s.
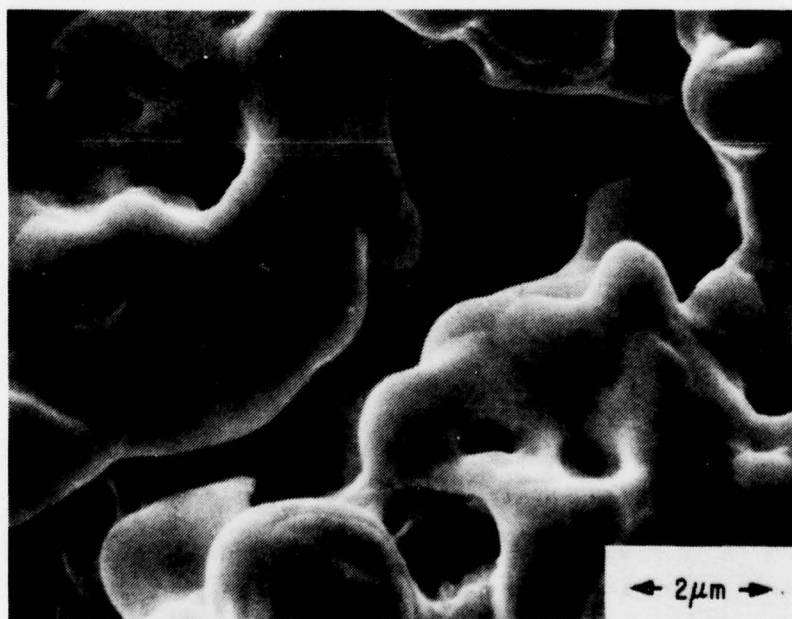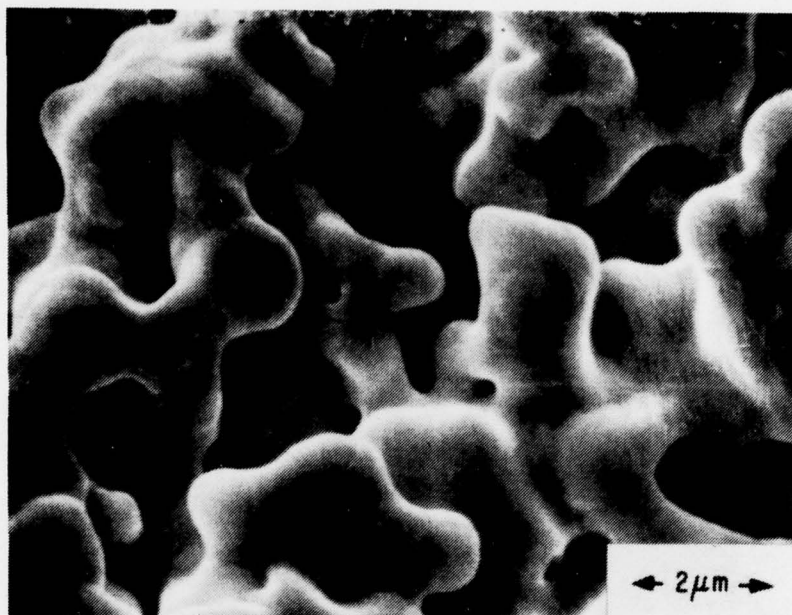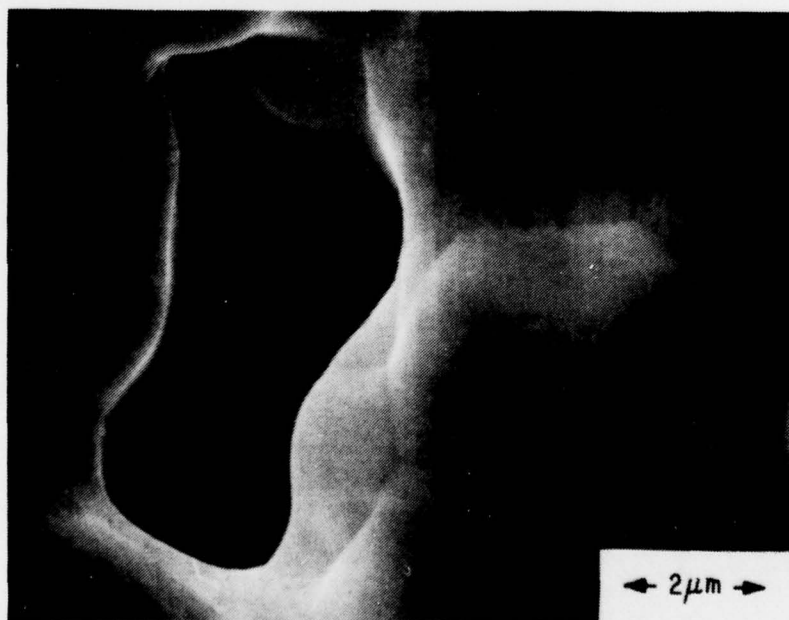

Figure F-12. SEM of MK-2 Au powder with 10 vol pct of E1527
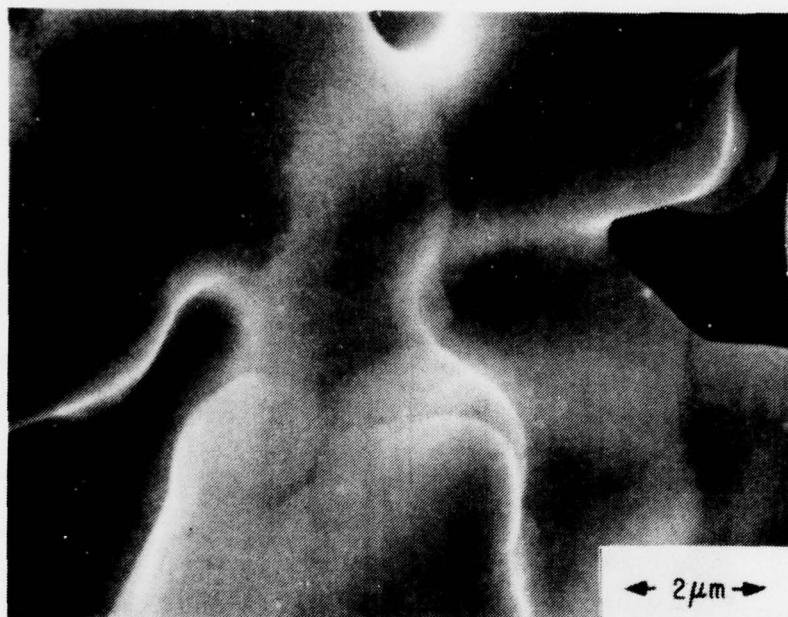   glass removed after sintering at 800°C for 600 s.

Figure F-13.   SEM of MK-2 Au powder with 50 vol pct of E1527
glass removed after sintering at 800°C for 600 s.
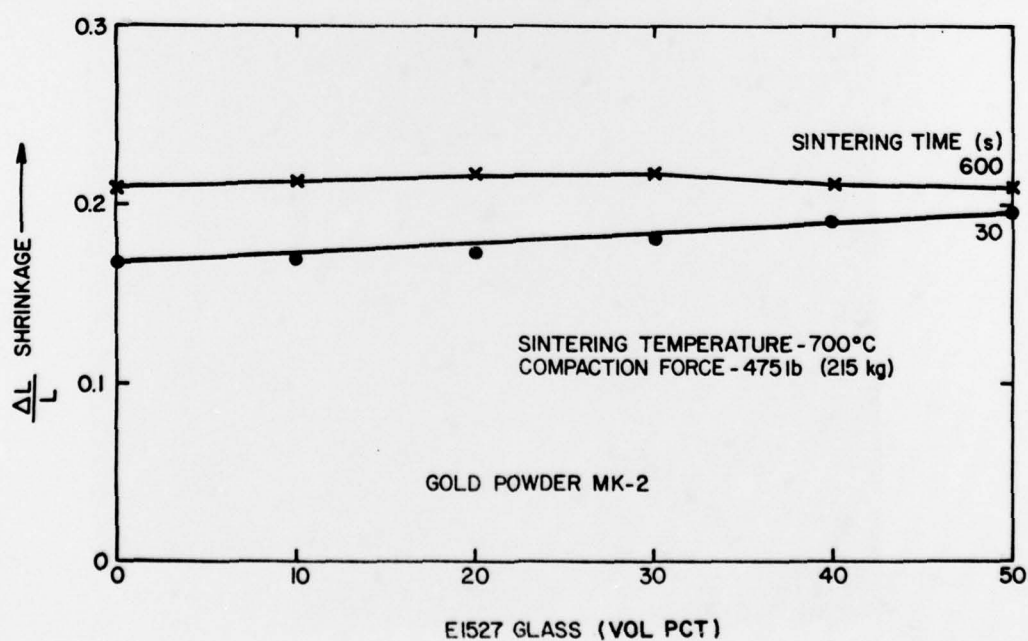
Figure F-14.   Isothermal densification rate at 700°C for MK-2
Au powder vs E1527 glass content.

% OF THEORETICAL DENSITY

110

100

90

800°C-600s

700°C-600s

80

800°C-30s

70

700°C-30s

COMPACTION FORCE
475 lb (215 kg)

GOLD POWDER MK-2

60

50

0   10   20   30   40   50
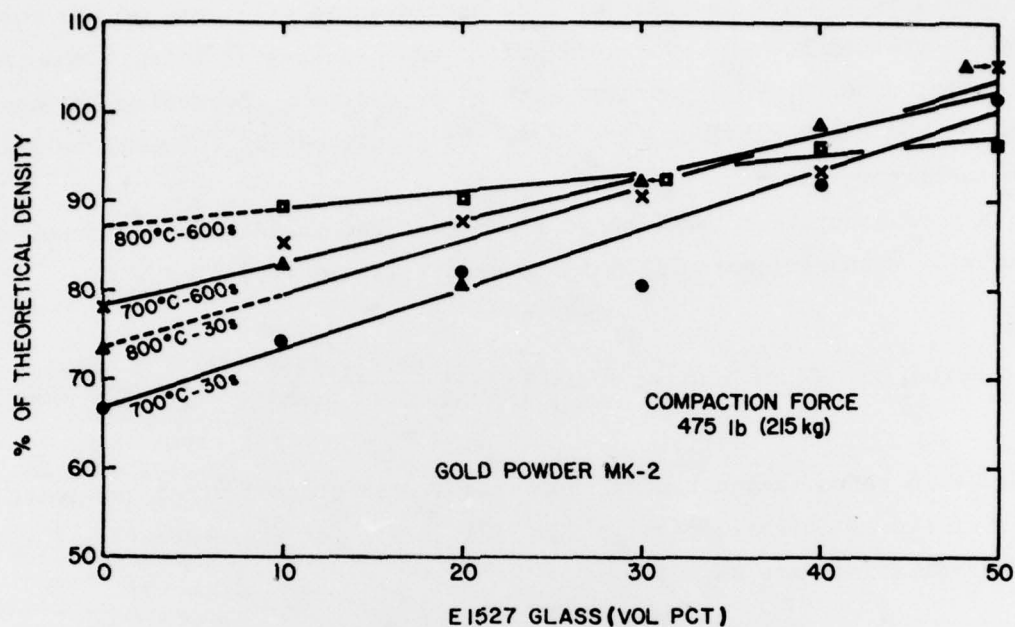
E1527 GLASS (VOL PCT)

Figure F-15.   MK-2 Au powder as percent of theoretical density vs
E1527 glass content.

TABLE F-1.   PERCENT OF THEORETICAL DENSITY OF MK-2 GOLD BEFORE AND
AFTER SINTERING WITH E1527 GLASS (475-1b (215 kg)
COMPACTION FORCE)

Glass Vol Pct	700°C-30 s Before	700°C-30 s After	700°C-600 s Before	700°C-600 s After	800°C-30 s Before	800°C-30 s After	800°C-600 s Before	800°C-600 s After
10	44	74	43	85	44	83	39	89
20	46	82	44	88	44	81	44	90
30	48	80	47	90	48	92	47	92
40	50	92	50	93	51	99	51	96
50	56	102	54	105	55	105	55	96

frit has a sufficient quantity of fine particles to fill some of the voids
normally present between some gold particles. Packing efficiency and con-
sequently, density, thus improved with glass content. Superfically, a plot
based on the theoretical density gives the appearance of enhanced densification
with increasing glass.

A more accurate comparison would account for variations in presintered
density by comparing normalized improvements in density, i.e.,

$$\text{Pct normalized densification} = 100 \left(\frac{\text{Final density} - \text{initial density}}{\text{theoretical density} - \text{initial density}} \right)$$

Figure F-16 shows this corrected comparison with glass content for which the
coefficients of determination, r^2, of the slopes for the respective temperature-
time combinations are as follows:

Temp.($°$C)-Time(s)	r^2
700-30	0.91
700-600	0.87
800-30	0.91
800-600	0.92

Therefore, it may be safely assumed that densification improvement is directly
and linearly proportional to glass volume fraction. Note, however, that the
slopes are more positive for the short sintering time (30 s) samples. This
implies that sintering during the initial stage of sintering, i.e., rearrange-
ment, is aided more by the presence of glass than during the final stage
(600-s-sintered samples) where solid-state processes predominate. The latter
observation becomes more vividly apparent when percent change in actual density
is compared, as in Fig. F-17, where the slopes of 600-s-sintered samples become
negative.

94
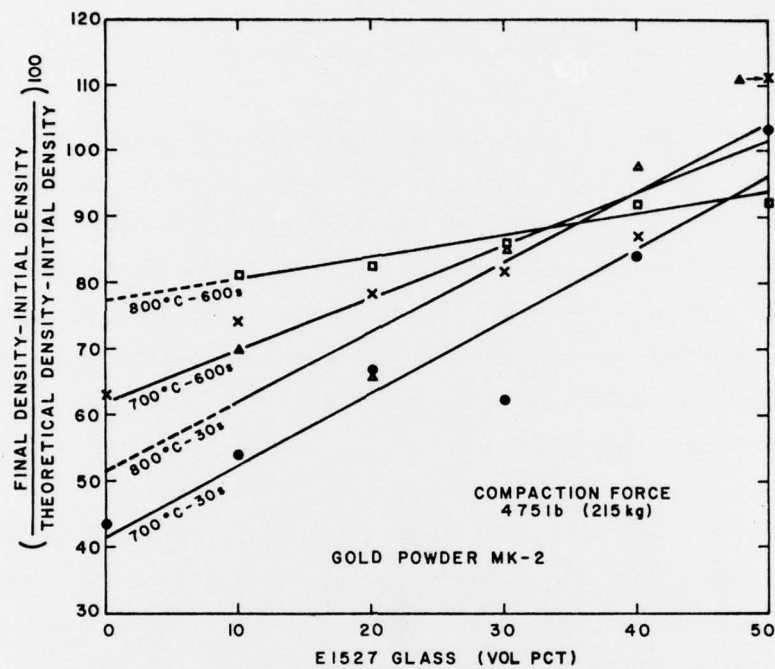
Figure F-16. MK-2 Au powder as normalized densification
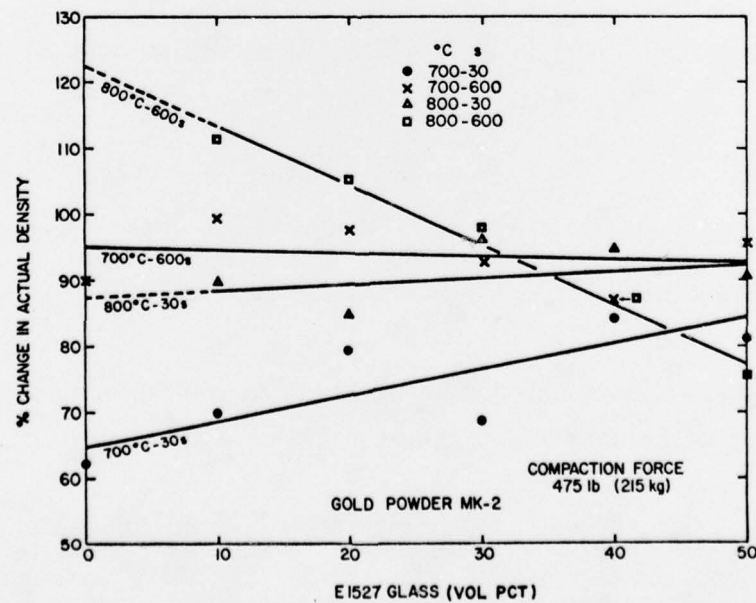vs E1527 glass content.

Figure F-17. MK-2 Au powder as percent change in actual
density vs E1527 glass content.

95

APPENDIX G

AIR BUBBLE ESCAPE IN MOLTEN GLASS

Since metal powder is densifying simultaneously with the glass frit, a
limiting factor is the rate of air bubble escape from the molten glass. This
escape rate is, in turn, controlled by the glass viscosity, which decreases
exponentially with increasing temperature. To determine the escape rate, an
experiment was conducted at 900°C, the temperature of fastest metal powder
densification studied in this program. A sample of E1527 glass frit weighing
1.05 g was placed in a Pt foil boat which measured 1 in. x 1 in. ($6.45 \ cm^2$).
The glass and Pt boat were then heated for varying times at 900°C with inter-
mediate determinations of the glass density. The density was determined
pycnometrically by hanging the Pt boat and solidified glass from a fine wire
and measuring the weight in air and water. The glass density was then computed;
the density, weight, and volume of the Pt boat were known. Table G-1 lists
the change in glass density and percent weight loss and shows that air bubble
removal was essentially complete after 90 min at 900°C. The cumulative weight
loss indicates that after initial moisture removal, little PbO evaporated at
this temperature.

TABLE G-1. DENSITY OF E1527 GLASS VS FIRING TIME AT 900°C

Time, min	10	20	30	90	120
Density, g/cm^3	3.48	3.70	3.85	4.02	4.07
% of Theoretical Density	86	91	95	99	100
Cumulative Weight Loss, %	0.48	0.50	0.51	0.55	0.65

If we assume a uniform coating of glass in the Pt boat, ignoring the
slight buildup at corners and edges, the glass thickness is

$$\text{thickness} = \frac{\text{volume}}{\text{area}} = \frac{\text{mass/density}}{\text{area}} = \frac{1.05 \ g/3.48 \ g/cm^3}{6.45 \ cm^2} = 0.047 \ cm$$

96

and the slowest possible bubble escape rate is

$$\text{rate} = \frac{\text{thickness}}{\text{time}} = \frac{0.047 \text{ cm}}{90 \text{ min}} = 5.2 \times 10^{-4} \text{ cm/min}$$

In a conventional thick film with a fired deposit of 15 μm containing 10 vol pct of glass, the glass film would be 1.5 μm (1.5×10^{-4} cm) presuming uniform dispersion. The time required for complete bubble escape is

$$\text{time} = \frac{\text{distance}}{\text{rate}} = \frac{1.5 \times 10^{-4} \text{ cm}}{5.2 \times 10^{-4} \text{ cm/min}} = 0.29 \text{ min (17 s)}$$

Referring to Fig. E-1 in Appendix E, the densification of MK-2 Au is about half-completed in 17 s at 900°C. Therefore, it is not probable that air would be confined in the glass by lack of an open path in the simultaneously densifying metal powder.

APPENDIX H

SYNOPSIS OF MIT MASTER'S THESIS BY

R. J. LISAUSKAS

The findings of this work, an MIT Master's thesis by R. J. Lisauskas, are so directly applicable and complementary to our study of reactively bonded and mixed-bonded conductor adhesion that we are presenting a synopsis of his work here, since it is not generally available [27].

Lisauskas studied the mechanism of adhesion in gold mixed-bonded and reactively bonded inks. He investigated four commercial materials. The two reactively bonded inks contained Cu and Cd binders in a nominal 3:1 ratio to each other but with differing ratios of binder to gold. The two mixed-bonded inks he studied contained copper, cadmium, and bismuth as the binder additivies. He further studied two pastes he made himself - one from CuO and one from CdO -- which contained no gold or other inorganic material.

All were printed and fired onto Coors 96-wt pct alumina, which he characterized as containing ∿4-wt pct silica and minor amounts of Ca, K, Na, and Mg. The films were fired in a belt furnace at a series of temperatures from 850 to 1050°C with 15-min dwell at peak temperature.

Analysis of the binder phases and interfaces was accomplished by use of the following techniques: selective etching, either with aqua regia or nitric acid to remove gold, glass, and metal oxides or with a $KI-I_2$ etchant solution which removed only gold; determination of the weight gain of fired specimen substrates after printing, firing, and etching; determination of the adhesion strength of unetched films; x-ray diffraction of etched film surfaces; SEM-ography; and EDAX analysis of features detected in the SEM. Table H-1 gives in detail some of the more important thesis findings.

The conclusions Lisauskas drew from this work are summarized below.*

A. At 1100°C the CuO paste and alumina substrate react to form the spinel $CuAl_2O_4$. No $CuAlO_2$ was detected, in agreement with the

_____
*In this summary the wording to Lisauskas's conclusions has been changed to restate them in the terminology we have used throughout the contract study, and to condense them.

Paste, Type, Composition of Additives to Gold	Adhesion Behavior	Thermally Activated Growth of Spinel at the Interface (grams). (Data normalized to wt at 850°C.)	Total Weight of Spinel and Metal Oxide Interfacial Materials	SEMograph after Etc and Metal Stated
CuO paste	N/A*	$W_{int}^{**} = 2 \times 10^{11} e^{\frac{-87 \text{ kcal/mole}}{RT}}$ Correlation factor was 99 pct for firing temps. from 900 to 1050°C.	N/A	Identific irregular ∿1- to 2- larger af surface c
CdO paste	N/A	$W_{int} = 3 \times 10^7 e^{\frac{-62 \text{ kcal/mole}}{RT}}$ Correlation factor was 99 pct for firing temps. from 900 to 1050°C.	N/A	∿80-pct c surface b 1050°C fi
Au paste No, 1, reactively bonded – 1.8 wt pct Cu 0.55 wt pct Cd	Nominally linear increase with firing temperature from 1 lb† at 900°C to 14 lb at 1015°C.	$W_{int} = 1 \times 10^5 e^{\frac{-49 \text{ kcal/mole}}{RT}}$ Correlation factor was 98 pct for firing temps. from 900 to 1015°C.	Not measured.	∿80-pct c by a phas spinel. than CdO samples.
Au paste No. 2, reactively bonded – 0.79 wt pct Cu 0.23 wt pct Cd	Nominally linear increase with firing temperature from 1.8 lb at 900°C to 9.5 lb at 1025°C.	$W_{int} = 1 \times 10^5 e^{\frac{-48 \text{ kcal/mole}}{RT}}$ Correlation factor was 87 pct for firing temps. from 900 to 1025°C.	No wt change at 900 to 1025°C.	
Au paste No. 3, mixed bonded – 0.23 wt pct Cu 1.43 wt pct Cd 1.10 wt pct Bi	Approximately constant at 9.5 lb with firings between 900 and 1025°C.	$W_{int} = 1 \times 10^{10} e^{\frac{-77 \text{ kcal/mole}}{RT}}$ Correlation factor was 99 pct for firings from 900 to 1025°C.	∿ constant wt at 900 to 1000°C (strong increase over 850°C value; decreases from 1000 to 1025°C).	Failed at when test not etche
Au paste No. 4, mixed bonded – 0.52 wt pct Cu 0.61 wt pct Cd 0.70 wt pct Bi 0.17 wt pct Ag	Approximately constant at 7.5 lb with firings between 900 and 1025°C.	$W_{int} = 1 \times 10^{10} e^{\frac{-78 \text{ kcal/mole}}{RT}}$ Correlation factor not given. Firing temps. 900–1050°C.	∿ constant wt at 950 to 1025°C (strong increase over 850°C value).	Failed at After aqu look simi paste No.

*N/A – Not applicable.
**W_{int} – Weight gain of interfacial compounds.
†lb – The strengths of the films expressed in psi in the thesis are shown here as failure load for a $(0.08\text{-in.})^2$ pad, by multiplying Lisauskas's stress value by his pad areas.
††d_{220} – The lattice spacing between adjacent planes of Miller index 220.

eight of Spinel and xide Interfacial s	SEMographic Data – after Etch Removal of Au and Metal Oxides unless Otherwise Stated	EDAX Analytical Data	x-Ray Diffraction Data
N/A	Identification of new phase growing irregularly on alumina. Particles $\sim$1- to 2-μm diam after 975°C firing; larger after 1050°C firing but surface coverage only $\sim$30 pct.		Spinel identified, d_{220}^{++} = 2.86 Å for 1050°C sample, 2.846 Å for ASTM standard, and 2.84 Å for standard prepared by Lisauskas.
N/A	$\sim$80-pct coverage of alumina surface by a second new phase after 1050°C firing.	New phase contains only Cd and Al, i.e., no glass present.	Spinel identified, d_{220} = 2.88 Å for 1050°C sample (2.86 Å calculated). x-Ray peak intensities less than with CdO-based material. No glass present.
sured.	$\sim$80-pct coverage of alumina surface by a phase identified as mixed spinel. Different appearance than CdO or CuO paste samples.	Cu and Cd in spinel particles.	Spinel identified, d_{220} = 2.86 Å; unreacted CuO identified.
ange at 900 to			Spinel identified, d_{220} = 2.86 Å.
nt wt at 000°C (strong in- ver 850°C value; s from 1000 to	Failed at glass-gold interface when tested. (Failure surface not etched.)	Spinel phase contains Cd and Cu but no Bi.	Spinel identified, d_{220} = 2.86 Å.
nt wt at 950 to strong increase °C value).	Failed at glass-gold interface. After aqua regia etching, samples look similar to those of gold paste No. 3 after etching.		Spinel identified, d_{220} = 2.86 Å.

phase diagram of Jacob and Alcock shown in Fig. 19 of the text and a model according to which spinel formation occurs at the $CuAl_2O_4$-Al_2O_3 phase boundary.

B. The pastes of CuO and CdO react with the substrate to form $CuAl_2O_4$ and $CdAl_2O_4$ (also a spinel), respectively. The amount formed is a thermally activated function of the firing temperature, which ranged from 850 to 1050°C.

C. The activation energies for spinel formation from the CdO and CuO pastes agree in general with the activation energies for M^{2+} ion diffusion through MAl_2O_4 spinels determined by galvanic cell experiments. The same mechanism is suggested to control the kinetics of spinel formation from the CdO and the CuO pastes.

D. Reactively bonded thick-film gold pastes based on a 3CuO:1CdO binder wt ratio form a spinel at the substrate interface. The fit to an Arrhenius relationship is not as good as that for the CdO and CuO pastes, but the slopes and the activation energies of spinel formation for the two reactively bonded inks are clearly different from those of the metal oxide pastes. The rate-limiting mechanism for spinel formation is judged to be different from that in the case of the metal oxide pastes.

E. The spinel which formed for the reactively bonded inks consists of both $CuAl_2O_4$ and $CdAl_2O_4$. Lisauskas could not determine whether the spinel was an intimate mixture of crystallites of each or a partially substituted spinel of the form $Cu_xCd_{1-x}Al_2O_4$.

F. For the reactively bonded gold pastes, a layer of metal oxide was found between the gold and the spinel on the substrates. The gold adheres to the oxide. The layer structure consists of alumina, spinel, metal oxide, and gold containing minor amounts of dissolved copper.

G. For the reactively bonded inks, higher adhesion strengths are obtained with higher firing temperatures. Adhesion is a direct function of the amount of spinel at the interface, an amount that increases with the firing temperature.

H. The character of the Bi_2O_3-containing mixed-bonded inks is different
    from that of the reactively bonded materials. The amount of spinel
    in the mixed-bonded films increased with the firing temperature, but
    the amount of glassy phase, and therefore the adhesion strength, re-
    mained nearly constant for firing temperatures from 900 to 1025°C.

I. For Bi_2O_3-containing mixed-bond films, the interface structure con-
    sists of a nearly continuous glassy layer, which covers the spinel
    and the substrate. The gold adheres principally to the glass surface
    and peels away from it during adhesion testing.

J. Reactively and mixed-bonded inks require different firing processes.
    The required firing process can be predicted if the binder system is
    known. Reactively bonded inks such as those which Lisauskas studied
    required higher-temperature firing, e.g., at 1000°C. Mixed-bonded
    inks are less firing-temperature sensitive; Lisauskas claimed his
    materials can be fired from 900 to 1025°C without significant changes
    in the adhesion strength.

In some of these conclusions, particularly J and parts of G and H, Lisauskas
has restated RCA findings in terms of the materials he studied. Concerning
certain points in the conclusions and other statements of the thesis, the RCA
study team would prefer an alternative interpretation of the results. In
general, however, Lisauskas's experimental findings agree with our findings,
and can be reconciled in the few places where they do not.

102

APPENDIX I

EXAMPLES OF BINDER PHASE AND SUBSTRATE REACTIONS

The reactions between the various phases of inks and ceramics in thick-film materials are complex. Some insight into these reactions can be gained by studying the phase diagrams for some of the phases, where they have been described. The following is a short list of some reactions which it is believed may be important to thick films and their adhesion. The information is taken from a set of compilations of such information [I-1 through I-3].

Reactants	Reaction Data	Ref.	Fig. No.
Al_2O_3-Bi_2O_3	Eutectic at 97 mol pct Bi_2O_3 and 820°C. Liquidus at 93 mol pct Bi_2O_3 and 1070°C.	I-3	4365
Al_2O_3-MgO-SiO_2	For a 96 wt pct substrate with 3 pct SiO_2 and 1 pct MgO, cordierite is not as likely to occur as are sapphirine, corundum, or spinel.	I-2	2535
Al_2O_3-CdO	$CdAl_2O_4$ was found to be rhombohedral. The spinel form was not observed.	I-3	4318
Bi_2O_3-CdO	Eutectic at 17 mol pct Bi_2O_3 and ∿795°C.	I-1	326
Bi_2O_3-PbO	Eutectic at ∿25 mol pct Bi_2O_3 and ∿730°C.	I-1	326
Bi_2O_3-CuO	Eutectic at 90 mol pct Bi_2O_3 and ∿600°C.	I-3	4178
CuO-SiO_2	Eutectic at 8 wt pct SiO_2 and 1050°C.	I-2	2142
CuO-Al_2O_3	Phase diagrams by Misra and Chaklader [32] and by Gadalla and White [33] are shown.	I-2	2085-2094
PbO-SiO_2	Several eutectics at high PbO concentrations and ∿720°C.	I-1	284

I-1. E. M. Levin, et al., *Phase Diagrams for Ceramists*, The American Ceramic Society, Columbus Ohio (1964).
I-2. E. M. Levin, et al., *Phase Diagrams for Ceramists 1969 Supplement*, The American Ceramic Society, Columbus Ohio (1969).
I-3. E. M. Levin and H. F. McMurdie, *Phase Diagrams for Ceramists 1975 Supplement*, The American Ceramic Society, Columbus Ohio (1975).